Controlling Colloidal Stability using Highly Charged Nanoparticles

David J. Herman

Dissertation submitted to the faculty of Virginia Polytechnic Institute and State University
in partial fulfillment of the requirements for the degree of

Doctor of Philosophy
In
Chemical Engineering

John Y. Walz
Richey M. Davis
William A. Ducker
Stephen M. Martin

February 4, 2015
Blacksburg, VA

Keywords: Colloidal stability, nanoparticle adsorption, electrostatic forces, van der Waals interactions, atomic force microscopy

Controlling Colloidal Stability using Highly Charged Nanoparticles

David Herman

ABSTRACT

This dissertation focused on the potential use of highly charged nanoparticles to stabilize dispersions of weakly charged microparticles. The experimental components of the project centered on a model colloidal system containing silica microparticles at the isoelectric point where the suspensions are unstable and prone to flocculation. The stability of the silica suspensions was studied in the presence of highly charged nanoparticles. Initial experiments used polystyrene latex with either sulfate or amidine surface groups. Effective zeta potentials were measured with nanoparticle concentrations ranging from 0.001% to 0.5% vol. Adsorption levels were determined through direct SEM imaging of the silica microparticles, showing that the nanoparticles directly adsorbed to the microparticles (amidine more than sulfate), producing relatively large effective zeta potentials. However, stability experiments showed that the latex nanoparticles did not stabilize the silica but merely provided a reduction in overall flocculation rate. It was concluded that the zeta potential was an insufficient predictor of stability as there was still sufficient patchiness on the surface to allow for the silica surfaces to aggregate.

Experiments using zirconia and alumina nanoparticles did achieve effective stabilization; both types stabilized the silica suspensions for longer than the observation period of approximately 15 hours. Stability was observed at concentrations of 10^{-4}% to 1.0% (zirconia) and 10^{-2}% vol. (alumina). These particles adsorbed directly to the microparticles (confirmed via SEM) and produced increasing effective zeta potentials with increasing nanoparticle concentrations. The adsorption resulted in significant electrostatic repulsion that was determined to be effectively irreversible using colloidal probe AFM. The improved stabilizing ability was attributed to the increased van der Waals attraction between the oxide nanoparticles (compared to polystyrene).

Finally, an unexpected result of the CP-AFM force measurements showed that the repulsive forces between a nanoparticle-coated particle and plate lacked the normal dependence on the radius of the probe as predicted by the Derjaguin approximation. The forces observed in nanoparticle suspensions were virtually identical for 5 μm and 30 μm probes. Based on calculations of the shear rate in the gap, it was theorized that this phenomenon may have resulted from the shearing of adsorbed particles from the surfaces, which leads to similar interaction geometries for the two probe sizes.

Acknowledgements

I want to thank Dr. John Walz for his guidance during my time in graduate school. I am particularly grateful for his commitment to me and the rest of his research group here at Virginia Tech and continuing to guide us and make our projects a priority, all while simultaneously taking on the significant responsibilities with his current position at the University of Kentucky. It was no simple feat, and he made the process far easier than we could have anticipated. I would also like to thank the rest of my committee members, Dr. Richey Davis, Dr. William Ducker, and Dr. Stephen Martin. I have learned a lot both in class and through lab work, and I am particularly appreciative for your collaboration, as well as the sharing of lab space and equipment throughout my time here.

To the staff in the Department of Chemical Engineering: thank you for your dedication to keeping the department and labs running smoothly.

Thank you to my lab mates (and friends) from the Walz group, Greg, Shunxi, Wenle, and Francisco, as well as Dean, DJ, and Milad in the Ducker group. We spent a large part of the last few years together, in and out of the lab, and it has been a great and fun experience. Thank you to all the friends I have made in the department and elsewhere for helping me enjoy (and survive) graduate school.

Finally, I want to thank my parents for their unending support. I never would have made it this far without your love and encouragement.

Contents

List of Figures

List of Tables

Chapter 1: Overview of Dissertation

1.1 Introduction

Colloidal dispersions are instrumental in a wide array of applications, ranging from inks, environmental systems, petroleum processes, self-assembled materials, and bio-colloids.[1-10] In each case the ability to control the particle interactions within the suspension is essential for tailoring of the colloidal properties for a particular application. A stable colloid requires balancing the multiple forces, both attractive and repulsive, that are present between individual particles. Stability can be achieved through direct modification of particle surfaces to increase repulsive forces, such as the addition of charged surface groups or polymer layers. This can provide electrostatic or steric forces that counteract long range attractive forces, such as the van der Waals interaction.[8]

Depending on the use, different levels of stability may be desired, and they require control of aggregation behavior. In inks or paint and many processing applications, need the colloid to remain as individual particles. Self-assembly typically needs a regulated aggregation or deposition process, and environmental processes may require quick and simple aggregation mechanisms to easily remove colloidal contaminants from a system. Given many applications for colloidal dispersions require suspensions containing multiple particle types, it is important to investigate and understand how different combinations of particles interact with one another and how it relates to the stability of the suspension. The results and understanding gained from studies using model colloidal systems can be applied to a broad range of more specific applications. Furthermore, it is beneficial to produce colloids that are stable without requiring extensive surface modifications that may be detrimental to the desired application of the suspension. Understanding and implementing particle interactions to control the stability of colloidal suspensions is essential to creating novel methods of stabilization.

1.2 Motivation

The purpose of this dissertation was to investigate the stability behavior of model colloidal systems in the presence of highly charged nanoparticles. The specific systems studied involved silica suspensions which are weakly charged and unstable, which are in suspension with either polystyrene or metal oxide nanoparticles. These systems were chosen for the ability to easily control the electrostatic interaction between the particles by adjusting the pH. The silica microparticles are unstable near the IEP, which can easily be determined; the polystyrene particles are highly charged (either positive or negative) across the entire pH range, and the oxide nanoparticles are highly positively charged at low pH (when the silica is weakly charged). This allows for tuning the net interactions between microparticles and nanoparticles; both weak and strong interactions are possible, both repulsive and attractive.

The silica-based suspensions were previously used to investigate the nanoparticle haloing effect, as well as more recent studies that indicated that repulsive electrostatic forces result from

direct nanoparticle adsorption. Prior to these studies, there was very little research available in the literature that studied bidisperse systems of microparticles and nanoparticles where significant adsorption occurred. The goals of the following work are to clarify the adsorption behavior of the nanoparticles as well as to further understand the role the adsorption played in the stability of weakly (or negligibly charged) silica suspensions. Additionally, there have been very few studies where colloidal probe force measurements were performed in systems of adsorbing nanoparticles, and this work

1.3 Overview of chapters

This dissertation follows the manuscript format, in which the primary experimental work is presented in chapters as journal article manuscripts that either have been published in peer review journals, or will be submitted for future publication; therefore, Chapters 4 through 7 are co-authored by John Y. Walz. Chapters 2 and 3 give the background on the relevant topics and techniques that are utilized in the work presented in this dissertation, including a review of the literature in Chapter 2, and in Chapter 3 an overview of the AFM technique used in this dissertation.

Chapter 4 presents the initial investigations into the adsorption potential stabilizing effects of charged nanoparticles. The experiments use a model system of silica microparticles and charged polystyrene nanoparticles to explore the relationships between zeta potential, adsorption, and stability. These experiments indicate that stabilization is possible through direct adsorption of nanoparticles, but that the zeta potential is an insufficient measure of the potential effectiveness of the adsorbed particle layer. Chapter 5 continues the work with latex nanoparticles, and aims to clarify the effects that were initially observed. The resulting conclusions were that the adsorption of the nanoparticles merely reduced the flocculation rate, and that ultimately the nanoparticles were insufficient stabilizers.

Chapter 6 presents further stability work utilizing metal oxide nanoparticles, rather than latex nanoparticles. Zirconia and alumina nanoparticles were both used. The experiments involved the different measurements performed previously, including zeta potential, adsorption, stability, and colloidal probe force measurements. The findings in this chapter show that long term stabilization is achievable, as both the zirconia and alumina nanoparticles were observed to consistently and effectively prevent flocculation for the duration of the observation period.

Chapter 7 presents work focusing on the scaling of measured forces in systems of adsorbing nanoparticles. The unexpected results show that the apparent force lacks the scaling based on the colloidal probe radius that is predicted by the Derjaguin approximation.

Chapter 8 summarizes the results and overall conclusions from this dissertation, along with discussing the contributions to the field and recommendations for future work. Finally, a set of appendices are included, which contain additional experiments, data, and information on methods used in the body of the dissertation.

Chapter 2: Literature Review

2.1 Introduction

The field of colloid and interface science dates back to the 19th century. Early investigations of dispersed systems include the work of physicist Michael Faraday, who studied the effects of salt on gold suspensions. His experiments showed that added salt caused rapid destabilization of the gold particles and that particle detection was possible using focused light.[11]

The term "colloid" was first used by Thomas Graham in 1861. In a publication on liquid diffusion, Graham described two types of substances: crystalloids and colloids. He categorized crystalloids as a "volatile" class of substances with regards to diffusion. This category includes compounds such as salts and sugars which form crystals on their own but would readily diffuse through a membrane when dissolved in a solvent. In contrast a colloid was "fixed" and would not pass through the separation membrane, yet was able to still be dispersed in a fluid. Graham commented on the often gelatinous nature of hydrated colloidal suspensions, and listed materials such as various gums, tannins, and starches as possessing the "colloidal condition of matter".[12]

The modern definition can vary between sources, but the designation of a substance as a colloid is typically based on size. A colloidal particle is that which has at least one characteristic length that falls on the nano-scale between the molecular and macroscopic regimes, with a size range roughly spanning 10 Å to 1 μm.[11, 13] This size yields unique functionality due the high surface area to volume ratio of the particles. This is a size regime where the Brownian motion of the particles begins to dominate the gravitational sedimentation forces acting on the dispersed particles, such that dispersions of small particles can remain suspended indefinitely if aggregation is prevented.

Additionally, the substance is usually composed of two or more discrete phases, a dispersed (or colloidal) phase and the continuous phase, within which many different interactions, forces, and behaviors can be observed. These systems can arise both in nature as well as in manufactured systems. As such, the study of colloidal science often intersects with many different fields, ranging from physics, biology, and chemistry to manufacturing and environmental science.[13]

2.2 Colloidal forces and stability

The behavior of a colloidal system is typically defined by the cumulative forces acting between the dispersed particles. The most significant forces are the electrostatic force and van der Waals force, though other significant forces include depletion interactions, steric or polymeric forces, and hydrophobic forces.[11, 13-15]

2.2.1 Electrostatic double layer

At the interface of two phases, there is almost always an electric potential present.[15] One of the most common cases, and one that is very relevant to most colloidal systems, is the immersion of a particle or surface (including solids, liquids, micelles, polymers) in a liquid, where the a charge or electric potential is generated at the interface.[14, 15] This can occur by various means: the surface molecules or atoms can ionize or charge groups can dissociate, or ions that are present in the continuous phase can preferentially adsorb to the surface. However, these systems must follow the requirement of electroneutrality, and therefore any charges generated on the surface must be balanced by counterions in solution at the interface.

This behavior forms what is known as the "electrical-double layer". This was first observed by Helmholtz, in the mid-19th century.[16] The layers are composed of the fixed ions of the surface, and the more diffuse layer of counterions, as shown in Figure 2-1. This double-layer can be effectively treated as capacitors; however there have been many investigations and proposed models as to the exact structure of the double-layer.

One of the prominent models is the Gouy-Chapman theory, which was developed concurrently by the two researchers.[17, 18] The model improved on the understanding with the observation that the capacitance was not constant in the diffuse layer. The primary assumptions of the theory are that of an infinite flat surface, the ions are point charges uniformly spread over the surface, and that the solvent properties are uniform and independent of the surface. One of the limitations is that this model breaks down at high electrostatic charges. From this theory was developed the Poisson-Boltzmann equation to calculate the electrostatic potential as a function of distance from the charged surface. Further modifications include those by Stern who proposed that in addition to the diffuse layer of counterions there is an immobile layer directly fixed to the surface (Stern layer), and also by Grahame who proposed that it was possible for some ions to penetrate the Stern layer.[14]

The effects of the double layer are directly tied to the ionic strength of the solution. The electrostatic potential decays exponentially from the surface and the characteristic decay length is tied to the Debye length of the system (which is a function of ionic strength). As the quantity of ions in the system increases, the effective range of the charged surface is reduced as the additional ions screen the surface charge from the rest of the system. Furthermore, the type and valency of ion has an effect on the critical concentration of ions required to aggregate a suspension.[13]

2.2.2 Zeta potential

In charged colloidal systems, the exact determination of the surface potential or surface charge is quite difficult. Instead, the much more easily measured quantity known as the zeta potential is used. The zeta potential is the potential at the plane of shear, which is the distance from the surface at which the fluid molecules are not bound to the surface relative to the bulk solution. While not equal to the surface potential, the zeta potential is commonly used as an

approximate value, given the close proximity to the surface. Figure 2-1 shows a schematic of the charged double layer with corresponding potential curve indicating the location of the zeta potential. The zeta potential is typically measured using one of the different electrokinetic techniques. The most prominent techniques are electrophoresis and streaming potential, but others exist, including electro-osmosis.

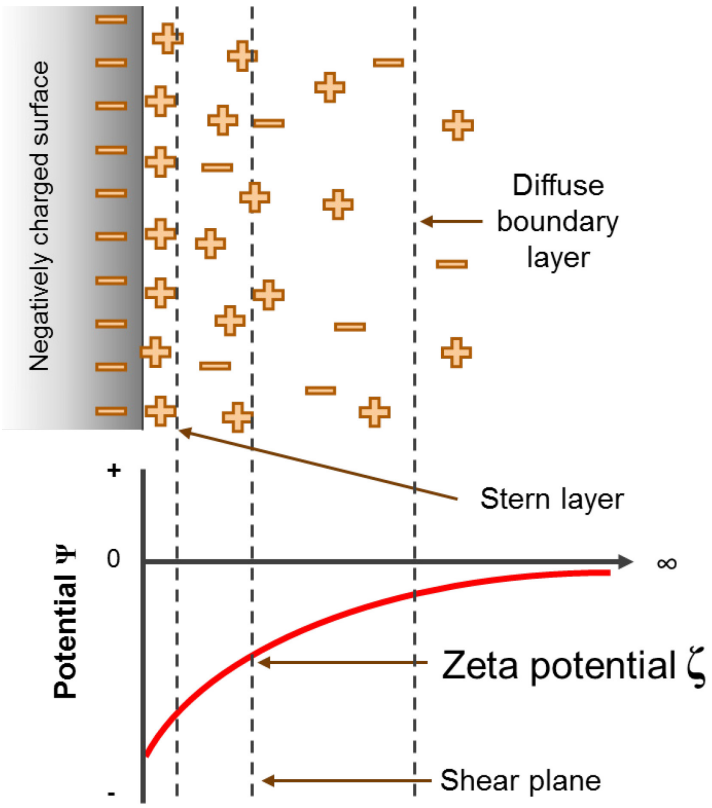

Figure 2-1: Schematic of the electrical double layer, with corresponding surfaces and zeta potential.

Electrophoresis is one of the earliest observed electrokinetic phenomena, with the first observations published by Ruess in 1809.[11] In those experiments, clay particles were observed to migrate based on the application of an electric field. The velocity of the particles was later related to the electrostatics and applied field by Helmholtz and Smoluchowski.[11] These measurements are quite straightforward and the zeta potential can be simply calculated using the particle velocity to determine the electrophoretic mobility. The velocity can be measured with various techniques; larger particles can be observed optically, while the potential of nano-scale particles can be determined using light scattering.

While electrophoresis applies an electric field to a stationary fluid and measures the velocity of particles, streaming potential can be used to measure the zeta potential of a stationary surface by flowing a fluid across the surface and measuring the induced potential.[19] This is useful for measuring large surface areas (e.g. slides or packed columns).

One of the primary drawbacks for using zeta potential to characterize the effective charge or predict the behavior of particles is that the measurement assumes that the surfaces are homogeneous. The measurements do not account for uneven or patchy charge distribution. It has been observed that suspensions where stability is predicted can still aggregate due to charge nonuniformity. This can cause fluctuations in the interaction energy at a given separation distance, as colloidal particles with uneven charge distribution move in solution, with the movement due to Brownian motion or fluid velocity.[20] Methods of characterizing the charge nonuniformity or zeta potential distribution is rotational electrophoresis which can also be combined with light scattering for improved practicality.[21, 22] However, the application of these techniques can be limited by the size of the particles as well as the extent and type of charge distribution.

2.2.3 Colloidal stability

The stability of a suspension can be discussed in terms of either kinetic or thermodynamic stability. Thermodynamic stability refers to a system that is at a minimum overall free energy. Micellar suspensions and macromolecular are the types of systems are typically dealt with in terms of thermodynamic stability, though colloidal crystal structures are also examples.[13] However, given that the dispersed phase often has inherent thermodynamic instability, discussions of colloidal stability predominantly refer to kinetic stability. In a kinetically stable system, the system is not at a free energy minimum, however the time required to reach this minimum is so large that the system essentially behaves as stable. In order to achieve this, there must be a significant *interaction energy* barrier, often occurring due to electrostatic forces as the van der Waals forces are usually strongly attractive at short separation distances. Without a repulsive barrier, the Brownian motion of the colloidal particles is sufficient to bring the surfaces into close contact and cause aggregation (or destabilization).

This approach is known as DLVO theory, and it states that the total interaction is can be reached by summing the attractive and repulsive interactions. The standard DLVO interactions are simply the double layer and van der Waals forces, which are assumed to be additive.[15] This was initially proposed by Derjaguin and Landau, and later through separate work by Verwey and Overbeek. Based on this approach, it is assumed that as the surfaces approach contact, there will always be an infinitely attractive interaction (due to the van der Waals, which is essentially independent of solution conditions such as ionic strength). In reality, it is assumed that a truly infinite attraction is not physically possible, however this can be dealt with in calculations simply with slight adjustments to the separation distance.[15] The shape of the rest of the curve results from the magnitude the double layer force which may be either attractive or repulsive. In a purely DLVO system, kinetic stability is achieved when the energy barrier is sufficiently large to prevent particles from approaching or reaching contact. Figure 2-2 shows a simple depiction of an energy barrier (ΔE) in a system with DLVO interaction. It is possible with the standard double layer and van der Waals forces to cause a secondary minimum as well at larger separations.

Given that the size and shape of the electrostatic barrier is what provides the stability in DLVO theory, being able to control the electrostatics is a way to control the aggregation. Many materials have a relatively fixed surface potential in a given solvent, however (as mentioned previously) the ionic strength can be used to greatly affect the range of the electrostatic force. Increasing the ionic strength to the critical coagulation concentration lowers the energy barrier to the point where the energy of the particles can easily overcome the barrier. Additionally, materials such as metal oxides can be sensitive to pH, as the surface charge is sensitive to the bulk hydrogen ion concentration. The surfaces typically are dominated by hydroxyl groups and the hydrogen dissociates at high pH leaving a negative charged. Increasing the H^+ concentration (lower pH) pushes the zeta potential towards the positive. The isoelectric point is where the surface is effectively neutral (i.e. equal number of positive and negative charge sites) and is likely to allow aggregation; therefore a careful adjustment of the pH can either stabilize or flocculate a system.

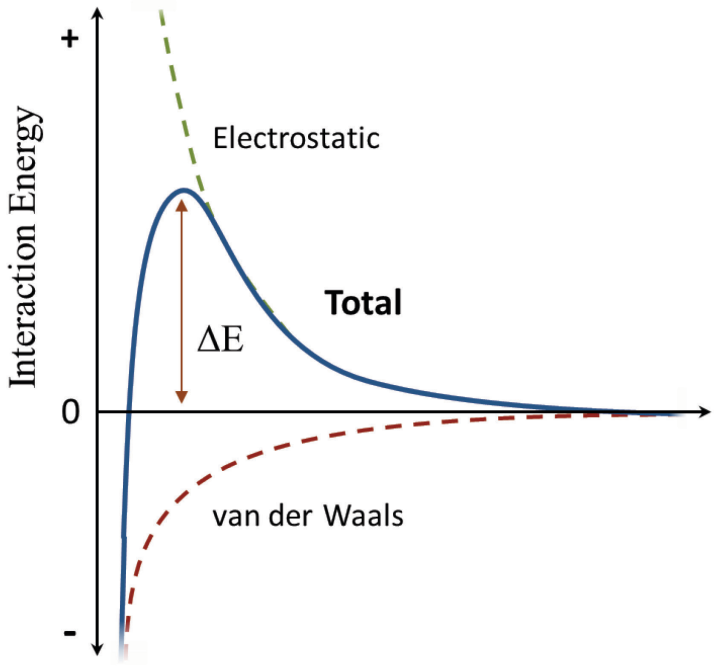

Figure 2-2: Simple schematic of DLVO energy barrier.

2.2.4 van der Waals forces

In general, it can be assumed that there is always a component of the overall force due to the van der Waals interaction. This interaction effectively the sum of the molecular interactions, which arise due to dipoles of interacting molecules (dipoles can either be permanent or induced by other dipoles). The "classical" theoretical approach forms the basis Hamaker theory, which separates the interaction into two parts: a purely geometrical equation, and a constant *A* (now known as the Hamaker constant) which is dependent on the number of interacting atoms and the coefficient from the pair potential between two interacting atoms.[14, 23]

A different approach, termed Lifshitz theory, can be used as well. It is a more "macroscopic", or continuum, approach based on the electromagnetic properties of the system.[15, 24] This method incorporates many-body effects of the system, and can be applied to systems with retardation effects as well as various geometries including multilayered surfaces, spheres, and cylinders.[24, 25] The van der Waals interaction energy per unit area, E_{vdW}, between two surfaces can be calculated by using a modified Hamaker-like term, $A(l)$, as a function of the separation distance l, which is shown in.[24] $A(l)$ is a function of material and dielectric properties of the interacting materials and medium and is given in the literature.[26-28] One of the primary drawbacks from this procedure is the necessity of obtaining dielectric spectral information, the availability of which is limited to a relatively small selection of materials.

Generally, the net van der Waals interaction is attractive; however certain conditions can lead to repulsive van der Waals forces. This can occur in systems with highly dissimilar surfaces separated by a non-polar medium. Examples of repulsive systems are the interaction between PTFE and materials such as alumina, silica, or gold.[29, 30] These surfaces are attractive in intervening media such as air or polar solvents; however in non-polar solvents such cyclohexane, the force is repulsive. These interactions have quantitatively predicted by multiple researchers, and when using either Hamaker theory or Lifshitz theory, the calculated interaction is repulsive (e.g. results in negative Hamaker constants). These interactions have been confirmed with colloidal probe force measurements and exhibit a high degree of agreement with the theoretical predictions.[29, 30]

2.2.5 Steric forces

Steric stabilization typically occurs through the use of polymer chains which can be adsorbed, grafted, or otherwise attached to the surface of the dispersed particles.[31-35] This interaction has stabilized suspensions such as inks and paints as far back as the ancient Egyptians, and naturally occurring environmental colloids often have a steric organic layer adsorbed.[15, 36] The polymer chains extend away from the particle surface and physically inhibit the particles from approaching other particles close enough to be in the range of the van der Waals attraction. In order for polymers to be effective steric stabilizers, it is necessary for the thickness of the polymer layer to be greater than the interaction range of the attractive forces between the particles in solution. The necessary thickness will vary, but for some materials, such as heavy metals, this may require polymer layer thicknesses on the order of the particle size itself.[34] The most effective stabilization occurs when the molecules extend perpendicular to the surface, such as block copolymers that have one segment that strongly adsorbs, while the other segment has a high affinity for the continuous phase.[15] The diversity of available polymers allows for customization of the surface, with different combinations of polymer blocks leading to different levels of stability, such as by combining polymers that attach strongly to the particle surfaces with long chains that provide steric repulsion.[33] The polymer adsorption must be controlled, as adverse effects such as bridging flocculation can occur when a polymer chains

adsorb to more than one particle simultaneously.[37] Ultimately, steric effects on stabilization are most effective when coupled with electrostatic repulsion.[31, 32]

Sterically stabilized colloids can be created *in situ*, in which the colloidal particles themselves are grown or formed in an environment that already contains the stabilizer. Alternately, the stabilizer can be added to already formed dispersions; this requires some level of initial stability in order for the individual particles to be properly coated with polymer.[36] The molecular weight and concentration of a polymer is usually related to how effective it is as a stabilizer. At lower concentrations, polymers tend to promote bridging flocculation, reducing the stability, and in this regime it has been shown to have little dependence on molecular weight. In general, once the concentration has increased to where stabilization occurs, higher molecular weight polymers are more effective stabilizers at a given polymer fraction.[38]

The drawback of steric stabilization is that significant modification to the particles is sometimes required. The stabilizers must be strongly anchored to the colloidal particle in order to be fully effective. Without sufficient attachment, the molecules can migrate across the surface (which is reduced with a fully coated surface) or can even desorb.[36] Directly altering the surfaces can significantly affect the properties and behavior of the dispersion, potentially reducing the performance or usefulness of the suspension in the desired application. Additionally, these modifications can be difficult to reverse. To avoid these complications, it is desirable to develop stabilization methods that do not directly alter the properties of the unstable particles and allow for reversible control of stability. Whether it is with the addition of macromolecules, polyelectrolytes, nanoparticles, or even other microparticles, the behavior and stability of these suspensions can be significantly altered through specific interactions between the distinct colloidal species[38-42], either to provide stability or to induce flocculation.

2.2.6 Depletion and structural forces

An area of particular interest since the early 20th century is the depletion force, which occurs in multi-particle systems containing some particles (or other solute) that are much smaller than others. The first publications on this force were focused on concentrating rubber latex suspensions through “creaming”, where negatively adsorbing polymer was added to induce flocculation and separating the rubber from the suspending liquid.[43] This mechanism was not completely described until the 1950s, when Asakura and Oosawa produced the first depletion model.[44, 45] The depletion force occurs in systems of larger particles dispersed with smaller charged “depletants”, such as small particles, polymer, or macromolecules which are repelled from the surface of the larger particles. Depletion attraction occurs when two of the larger approaching surfaces in suspensions of depletants exclude the smaller particles from the gap between surfaces. This results in an osmotic pressure differential between the gap and the bulk, which can produce a net attractive force between the two otherwise repulsive surfaces. This produces an energy well at a given separation which can be deep enough to result in flocculation. As such, if there was no repulsion between depletant and the larger colloidal surfaces, the exclusion does not occur and the force is not present.[46, 47]

In terms of concentration dependence, the added depletants have no effect on the colloidal stability until a critical flocculation concentration is reached. The attractive depletion force increases with the concentration until the concentration is large enough to result in a long range oscillatory force.[48, 49] These forces are due to the ordering or structuring of the high concentrations depletants in the gap region. This can effectively restabilize the system, which is sometimes referred to "depletion stabilization".[50] This type of stabilization results entirely from free or negatively adsorbing species, in contrast to steric stabilization, which relies on direct adsorption or attachment of the stabilizers.

2.2.7 Nanoparticle haloing

A recently discovered phenomenon in colloidal stability is the "nanoparticle halo", which was first described by Tohver et al.[8, 35, 51-58] The basic principle is that larger weakly charged microparticles in suspension with highly charged nanoparticles (both are of like charge), there is sufficient electrostatic repulsion to prevent nanoparticle adsorption, yet a van der Waals or other attractive force is sufficient to attract the nanoparticles to relatively short separation distances. In systems that were explored both experimentally and through simulations, it was shown that this allows a small energy well to develop a short distance from the weakly-charged microparticle surfaces which are in suspension with the highly charged nanoparticles. The nanoparticles then can form a highly-charged "halo" around the microparticle, which could essentially stabilize the microparticles. The key feature of this interaction is that the nanoparticles are not in direct contact with the surface, but are essentially adsorbed a short distance (on the order of a Debye length[59]) from the surface.

Nanoparticle halos have been reported in various micro-nanoparticle systems including alumina-ceria,[52] silica-zirconia,[60] and silica-polystyrene[55]. Various experimental methods were used, including measuring the sedimentation velocity, and confocal microscopy of settled particles to observe packing structures, as well as numerical studies of the interaction energies. Ultra-small x-ray scattering was to determine a microparticle-nanoparticle separation distance of 2.15 nm for a silica-zirconia system; this compared to a solution Debye length of 1.8 nm at pH 1.5.[54] Other researchers have used colloidal probe AFM to investigate this mechanism. Force measurements between silica surfaces in increasing concentrations of zirconia nanoparticles indicated a transition between purely attractive and purely repulsive forces occurred at a volume fraction of 10^{-5}. Additionally, a small peak at approximately 2.3 nm separation was observed at this concentration, which was attributed to the distance that the nanoparticles were separated from the surface.[61] These studies indicated that the nanoparticles prevented flocculation of the microparticles, that they formed an electrostatically charged layer at a non-zero separation distance, and that this was due to small energy wells.

Additionally, a similar behavior has been predicted in three-particle systems of micron, submicron, and nanoparticles in a computational study.[62] In this system, the nanoparticles produce a depletion attraction between the micron and submicron particles with an energy well at non-zero separation distances. This attraction is predicted to be sufficient to hold the submicron

particles in a halo around the microparticles. Additional long range features in the calculated particle distribution were predicted, although they have not been experimentally investigated.

2.2.8 Nanoparticle adsorption

In contrast to the nanoparticle haloing, other researchers have concluded that repulsive interactions resulting from charged nanoparticles are due to the direct adsorption of the particles onto the weakly charged surface. Monte Carlo simulations by Trulsson and coworkers have demonstrated that even in the case of a weak repulsion between silica spheres and zirconia nanoparticles (which was the system previously predicted to allow a halo to form), the nanoparticles will adsorb to the silica and produce a purely electrostatic stabilization.[59] One interesting detail that the authors discussed was that in the weakly repulsive system a charge-regulation occurs and the highly positive zirconia nanoparticles actually induce a deprotonation of the silanol groups on the surface of the weakly positive silica. This leads to the silica surface becoming weakly negatively charged, and thus being attractive to the zirconia, which then leads to direct adsorption of the nanoparticles.

Experimentally, McKee and Walz investigated the forces present between glass surfaces interacting in suspensions of either zirconia or polystyrene nanoparticles. With the zirconia, experiments were done at pH 1.5 (weakly positive glass and highly positive zirconia), and the results provided further evidence of direct adsorption. AFM images of the surface in the presence of the nanoparticle solution showed distinct protrusions from the surface with sizes comparable to the size of the nanoparticles (compared to the very smooth images with no nanoparticles present), and the authors concluded this would only occur in the event of strong adsorption on the glass surface. Additional force measurements indicated increasingly repulsive forces as the nanoparticle concentrations increased. The forces were measured both where the glass was effectively uncharged, as well as weakly like-charged (positive for the zirconia, negative for the polystyrene).

Further force measurement work by Ji et al. showed that in systems of silica and negatively charged polystyrene latex, the repulsive forces due to nanoparticle adsorption were largely irreversible.[63] Force profiles were measured before and after the introduction of nanoparticles, as well as after the nanoparticles were rinsed from the system. These showed that while the nanoparticles increased the total force upon introduction, the force remained virtually unchanged after the nanoparticle solution was flushed from the cell. Additionally, direct imaging of silica surfaces that had been exposed to the polystyrene were imaged (using SEM) and showed that a significant number of particles remained attached to the surfaces. From the force measurements, a charge density was determined and converted to an approximate number of particles per square micrometer; these values were in reasonable agreement with the approximate number density of adsorbed particles observed in the SEM images. The authors concluded that even a relatively small number density could have a significant effect on the total force.[63]

2.3 Measurement of colloidal and surface forces

Given the importance that colloidal forces have on stability and particle or surface interactions, different methods of experimentally measuring these forces have been developed. Some of the earliest force measurements were carried out by Overbeek and Sparnaay, in which experiments were conducted using flat glass and quartz plates in air.[64] The forces were calculated from the bending of a stiff spring, determined using the electric capacity method with an accuracy of about 10 Å. These experiments were used to investigate long range attractive forces, and Hamaker constants were calculated for the different systems, though at short separations dust or surface roughness caused significant difficulties. This experimental setup was later used to measure interactions between metal plates, such as chromium.[65]

Experiments by Derjaguin and co-workers were performed to measure repulsive as well as attractive forces between metal filaments in liquid environments.[66] Platinum filaments were used in various electrolytic solutions (including potassium chloride, magnesium sulfide, and butyric acid). The filaments were polarized and the force was measured while moving one filament using a potentiometer attached to the second. These measurements indicated the presence of non-electrostatic repulsion due to films on the filaments in addition to repulsive electrostatic forces. Further measurements were done with gold filaments at the point of zero charge and Hamaker constants were determined.

In order to effectively measure interactions at very small separation distances, the surface forces apparatus (SFA) was developed.[67] The technique was first described in 1968 by Tabor and Winterton, where the van der Waals interactions were measured between two crossed cylinders of mica in air. The movement of the surfaces was controlled by a piezoelectric transducer, the separation distances were determined using multiple beam interferometry, and the force was calculated from the deflection of a spring. This method was capable of operating at separation distances as small as 5-30 nm with accuracy of 0.3 nm.[68]

The SFA technique was further modified by Israelachvilli and Tabor, reducing the separation to 1.5 nm.[69] Different measurement methods included the “jump method” for short separations as well as the “resonance method” using oscillatory measurements at known frequencies for larger separations. Additional measurements between monolayer coatings on the mica cylinders were performed.[70] Subsequent iterations of the device allowed for measurements to be carried out in liquid systems, and the addition of lateral movement strain gauges made possible the measurement of friction in various conditions. In the following years, many modifications and attachments have been implemented, permitting a very wide variety of measurements. Currently, separation distances less than 1 Å can be resolved, equilibrium and dynamic experiments can be made even in biological or electrochemical systems, and the measurements can be simultaneously performed with techniques such as x-ray scattering and IR spectroscopy on a single sample.[70]

The development of the technique known as total internal reflection microscopy (TIRM) allowed for the measurement of forces between microscopic surfaces.[71, 72] Using TIRM, the

forces and interactions can be measured between a single colloidal particle and a flat, transparent plate. One of the primary advantages of TIRM is that the method is non-invasive. This method utilizes an evanescent light wave, which is reflected off the plate (at an angle where total reflection occurs) and illuminates a colloidal particle. The light scattered from the particle then can be used to determine the instantaneous separation distance between the particle and plate which, due to Brownian motion of the particle, is constantly fluctuating. Statistical analysis of a large number of separation measurements can then be used to form a probability density function, which can be converted to the interaction potential energy using the Boltzmann equation. The scattering intensity is very sensitive to the separation distance, allowing for nanometer-scale resolution.[71] To prevent migration around the surface, the particle can be effectively trapped in the sampling area using optical radiation pressure without affecting the measured energy profiles.[73]

TIRM can be used to measure van der Waals, electrostatic, and even gravitational forces, but it is particularly useful for measuring the depletion force, as the technique can measure depletion attractions with much greater sensitivity than other methods, including SFA.[71] Walz and coworkers have measured depletion interactions with a charged polystyrene particle in suspensions of charged silica nanoparticles as well as in the presence of surfactant micelles.[73, 74] The high degree of sensitivity allowed for the detection of depletion forces with as little as 0.02% vol. micelles at separation distances greater than 100 nm. Forces as small as 0.01 pN can be detected with this technique however other methods may be more appropriate for the stronger forces such as adhesion.[71]

Other less common force measurement techniques between colloidal particles (rather than macroscopic surfaces) include the osmotic stress method[75] and colloidal particle scattering[76]. The osmotic stress method relies on using osmotic pressure to control the structure of colloidal dispersions, which is characterized using x-ray diffraction. The particle interactions are described in terms of pressure versus distance curves.[77] The colloidal particle scattering technique is a dynamic method that characterizes individual collisions between two particles in solution, and by determining the particle positions before and after colliding the position data can be fitted to trajectory equation to determine the interaction forces as a function of separation distance.[76]

Finally, one of the most common colloidal force techniques is colloidal probe atomic force microscopy (and which is used experimentally in this dissertation) will be discussed in more detail in the following chapter.

Chapter 3: AFM Force Measurements and Technique

3.1 Introduction and background

The atomic force microscope was developed in 1986 by Binnig, Quate, and Gerber.[78] The instrument effectively combines the function of a scanning tunneling microscope and a stylus profilometer, and allows for sub-nanometer scale imaging and investigation of surfaces. Imaging is carried out by monitoring the deflection of a cantilever tip across a surface and typically relies on short-range repulsive forces (Born repulsion) to provide image contrast.[77] In addition to imaging, the AFM is naturally suited to measuring surface forces, as the cantilever tips can be functionalized to perform measurements between a variety of materials or even single molecules.[79] The force experiments in this dissertation (Chapters 6, and 7) utilize the technique of colloidal-probe atomic force microscopy (CP-AFM) in which a colloidal microsphere is attached to an AFM cantilever, allowing for highly sensitive force measurements between an even wider variety of surfaces and in various fluid environments.[80]

CP-AFM measurements have been used to measure many different colloidal forces, including DLVO interactions[81, 82], steric forces[83], depletion and structural forces[84-86], adhesion forces[87-89], hydrodynamics[90], and friction[91-93]. Early measurements by Ducker et al. included silica sphere-silica plate interactions as a function of pH and salt concentration, as well as gold coated surfaces[80, 94]. The measurements can be carried out at low enough velocities to avoid hydrodynamic contributions to the force. The silica measurements showed very close agreement with predicted DLVO interactions at separation distances greater than 2-3 nm. The measured decay lengths were consistent with predictions and demonstrated a high level of precision and reproducibility.

Non-DLVO forces, including steric, depletion, and adhesion interactions, can also be measured. In the case of polymer adsorption, these forces can be present more than 200 nm from the surface, with the increased range attributed to compression of the polymer layer.[83] Depletion forces are easily measured between surfaces in various suspensions, including nanoparticles and micelles, with good agreement to theoretical predictions, and can clearly show oscillatory structural interactions.[84, 85] Finally, adhesion measurements focus on the force required to remove the colloidal probe from surface contact. The contact time and applied forces can be controlled before measuring the maximum force required to withdraw the cantilever from the surface. This dissertation contains further discussion and experiments on DLVO, steric, depletion and adhesion (either the main experiments or in the appendices).

Occasionally, particularly in the case of non-DLVO forces, it can become difficult to determine the zero-separation point from the raw force data. In these cases, a more precise determination of the separation distance can be achieved when CP-AFM is used in conjunction with additional independent methods, including evanescent wave measurements.[95] This is most important when comparing different systems. However even without the additional

measurement, the CP-AFM data can still be useful in understanding the stability of a dispersion, as an absolute value for contact is not required for evaluating a single system.[77]

3.2 AFM force measurements

The basic components of an AFM are shown in Figure 3-1. The sample surface is typically mounted on an XY scanner, and the cantilever is attached to a piezoelectric translator, which can precisely control the cantilever position. Cantilevers usually have a sharp tip with a nanometer-scale radius for better imaging resolution, though they may have other surfaces mounted or even be tip-less. A laser beam is directed onto the cantilever reflected onto a photo-detector, which is used to determine the deflection of the cantilever.

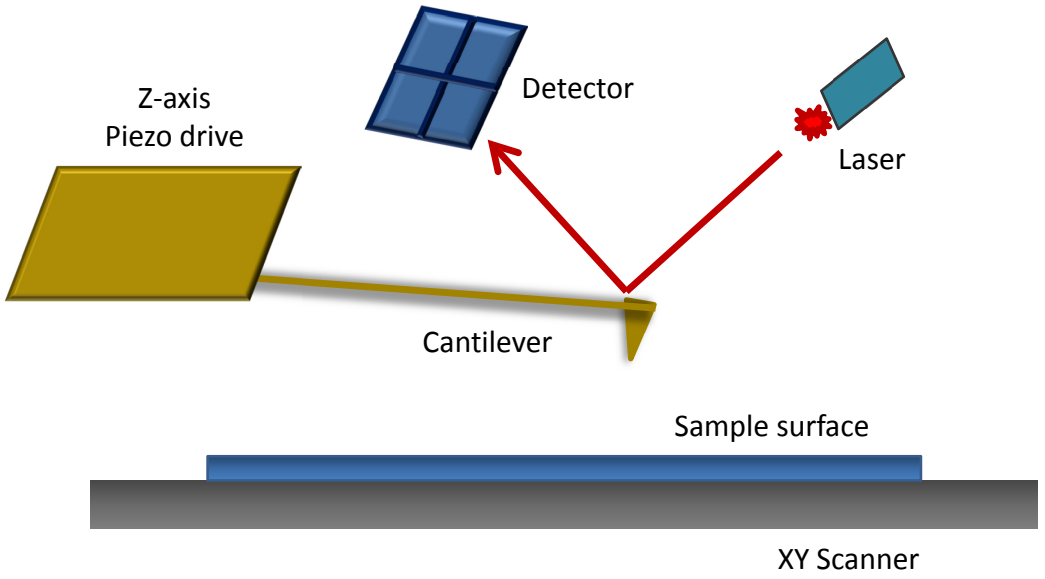

Figure 3-1: Simple schematic of an AFM.

Imaging of a surface can be done by applying a force to the cantilever and scanning it across a surface. Through a feedback loop, the instrument maintains a constant force by adjusting the height of the cantilever via the piezo drive. The surface image can be produced from the measured deflection of the cantilever as well as from the recorded height position of the piezo.[77] This method is typically referred to as "contact mode" imaging; however images may be taken in "tapping mode", which is useful for more delicate surfaces. In tapping mode, the cantilever is vibrated at its resonance frequency while scanning across a surface (without making contact). Surface features cause deviations in the vibration, which is then used to produce an image.

Force measurements with an AFM are simply done by driving the cantilever to the sample surface while measuring the deflection as the cantilever approaches and withdraws. The linear spring constant of the cantilever, which is needed to relate deflection to force, can be

obtained from the frequency of the thermal vibrations of the cantilever.[96] Equation 3.1 shows the relationship between the spring constant k and the thermal vibrations in the form of the mean square deflection of a freely vibrating cantilever, $\langle \Delta Z_c^2 \rangle$.

$$k = \frac{k_B T}{\langle Z_c^2 \rangle} \tag{3.1}$$

Here, k_B is the Boltzmann constant, and T is the temperature. The quantity $\langle \Delta Z_c^2 \rangle$ is equal to the integral of the primary resonant frequency (the area under the peak). The instrument software contains functions that allow for quick determination of the resonant frequency, from which the spring constant can then be calculated.

3.2.1 Colloidal probe preparation

To better mimic the interaction of specific surfaces, the technique of CP-AFM was developed in 1991.[77, 80, 94] This technique utilizes a colloidal microspheres ("probe") that is attached to the end of a cantilever. This provides a custom surface instead of the standard tip, which can be easily characterized for more accurate measurements. The probes can be functionalized further either before or after being attached to a cantilever. Depending on the desired application, the probes can be attached by glue, through sintering, or even through adsorption.[77] A schematic of the "colloidal probe mount", used to glue a microsphere to a cantilever for the experiments in this dissertation, is shown in Figure 3-2.

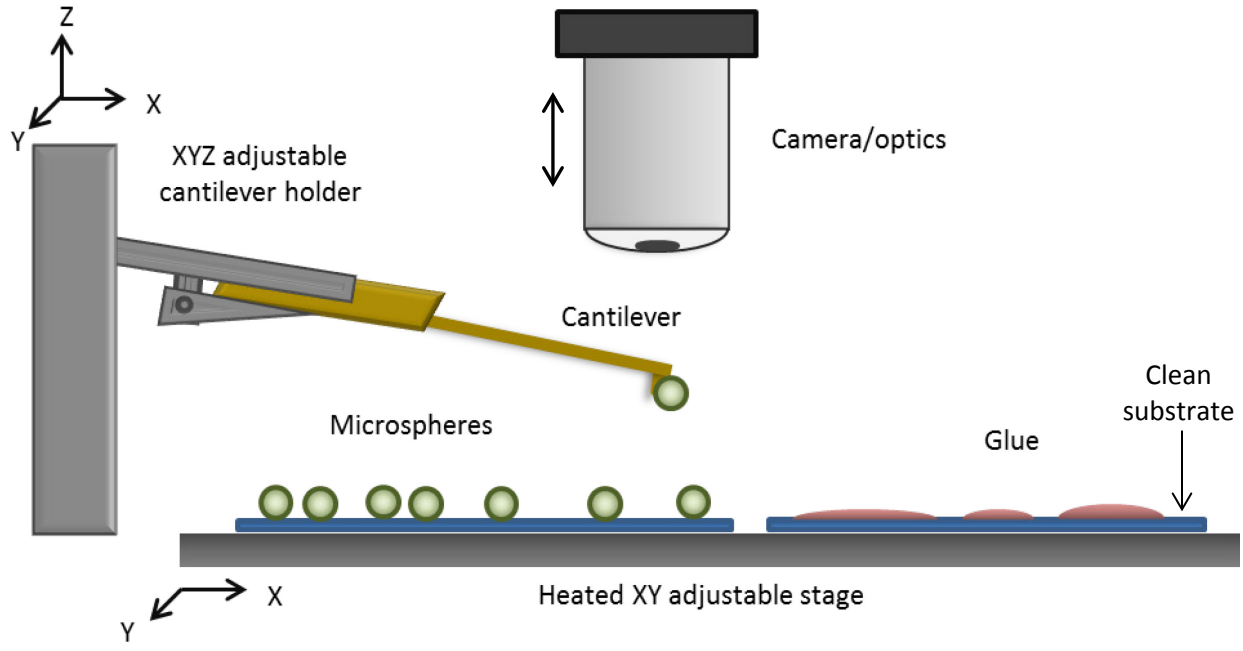

Figure 3-2: Schematic of the colloidal probe mounting apparatus used for mounting microspheres to AFM cantilevers.

To glue a microsphere, a cantilever is loaded into the holder. Two clean substrates are used and one dusted with microspheres, the other with glue. The cantilever is positioned over, and then dipped in, the desired adhesive (typically epoxy that is either heat-setting or UV-curable), before being moved to a region with spheres. The cantilever is gently lowered to pick up a single sphere. Once set, the cantilever (with sphere) is cleaned in a UV-ozone cleaner. Figure 3-3 shows an SEM image of a cantilever with attached colloidal probe. The cantilever shown has an approximately 3 μm pyramidal tip, which has no effect on the measurements, provided the probe is larger than the tip. Tip-less cantilevers can be used in situations where smaller spheres are desired.

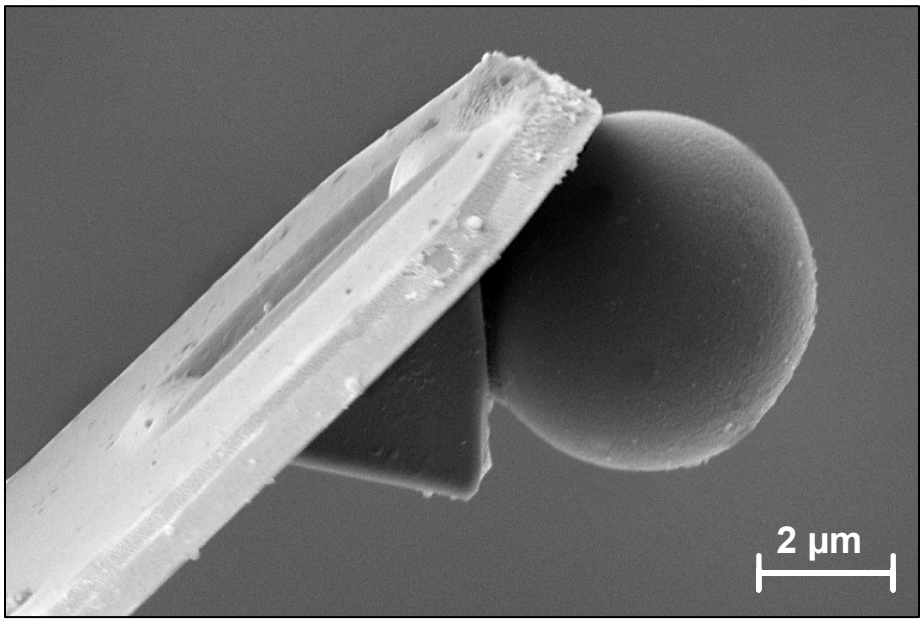

Figure 3-3: SEM micrograph of cantilever with attached spherical probe.

The surface clean sphere is then imaged using a reverse tip grating, which consists of an array of nano-scale tips arranged on a surface. The standard imaging procedure is used, with the grating acting as scanning probe, with the mounted sphere as the surface being imaged. Figure 3-4 shows a 3D contour image of a 5 μm silica sphere. The primary image of the sphere is in the center, and the clipped portions along the edges of the image are simply repetitions of the same sphere (because the grating has an array of tips, when imaging a single sphere the instrument produces an array of images of the sphere surface). These images can be flattened using the AFM software, and from the flattened image the probe roughness can be assessed. For the experiments in the following chapters, only spheres with an RMS roughness of less than 1 nm were used (typically the spheres were in the range of 600-800 pm roughness).

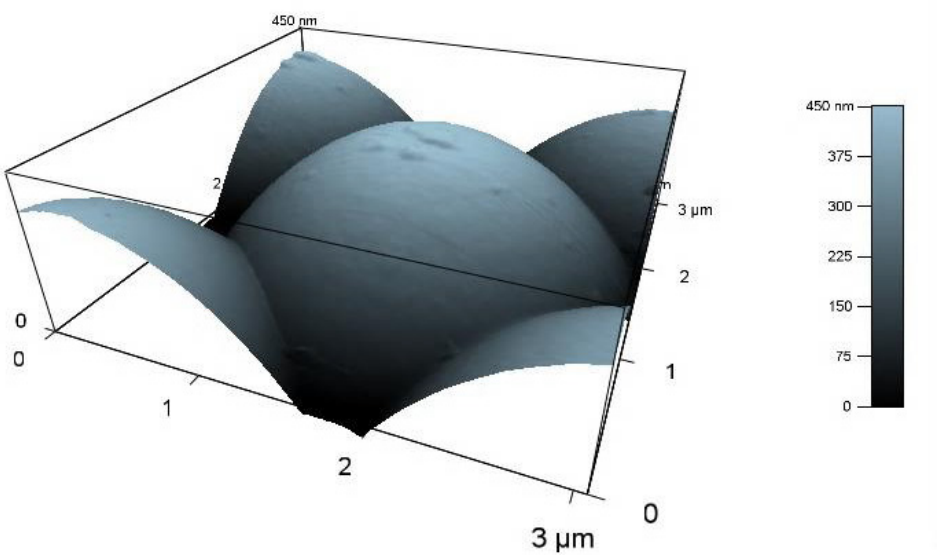

Figure 3-4: 3D AFM image of a 5 µm silica sphere that has been mounted on a cantilever. Small asperities are visible on the surface.

The final step before a force measurement is to determine the spring constant of the cantilever with the attached sphere. CP-AFM measurements then proceed identically to standard force measurements.

3.2.2 AFM Data Analysis

The raw data curves, as recorded by the instrument, are in terms of cantilever deflection (volts) vs. the piezo drive (nm). Figure 3-5 shows a single raw data curve, which is in terms of arbitrary deflection and position of the piezo. The data is divided into three regions. The region at large separation distances, where it can be assumed that there are no surface interactions, is considered to be zero deflection at low drive velocities. The interaction region is the range of separation where the colloidal interactions of interest occur. The constant compliance region is where the tip or probe is in contact with the sample surface and has a linear relationship between the deflection of the cantilever and position of the piezo.

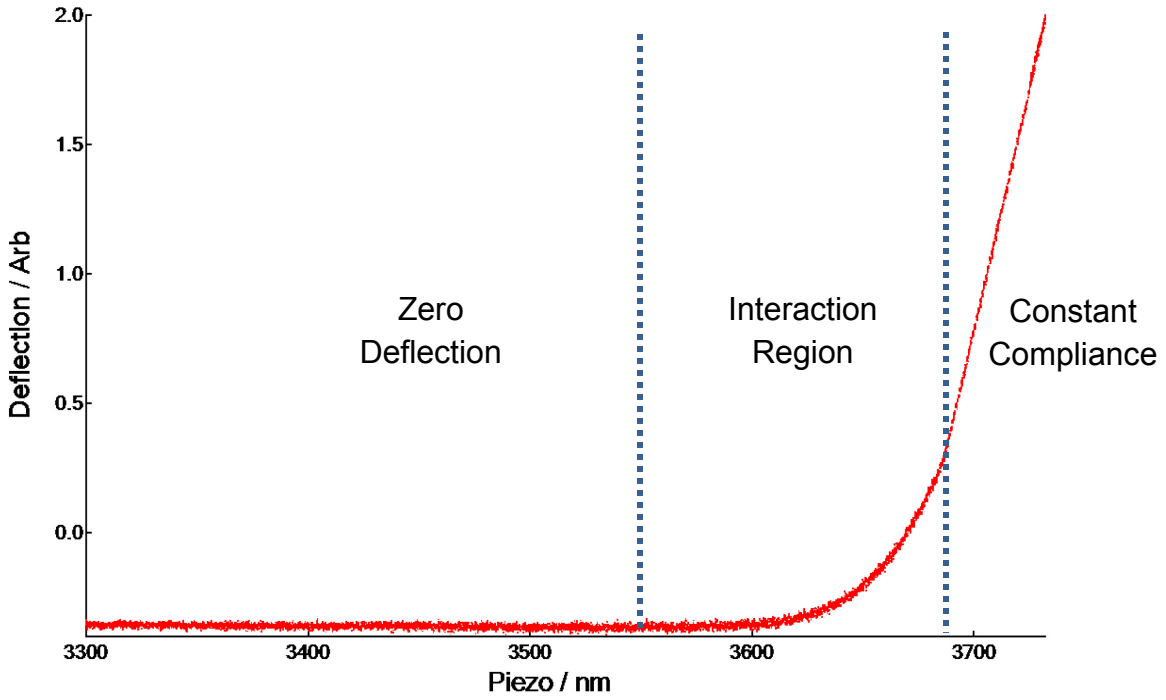

Figure 3-5: Raw data curve from AFM. The three important regions are designated.

The constant compliance region is used to convert the deflection vs. drive data into force vs. separation. Equation 3.2 defines the optical lever sensitivity (OLS), which is the ratio of the deflection to the drive distance, and is equal to the slope of the constant compliance region.

$$OLS = \frac{dDefl\ (V)}{dDrive\ (nm)} \tag{3.2}$$

The underlying assumption is that in the constant compliance region the two hard surfaces are in hard contact and therefore the distance the piezo drives the cantilever is equal to the distance the cantilever deflects.[94]

$$\frac{dDefl\ (nm)}{dDrive\ (nm)} = 1 \tag{3.3}$$

With the constant compliance assumption, we can take the inverse OLS (invOLS) and use it to convert the measured deflection (in volts) to deflection in nanometers.

$$Defl(nm) = invOLS \times Defl(V) \tag{3.4}$$

To complete the conversion to absolute deflection, the average value of the deflection in the "zero deflection" region is subtracted from the entire curve.

Finally, the separation distance h of the colloidal probe from the surface is simply defined by the sum of the deflection, drive, and arbitrary initial starting separation, h_0 (Equation 3.5). The deflection and drive are known, and h_0 is found by setting h=0 within the constant compliance region (hard contact).

$$h = Defl + Drive + h_0 \tag{3.5}$$

The force is simply determined from the deflection using the spring constant and the deflection, using Hooke's Law ($f = kx$) with x as the deflection. A single converted force curve is shown in Figure 3-6.

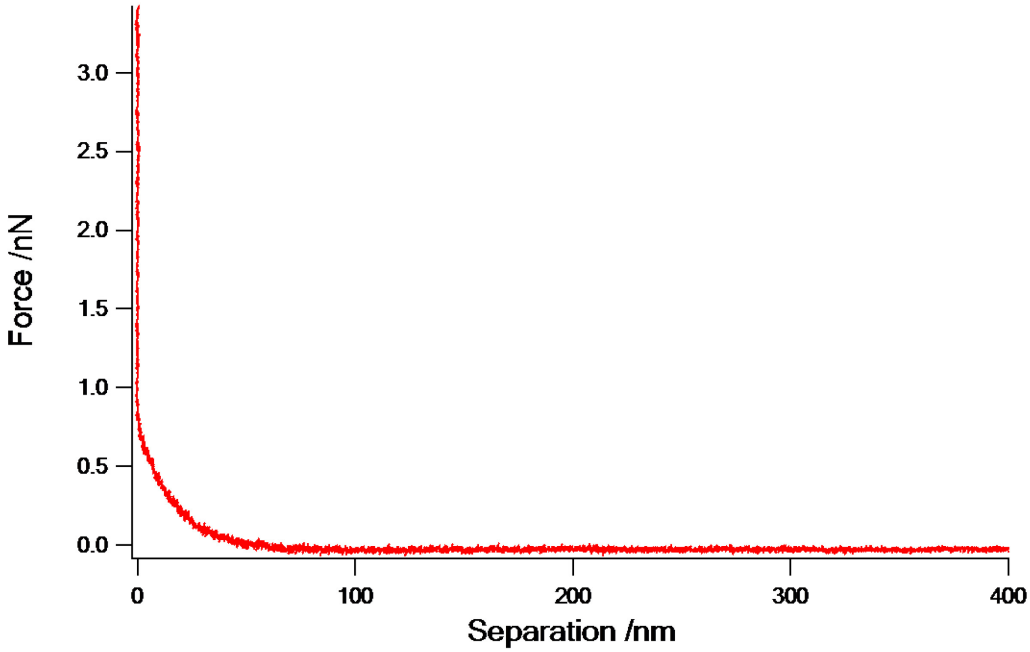

Figure 3-6: Final individual force curve.

Multiple such curves from a single sample measurement are typically averaged together into the final curve. The averaging procedure consists of dividing the curve into bins of varying size (e.g. smaller, <1 nm, bins for the interaction region to preserve fine details in the measured forces, larger bins for the zero deflection region) and averaging the bins into single points at a given separation. Once the force curves are averaged into a single measurement, any signal drift (or "virtual deflection", which is a steady change in the deflection signal that is not due to the measured surface forces) is removed from the curve by fitting a linear equation to the data at large separations (the zero force region) and subtracting the resulting equation from the overall curve.

Chapter 4: Nanoparticle Adsorption and Stability in Binary Colloidal Suspensions

This chapter consists of work that has been published. Reprinted with permission from: D. Herman, J.Y. Walz, Stabilization of weakly charged microparticles using highly charged nanoparticles. Langmuir, 2013. ***29****, 5982-5994.*

Experimental studies were performed to understand the ability of highly-charged nanoparticles to stabilize weakly-charged microsphere dispersions. The experiments involved adding either anionic (sulfate) or cationic (amidine) latex nanoparticles to dispersions of micron-sized silica spheres near the silica IEP. Although both nanoparticles increased the zeta potential of the microspheres above the value at which the silica-only dispersions were stable, only the amidine/silica dispersions were stable. Adsorption tests on silica slides indicated that amidine nanoparticles deposited more densely than sulfate nanoparticles, producing multi-layer surface coverage. Calculated DLVO energy profiles between nanoparticle-coated microspheres predicted stability for both systems. It is hypothesized that the relatively low coverage of the sulfate nanoparticles (≤25%) led to bare silica patches on the microspheres that could align during interaction due to Brownian motion. This indicates highly-charged nanoparticles can be effective stabilizers, provided sufficient levels of adsorption, and that zeta potential alone is insufficient for predicting coated microsphere stability.

4.1 Introduction and background

The impact of charged nanoparticles on the stability of a dispersion of colloidal 'microparticles' has been studied by several different groups. In 1997, Sharma et al. showed that negatively-charged silica nanoparticles added to an aqueous dispersion of negatively-charged polystyrene latex particles (approximately 0.5 and 1.0 μm in diameter) could induce flocculation at nanoparticle concentrations above approximately 2% vol.[39] The mechanism proposed was long range attractive depletion forces that created secondary energy wells (beyond the range of repulsive electrostatic forces between the charged latex particles). At nanoparticle concentrations above roughly 5% vol., the flocculation was no longer observed, which the authors postulated was due to the development of longer range structural forces caused by the layering of the free nanoparticles in the gap region. These structural forces, which are caused by repulsive interactions between the nanoparticles themselves, have been studied in great detail by numerous researchers.[41, 48, 49, 97-101] The critical flocculation and restabilization concentrations observed experimentally by Sharma et al. were consistent with predictions made using a force-balance model developed earlier by Walz and Sharma[47].

Several years later, the phenomenon of nanoparticle halos was proposed by Tohver et al. to explain some interesting stability behavior of a dispersion of weakly-charged silica particles.[8] Specifically, when highly positively-charged zirconia nanoparticles (6 nm in

diameter) were added at low concentrations (as low as 10^{-4} vol. fraction) to a dispersion of 0.570 or 1.18 μm diameter silica particles at pH 1.5 (slightly below the IEP of silica), gelation of the system was arrested. At higher nanoparticle concentrations, a re-entrant gelation concentration was noted.

Tohver et al. proposed that the strong electrostatic repulsion between the nanoparticles themselves, coupled with the weak repulsion between the nanoparticles and silica microparticles, led to the formation of a halo of nanoparticles around the microparticles. A key feature of this halo, which distinguished it from simple deposition, was that the nanoparticles were kept a fine distance from the microparticle surfaces by short-range electrostatic repulsion, a hypothesis that was supported by subsequent ultra-small angle X-ray scattering studies by Zhang et al.[54] Tohver et al. postulated that the re-entrant gelation observed at higher nanoparticle concentrations arose from attractive depletion forces between the microparticle/nanoparticle complexes caused by excess zirconia nanoparticles in solution.

This formation of a nanoparticle halo was later supported by Monte Carlo simulations of Luijten and coworkers, who suggested that in addition to the nanoparticle-nanoparticle repulsion, attractive forces between the microparticles and nanoparticles could also play a role in the formation of the halos.[35, 58, 102] The authors suggested that these attractions could arise from either van der Waals forces or from electrostatic attractions that can arise between two surfaces with charge of the same sign but greatly different magnitude.

Additional experimental work on the topic of nanoparticle halos has been performed by several different groups. Hong and Willing[61] measured the force between silica surfaces (micron-sized silica sphere and flat silica plate) in dispersions of zirconia nanoparticles using colloidal probe atomic force microscopy (CP-AFM) at conditions similar to those used by Tohver et al. The authors observed a slight inflection in the force profile measured at a nanoparticle volume fraction of 10^{-5} which they attributed to the formation of a nanoparticle halo. Chang et al. measured the effect of adding weakly positively-charged zirconia nanoparticles on the gravitational settling rate of polystyrene late particles (highly negatively-charged).[103] At low concentrations, the nanoparticles were able to reduce the settling rate, suggesting a more stable dispersion, which the authors attributed to nanoparticle halos.

In addition to these studies, focused specifically on nanoparticle halos, Walz and coworkers used CP-AFM to measure the general effect of highly-charged nanoparticles on the force profile between weakly-charged surfaces. McKee and Walz measured the force profile between a micron-sized glass sphere and glass plate in solutions of zirconia and polystyrene nanoparticles at pH values near the IEP of glass, such that significant deposition of the nanoparticles occurred.[84] The authors found that at low nanoparticle concentrations, both nanoparticles produced a significant increase in the repulsive force between the glass surfaces and that the decay length of the force was similar to that of the solution Debye length, suggesting a screened electrostatic repulsion arising from the deposition of the charged nanoparticles.

Ji et al. conducted a similar though more comprehensive study using weakly-charged silica surfaces with highly negatively-charged polystyrene latex nanoparticles.[63] It was found that the increased repulsion between the silica surfaces upon introduction of the nanoparticles was caused by nanoparticle deposition and that this force did not disappear upon flushing the nanoparticles from the solution. This latter finding indicated that the nanoparticles were depositing onto the silica surface into deep energy wells (i.e., essentially irreversible deposition).

These prior results suggest that whatever the fundamental mechanism (i.e., strong deposition of nanoparticles directly onto the surface or a weakly-bound halo of nanoparticles displaced slightly from the surface), highly-charged nanoparticles could be an effective means for stabilizing weakly-charged microspheres that would otherwise flocculation. Motivated by these findings, we decided to undertake a relatively comprehensive study to understand the general capability of using charged nanoparticles as stabilizers. Specifically, unlike polymeric stabilizers which can create a tightly-packed brush layer of polymer chains uniformly over the surface leading to repulsive electrostatic and steric forces, it was unclear to us whether charged spherical nanoparticles would consistently produce strong enough repulsive forces to overcome the attractive van der Waals forces driving aggregation.

Our experimental system consisted of weakly-charged silica microspheres (near the IEP of silica) in solutions of either anionic or cationic polystyrene latex nanoparticles. The nanoparticles were of similar average size and absolute zeta potential, though the cationic nanoparticles were significantly more polydisperse in size. Stability of the dispersions with and without added nanoparticles was measured visually and using optical absorbance, and the degree of nanoparticle adsorption was measured using direct visualization (scanning electron microscopy) and with a quartz crystal microbalance.

4.2 Materials and methods

4.2.1 Materials

Filtered, deionized water was used for all experiments, and was produced by a RiOs 8 reverse osmosis system (Millipore, catalog #ZR0S6008Y), followed by a Barnstead EASYpure II UV Ultrapure water system (Thermo Scientific, catalog #D7401). The water had a resistivity of 18.2 MΩ-cm. Fused silica slides (Corning 7980 fused quartz silica, item #3x1x1mm) were obtained from TGP (Technical Glass Products, Inc., Painesville, OH). The silica microspheres (Polysciences, Inc., Warrington, PA, catalog #24326-15) were supplied at a concentration of 10%w/v in water at a size specification of 1.0 μm. The nanoparticles used in the experiments were IDC brand latex nanoparticles ordered through the Invitrogen Corporation (Life Technologies, Carlsbad, CA). Both types of nanoparticles were specified to be 0.02 μm; the sulfate latex nanoparticles (catalog #S37200) were supplied as an 8%w/v suspension in water and the amidine latex nanoparticles (catalog #A37309) were supplied at 4%w/v.

4.2.2 Zeta potential

The zeta potential of the silica slide surfaces was determined using a SurPASS Electrokinetic Analyzer (Anton Paar GmbH, Graz, Austria). The SurPASS tubing was rinsed using the extended rinse program instructions with very dilute isopropanol (<1% vol. in water) and then with deionized water; rinse cycles were approximately 5 min for each. The fused silica microscope slides were cleaned with pure ethanol, rinsed in deionized water, and cleaned for 30 min in a UV/Ozone ProCleaner (BioForce Nanosciences, Inc., Ames, IA), before being mounted in the SurPASS "clamping cell" configuration. A 5 min rinse cycle was then run using the chosen electrolyte, which had been adjusted using 0.2 M NaOH to the highest pH to be used. After rinsing, the zeta potential was measured at pH intervals from high to low pH, using 0.2 M HCl as the titrant.

Measurements of the zeta potential of microspheres and nanoparticles (separately) were done via Dynamic Light Scattering (DLS) using a Zetasizer Nano ZS (Malvern Instruments Ltd, Worcestershire, UK), with samples measured in disposable folded capillary cells (catalog #DTS1060C), which were rinsed first with ethanol then deionized water and dried with compressed nitrogen gas. To measure zeta potentials across a range of pH values, the Malvern MPT-2 Autotitrator was used, with 0.25 M HCl, 0.25 M NaOH, and 0.01 M HCl used as titrants.

To measure the effective microsphere zeta potentials in binary microsphere/nanoparticle solutions, a Micro-Electrophoresis Apparatus Mk II (Rank Brothers Ltd., Cambridge, England) was used. The rectangular cell configuration was used to avoid the effect of sedimentation on observed particle velocity. Nanoparticle concentrations used with this instrument corresponded to those used in the flocculation and adsorption measurements, while the microsphere concentration was relatively dilute (<0.01% vol.) in order to be able to observe individual particles. All the measurements were taken at the stationary plane in the cell in order to eliminate the effects of the counter-flow of electrolyte in the cell. An electric potential was applied across the cell and the velocity of the particles was determined visually using a stopwatch to measure the time a particle took to travel a fixed distance.

4.2.3 Nanoparticle adsorption

Scanning electron microscopy (SEM) was used to determine the degree of nanoparticle adsorption onto fused silica slides. The slides were cleaned by sonication in ethanol. Initially, the slides were subsequently cleaned via UV/Ozone treatment; however this step was discontinued after the test images showed no difference in behavior between surfaces treated with and without the UV/Ozone cleaning. An appropriate volume of nanoparticle solution at the desired volume fraction was prepared, briefly sonicated, and then titrated to the desired pH using 0.2 M HCl or 0.2 M NaOH.

A beaker of deionized water to be used as the rinse solution was prepared and titrated using 0.2 M HCl to the same pH as the nanoparticle solution. The cleaned and dried silica slides were briefly immersed in the rinse solution before being placed in a beaker containing the

nanoparticle solution. After 30 minutes in the nanoparticle solution, the silica slide was removed from solution and gently rinsed in the rinse solution in order to remove any excess (non-adsorbed) nanoparticles from the slide. By using the same pH for both the adsorption and rinse solutions, the surface charge should remain approximately the same and the adsorbed particles (if they were present) would remain on the slide. The silica was then allowed to air dry, after which the surfaces were sputter-coated with a 1-2 nm layer of gold in preparation for SEM imaging.

4.2.4 Stability and flocculation

The stability of the silica microsphere dispersions was studied using both visual observation and optical turbidity measurements. To prepare samples for the flocculation experiments, appropriate concentrations of latex nanoparticles (either amidine or sulfate) were prepared and titrated to the desired pH using either 0.2 M HCl or 0.2 M NaOH (for experiments without added nanoparticles, only deionized water was titrated, using the same titrants). Equal volumes of the titrated solutions were then sonicated to help disperse the nanoparticles and then transferred to cuvettes. The appropriate amount of microspheres was sonicated and then added to the cuvettes to reach 0.1% vol. silica in each cuvette. The cuvettes were capped and inverted in order to evenly distribute the particles. When using the UV/Vis spectrometer, the samples were all sonicated briefly one more time before the experiment, as there was additional time in between the sample preparation and experiment.

Quantitative assessment of the rate of flocculation was performed by measuring the total absorbance in a UV/Vis spectrophotometer and then calculating a turbidity exponent, n, that depends on the size of the scattering particles. Specifically, for particles outside of the Rayleigh regime, the total absorbance (turbidity) of the sample can be expressed as an exponential equation (Equation 4.1).

$$A = k\lambda^n \tag{4.1}$$

Here, A is the turbidity at wavelength λ, n is the turbidity exponent, and k is a constant that depends on particle size, density, and refractive index.[39, 104, 105] This equation is derived from the classic relationship between the intensity of light scattered and wavelength in the Rayleigh regime (size << wavelength) where the scattered intensity scales as λ^{-4}. For particle sizes of order λ or greater (i.e., Debye scattering, which applies to the 1.0 μm silica spheres used in these experiments), the wavelength exponent increases with increasing size of the scattering objects.[37, 104, 106]

The spectrometer used for the UV/Vis measurements was an Ocean Optics SD2000 miniature fiber optic spectrometer with an Ocean optics DT-1000-CE Deuterium Tungsten light source (Ocean Optics, Inc., Dunedin, FL). The absorbance spectrum was recorded at regular time intervals in order to calculate the turbidity parameter. In the measurements, the absorbance spectrum from 500-700 nm (wavelength) was used. The turbidity parameter was determined as the slope of a log-log plot of absorbance versus wavelength.

4.3 Results

4.3.1 Zeta potential of the microspheres and nanoparticles

In Figure 4-1, the measured zeta potential for both the 1.0 μm silica microspheres and the fused silica slides is shown as a function of pH. For comparison, zeta potential data for silica slides, reported by Scales et al.[19], is also included. While there is a clear difference between the different experiments at a given pH value, the trends are quite consistent. The isoelectric point falls between pH 2.0 and 3.0, depending on the material geometry and type of zeta potential measurement.

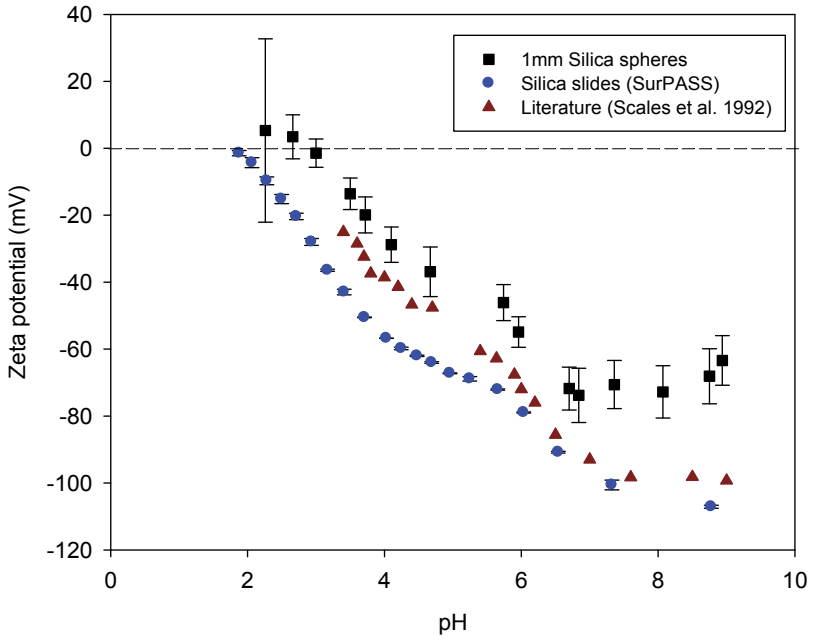

Figure 4-1: Measured zeta potential vs. pH for 1.0 μm silica microspheres and silica slides, compared with literature values[19].

Figure 4-2 shows the zeta potentials obtained using DLS for both amidine latex and sulfate latex polystyrene. For each data point, the Zetasizer software combined a minimum of 10 zeta potential measurements (more runs were automatically conducted if required to sufficiently fit the data; typically there were less than 20 runs required per data point). There is significant scatter in the data points (due to Brownian motion of the nanoparticles[63]), however for both types of particles, the zeta potentials remain consistent over the range of pH range. Furthermore, the average values were consistent over multiple measurements, suggesting the relatively large standard deviation arises from variation in the particles rather than in the measurement. By comparing the trends in Figure 4-1 and Figure 4-2, it is clear that the strength and direction of the electrostatic interaction between the microspheres and nanoparticles can be effectively controlled by altering the pH.

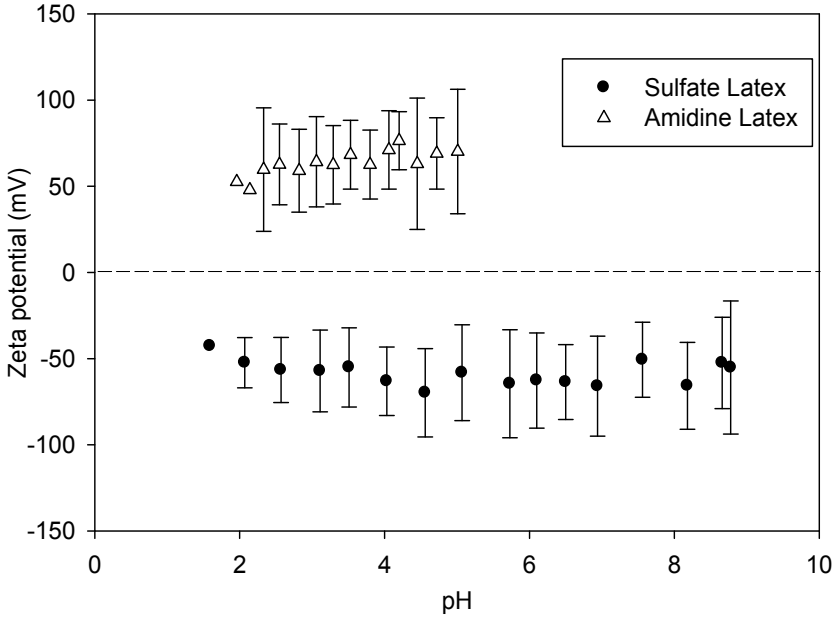

Figure 4-2: Zeta potentials of sulfate latex (circles) and amidine latex (triangles) nanoparticles. The standard deviation of the measured values is indicated by the error bars.

4.3.2 Zeta potential of microspheres with the nanoparticles

Table 4-1 shows the effective composite zeta potential for the binary mixtures of silica and polystyrene particles. The values reported here for the nanoparticles were taken from Figure 4-2. The measurements on both the silica-only and the binary solutions were done at pH 2.0 and 3.0 using the Rank Brothers Micro-Electrophoresis Apparatus Mk II. Because this measurement involves actually viewing the particles via a microscope, only the microspheres are large enough to be visually detected in measurements involving dispersions containing both nanoparticles and microspheres. It was noted that in solutions where the pH was near the IEP for the silica microspheres, a significant number of microspheres were effectively stationary.

As seen, the presence of the nanoparticles substantially increases the measured zeta potential of the silica microspheres, presumably due to adsorption of the highly-charged nanoparticles. For both the amidine and sulfate systems, the magnitude of the zeta potential is similar to, or even larger, than the zeta potential measured for bare silica particles at pH 6 (Figure 4-1).

Table 4-1: Comparison of composite zeta potentials (mV) for 1.0 μm silica microspheres and polystyrene latex nanoparticles.

	pH 2.0	pH 3.0
Sulfate latex nanoparticles	-52±20	-57±24
Amidine latex nanoparticles	+53±26	+64±25
Silica microspheres	+7.3±3	+2.1±3
Silica microspheres + 0.5% vol. sulfate latex nanoparticles	-63.2±15	-108.1±7
Silica microspheres + 0.5% vol. amidine latex nanoparticles	+79.6±12	+83.1±6

It is interesting to note that the zeta potential of the microspheres measured in the microsphere/nanoparticle mixtures is actually significantly greater than that of the nanoparticles themselves. Our hypothesis is that this discrepancy arises from the interpretation of the measured electrophoretic mobility. Specifically, the relationship between electrophoretic mobility and zeta potential depends on the radius of curvature, thus accurate determination of the zeta potential for micron-sized particles with adsorbed nanoparticles is non-trivial. For this reason, the values reported for microsphere/nanoparticle mixtures in Table 4-1 should be viewed as semi-quantitative. The key finding here is that the adsorbed nanoparticles greatly increase the apparent zeta potential of the microspheres.

4.3.3 Stability of dispersions containing only silica microspheres

Figure 4-3 shows the resulting turbidity curves for solutions containing only 0.1% vol. 1.0 μm silica microspheres. The pH ranged from pH 2.0 to 8.2. As particle size increases, the turbidity exponent becomes less negative, indicating larger scatterers. From the data, there is a clear difference between samples at pH 4.0 and lower, compared to 5.0 and higher. The solutions, at and below pH 4.0, show a relatively large and rapid change in the turbidity exponent, which becomes less negative. This indicates a significant increase in the size of the suspended particles which, for this type of system, is a direct indication that the silica microspheres are flocculating.[37, 106] From about a pH of 5.0 and higher, the microspheres are effectively stable, with the turbidity (and therefore the particle size) remaining constant over the observation time. The particle size, as gauged by the turbidity exponent, remains approximately unchanged over a period of two hours, while the lower pH solutions show a rapidly increasing particle size, with significant flocculation being visible almost immediately.

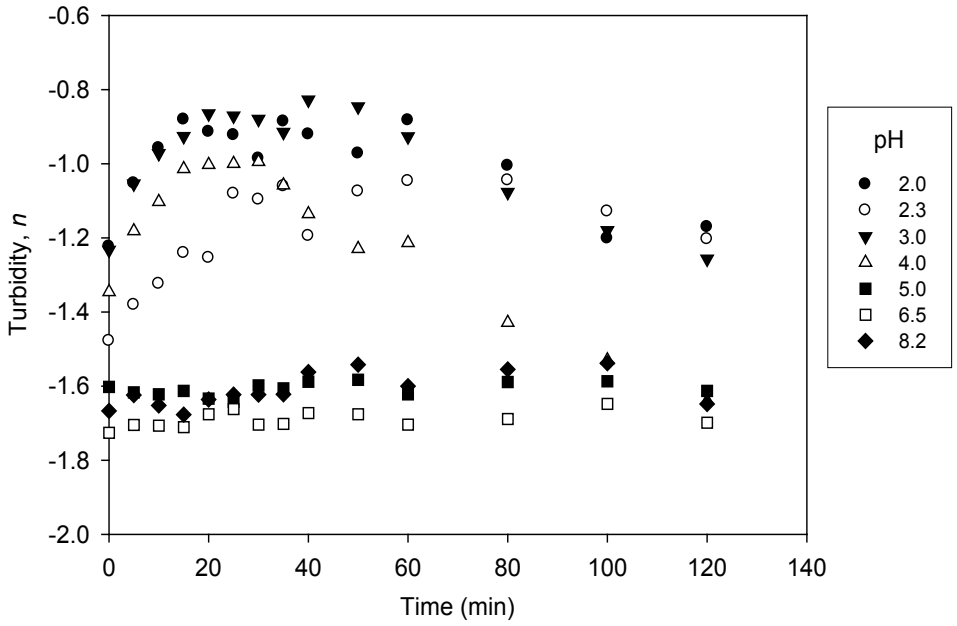

Figure 4-3: Turbidity curves of 0.1% vol. 1.0 μm silica microsphere dispersions at varying pH (no added nanoparticles). The pH values used are labeled in the legend.

For the purposes of the plots of turbidity exponents with respect to time, the first measurement is taken to be effectively t=0. In actuality, however, there was a short interval of approximately 10 minutes between the introduction of the microspheres into the solution and the beginning of the measurement process. The samples were all sonicated again briefly right before the measurements; however, it was difficult to begin the measurements before the particles began flocculating. Since the flocculation process is quite rapid when it was observed (at low pH), the unstable particles had already begun to aggregate before the initial turbidity measurement of each sample (at t=0), resulting in the slightly different starting values for n for the first measured point at each pH.

As flocculation continues, the larger flocs sediment out of solution, leaving smaller flocs and individual particles suspended. This sedimentation causes the turbidity exponent to decrease after reaching a peak value. Using the peak in the n-vs.-time curve as an indicator, a significant portion of the silica microspheres flocculate and begin to sediment out of solution in about 20 minutes.

Photographs of the flocculating silica-only solutions at different times are shown in Figure 4-4. Solutions that are stable are cloudy due to scattering of light by the suspended microspheres. The lower pH solutions clearly flocculate and most of the particles sediment within an hour. The pH 4.0 solution is somewhat in between the two extremes, as flocculation is visible but much slower than pH values that are slightly lower. At pH 5.0 and higher, there is a

very clearly defined boundary between the sedimenting spheres and the supernatant, indicating the spheres are sedimenting individually and uniformly.

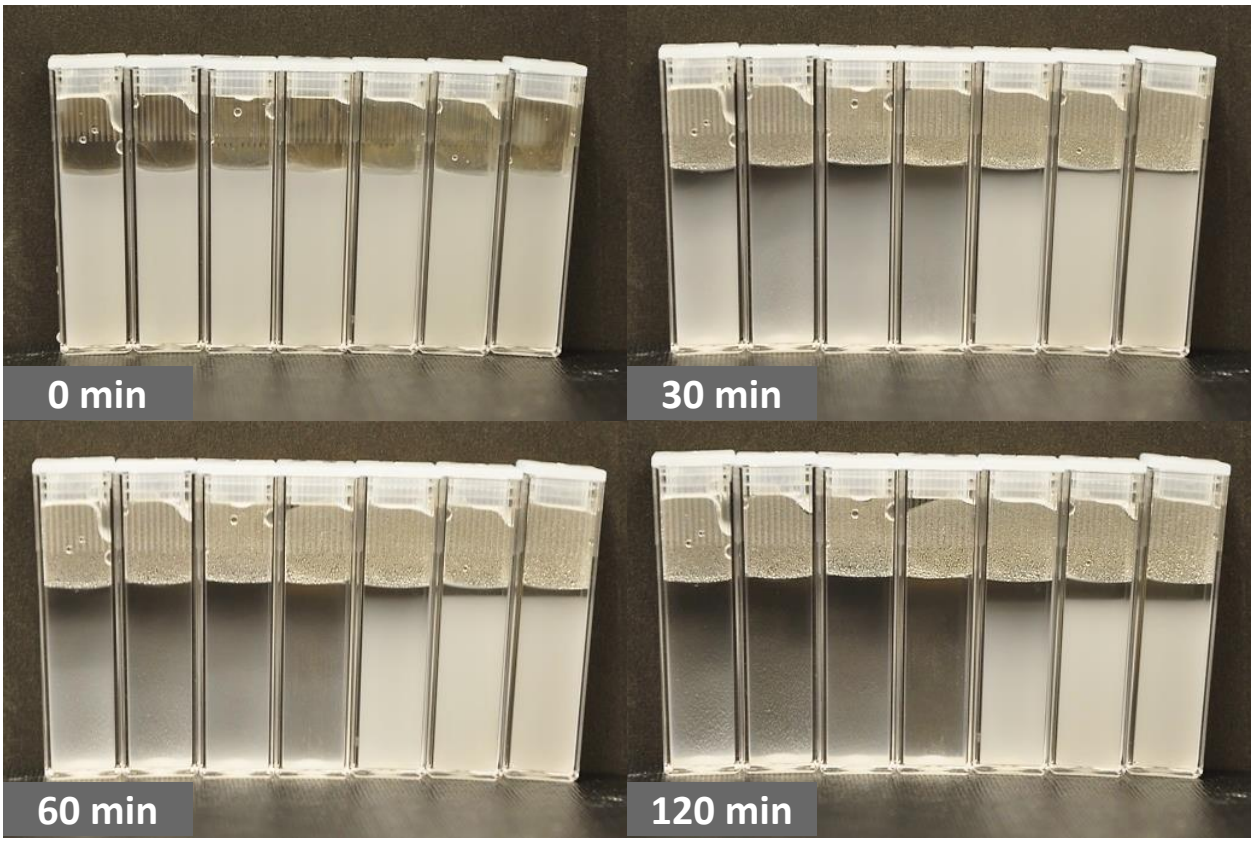

Figure 4-4: Stability of 0.1% vol. 1.0 μm silica microspheres. In each photograph, the cuvettes contain solutions at pH (L to R) of 2.0, 2.5, 3.0, 3.5, 4.0, 5.0, and 8.0.

4.3.4 Stability of dispersions containing silica microspheres and sulfate nanoparticles

A plot of turbidity vs. time at different pH values for dispersions of 0.1% vol. silica microspheres plus 0.5% vol. sulfate nanoparticles is shown in Figure 4-5. As seen, the stability of the microspheres remains essentially unaffected by the addition of the nanoparticles. This concentration of nanoparticles was chosen as it is in the range (approximately 0.1 to 1.0% vol.) suggested in the literature that would potentially exhibit a stabilizing effect.[8, 55] However, the microsphere/nanoparticle solutions studied in Figure 4-5 behave almost identically to the microsphere-only measurements (Figure 4-3), exhibiting the same characteristic rapid change in turbidity at low pH values. Indeed, based solely on the turbidity values, it appears that the microspheres may actually flocculate slightly faster or form larger aggregates when compared to Figure 4-3. Specifically, the peak in turbidity is approximately -0.7 for pH values ranging from 2.0 to 3.0 with the added sulfate latex nanoparticles, whereas without the nanoparticles the peaks

were between about -0.8 and -0.9. This difference could result from a slight depletion attraction between the microspheres produced by the nanoparticles in solution, though this is not certain.

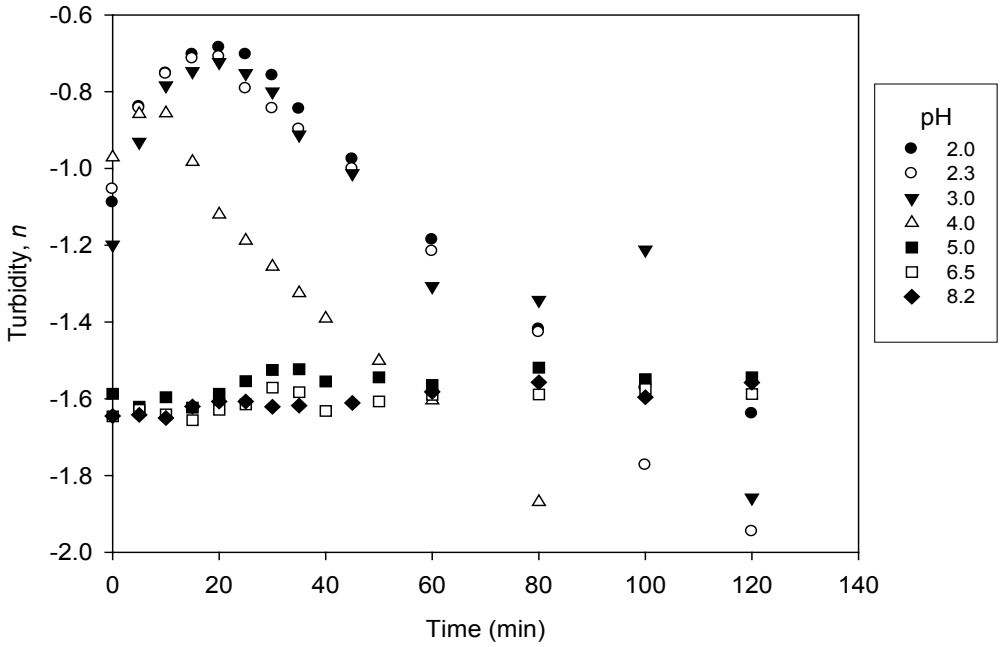

Figure 4-5: Turbidity curves of 0.1% vol. silica microspheres in solution with 0.5% vol. sulfate latex nanoparticles. The pH values used are labeled in the legend.

Figure 4-6 shows photographs of silica solutions at low pH values with and without the addition of sulfate latex nanoparticles at different times. The silica-only samples flocculate as usual, and the samples containing the sulfate latex do as well. However, in this instance the pH 2.0 sample is shown to flocculate slower than the rest. It still lacks as well of a defined boundary between the sedimenting particles and the remaining solution, however there are clearly more particles in suspension after 2 hours than the other cuvettes at the different pH values, and the image clearly differs from the behavior of the pH 2.0 sample shown in Figure 4-4.

It is important to note that dispersions containing the latex nanoparticles (both sulfate and amidine, presented below) exhibit a bluish color. When the dispersions also contain suspended silica microspheres with the nanoparticles, the color is less noticeable. However, as the microspheres flocculate and sediment, the remaining supernatant is distinctly bluish in color when compared to the silica-only solutions. In Figure 4-6 (as well as Figure 4-7), the focus should therefore be on the opacity of the solution and the interface between the uppermost silica particles and supernatant. Non-flocculated samples will appear white in all cases. With this in mind, as seen in Figure 4-6, every cuvette except the silica/latex at pH 2.0 is nearly transparent, indicating almost complete flocculation and sedimentation of the microspheres by the time of the final image (120 min).

The silica/latex solution at pH 2.0 is noticeably bluish with a less-defined sedimentation boundary, as some degree of flocculation has occurred, allowing the bluish nanoparticle-containing supernatant to be visible. Nonetheless, it is quite apparent that the pH 2.0 sample in Figure 4-6 appears to be more stable by comparison to the other pH samples. While this image suggests that the sulfate nanoparticles are tending to stabilize the dispersion at this pH, it should be noted that this result was not observed consistently. Furthermore, the turbidity results in Figure 4-5 indicate that this solution does, in fact, flocculate. This may indicate that the conditions for this sample are near a transition region between stable and unstable.

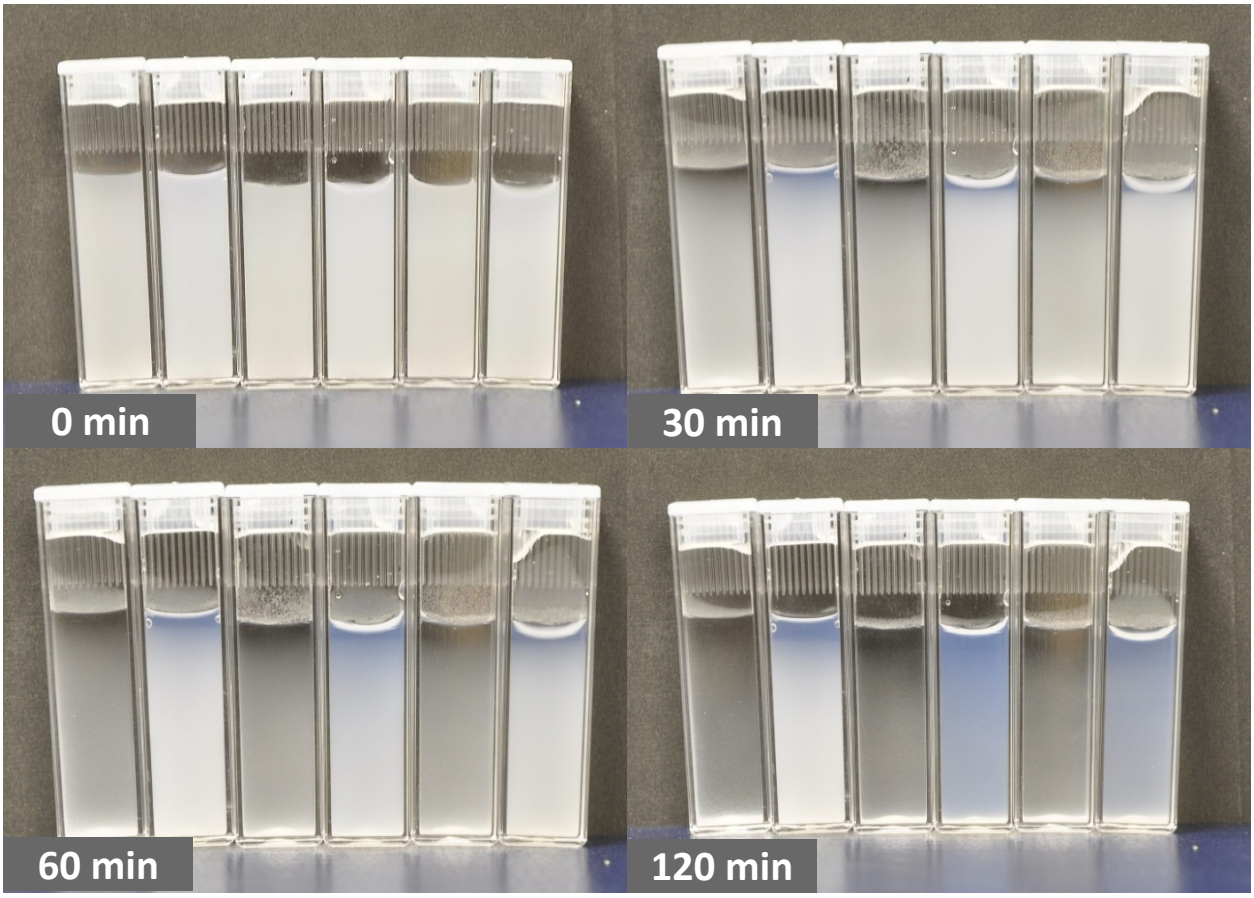

Figure 4-6: Dispersions of 0.1% vol. silica microspheres with and without 0.5% vol. sulfate latex nanoparticles. In the cuvettes from L to R: pH 2.0 SiO_2 only, pH 2.0 SiO_2 + sulfate nanoparticles, pH 2.5 SiO_2 only, pH 2.5 SiO_2 + sulfate nanoparticles, pH 3.0 SiO_2 only, pH 3.0 SiO_2 + sulfate nanoparticles.

Figure 4-7 shows the results of an experiment investigating the effect of the concentration of the sulfate nanoparticles on the stability of the microspheres. The solution pH was 2.5 and nanoparticle concentrations of 0.1, 0.5 and 1.0% vol. were used. As seen, the turbidity exponent showed the same initial increase as observed in samples without added nanoparticles (Figure 4-3), meaning that the solutions flocculated again. It was observed, however, that the turbidity curve for the lowest nanoparticle concentration (0.1% vol.) did not exhibit quite the same peak as observed in the higher concentrations, and appears to flocculate slightly slower.

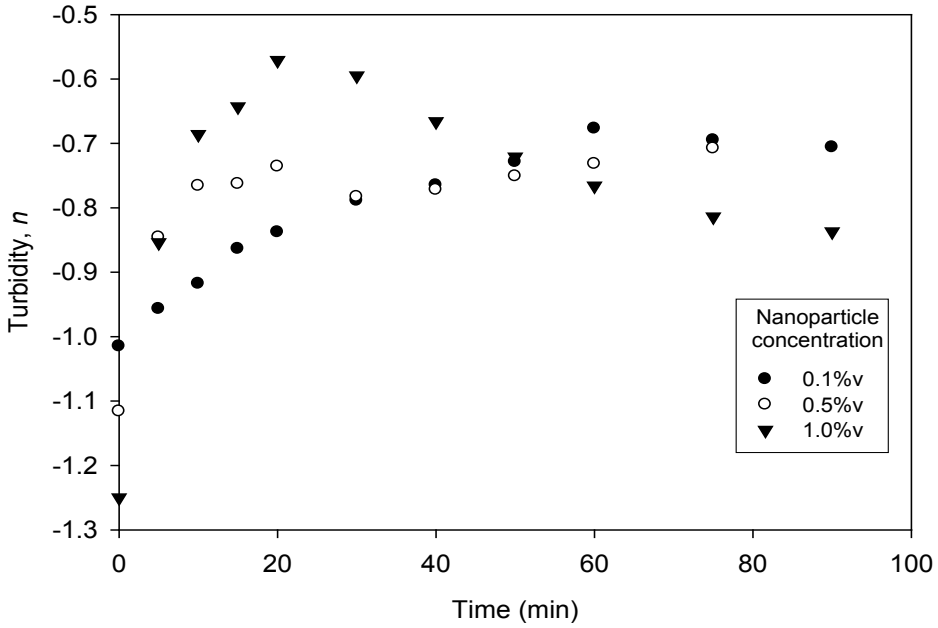

Figure 4-7: Turbidity curves for 0.1% vol. silica microparticles with varying concentrations of sulfate latex nanoparticles, all at pH 2.5. The legend indicates the nanoparticle concentrations that were used.

4.3.5 Stability of dispersions containing silica microspheres and amidine nanoparticles

Shown in Figure 4-8 are photographs of dispersion containing 0.1% vol. silica microspheres plus 0.5% vol. positively-charged amidine latex nanoparticles at varying times. Here, at all three pH values, the amidine latex very clearly stabilized the microspheres. Each solution has a well-defined sedimentation boundary layer, just as observed with the stable, silica-only solutions in Figure 4-4. This is somewhat unexpected, as the magnitude of the zeta potentials of the microspheres with the amidine nanoparticles are comparable to those with the added sulfate nanoparticles (Table 4-1). Clearly zeta potential alone is not sufficient for predicting the system stability.

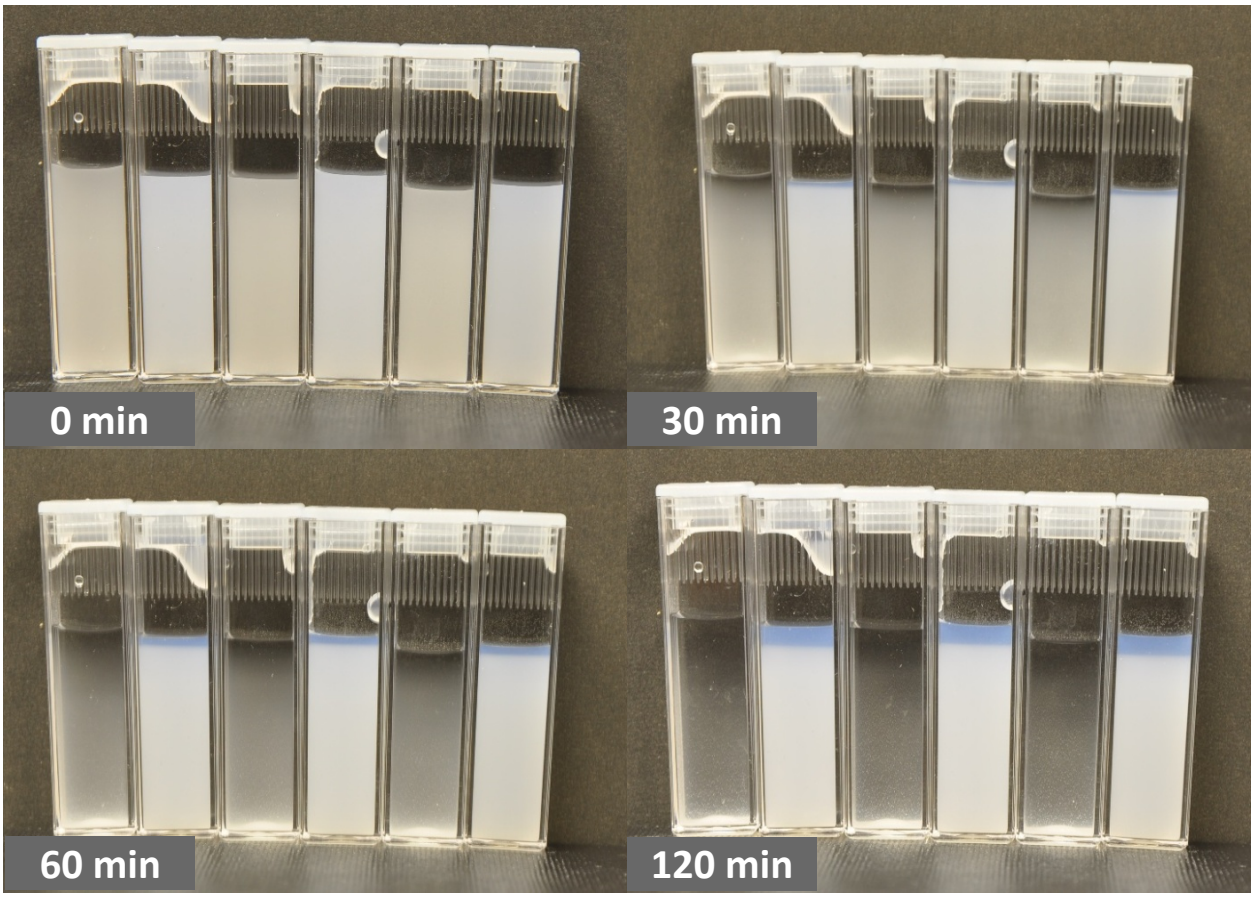

Figure 4-8: Dispersions of 0.1% vol. silica microspheres with and without 0.5% vol. amidine latex nanoparticles. In the cuvettes from L to R: pH 2.0 SiO_2 only, pH 2.0 SiO_2 + amidine nanoparticles, pH 2.5 SiO_2 only, pH 2.5 SiO_2 + amidine nanoparticles, pH 3.0 SiO_2 only, pH 3.0 SiO_2 + amidine nanoparticles.

Figure 4-9 shows the turbidity exponents for amidine latex (0.5% vol.) and 1.0 µm silica (0.1% vol.) at various pH values over the course of about 2 hours. As expected, based on the photographs in Figure 4-8, the turbidity exponents at each pH remain essentially constant over the course of two hours. The different samples had somewhat varying starting values, which could be due to small differences in concentration introduced during sample preparation, but the turbidity exponents nonetheless showed little change throughout the entire experiment time.

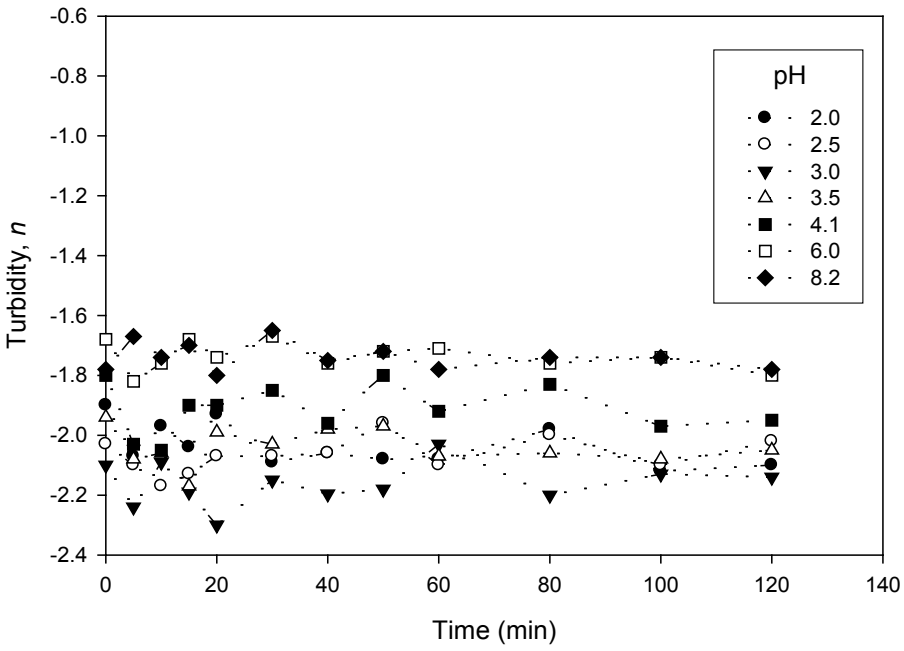

Figure 4-9: Flocculation behavior of 0.1% vol. silica microspheres in solution with 0.5% vol. amidine latex nanoparticles. The dotted lines serve only to guide the eye and connect the data points for a given sample. The pH values used are labeled in the legend.

4.3.6 Adsorption of nanoparticles on silica surfaces

In order to better understand the stability behaviors reported in Figure 4-4 through Figure 4-9, a series of tests to quantify the degree of nanoparticle adsorption were conducted. Figure 4-10 shows images of fused silica slides that had been immersed for 30 minutes in 0.1% vol. sulfate latex solutions, at varying pH values. The level of adsorption observed is negligible for higher pH values, and becomes noticeable at pH 3.5. Lower pH samples show significant adsorption, as the silica becomes positively charged.

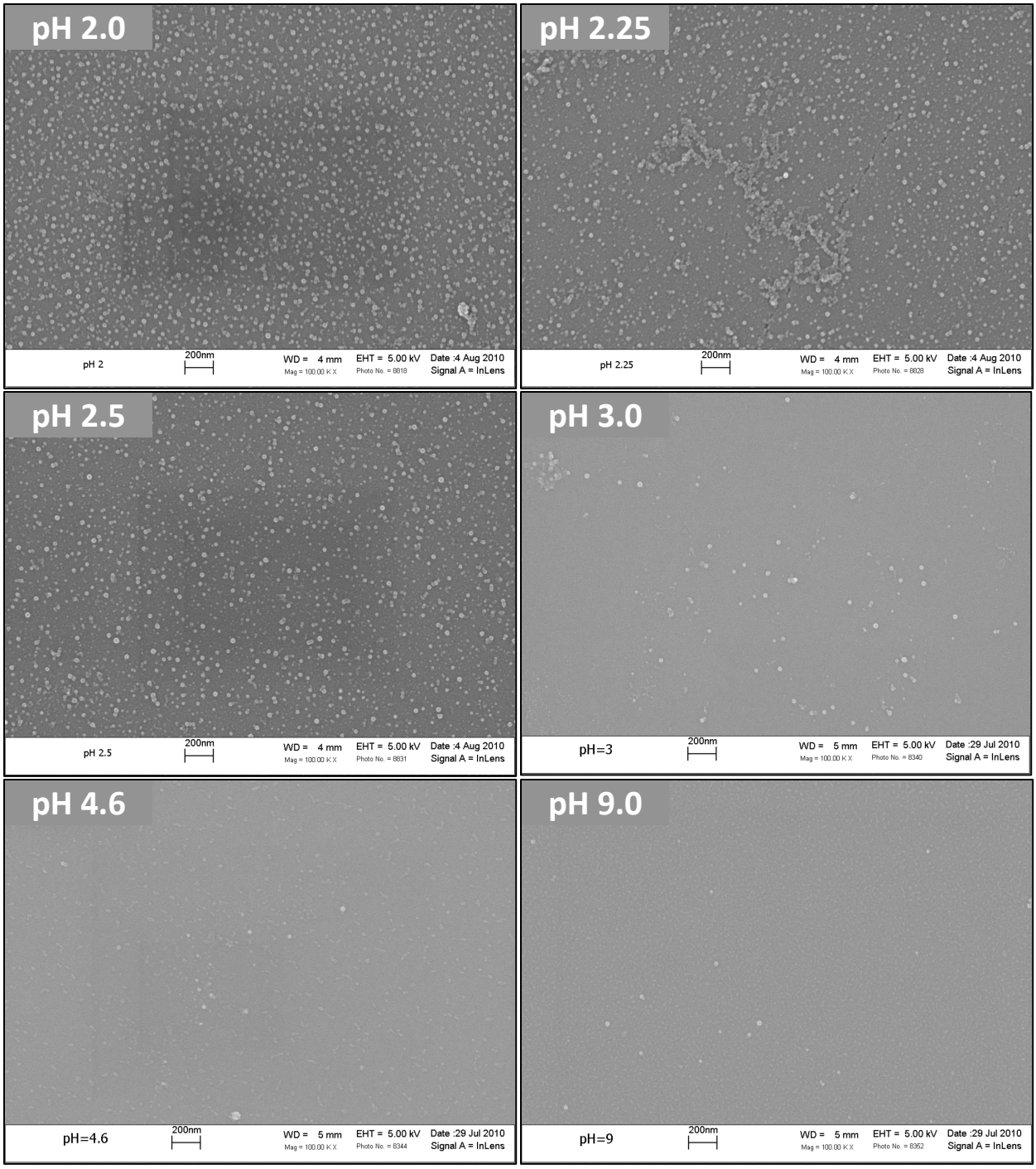

Figure 4-10: SEM images of fused silica after immersion for 30 min. in a 0.1% vol. sulfate latex nanoparticle dispersion at various at pH values. Images are 100kX magnification, showing increasing adsorption with decreasing pH.

Estimates of the surface density of adsorbed particles were determined from the SEM images in Figure 4-10. Multiple images were taken at each pH and the average density was estimated. Figure 4-11 shows the approxmate number of nanoparticles per square micron at each

pH. Above a pH of 4.5 there are effectively no adsorbed nanoparticles. By pH 3.5 there is noticable adsorption, which increases with decreasing pH.

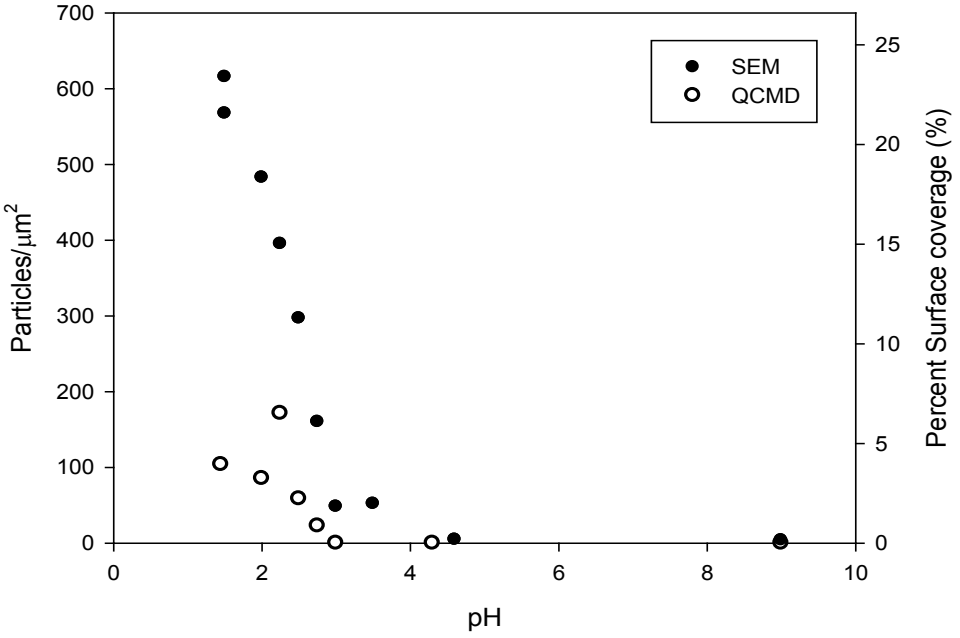

Figure 4-11: Number density of adsorbed sulfate latex nanoparticles (0.1% vol. in solution), displayed as both number per μm^2 (left axis) and in percent of surface covered (right axis).

To confirm that adsorption was in fact taking place, rather than non-adsorbed particles simply drying on the surface, quartz crystal microbalance (QCMD, Q-sense/Biolin Scientific, Linthicum, MD) measurements were performed using the same concentration of sulfate latex particles, 0.1% vol. The surfaces used were Q-sense silica sensors (catalog #QSX 303). The mass adsorbed was calculated using the Sauerbrey equation.[107] The trend in the QCM results in Figure 4-11 agrees with that obtained using the SEM micrographs, showing increasing adsorption with decreasing pH of the solution. The difference in magnitude between the two data sets likely results both from the difference in the measurement surface (QCM sensors are vibrating in a flow cell), and the fact that the SEM micrographs merely provide rough estimates of density.

By comparison, the images in Figure 4-12 show the adsorption of amidine latex nanoparticles on silica slides at four pH values. In each case there is significant adsorption; far more than what was observed using the sulfate nanoparticles at the same conditions. Based solely on visual estimation of the number of adsorbed particles, the particle density on the surfaces actually appears to decrease with increasing pH, which is essentially the opposite of what was expected, as the silica surface becomes more negatively charged with increasing pH while the zeta potential of the amidine latex nanoparticles remains highly positive over this pH

range. Thus, surprisingly, the adsorbed nanoparticle density is highest when both the silica plate and amidine latex nanoparticles are positively charged (pH 2.0).

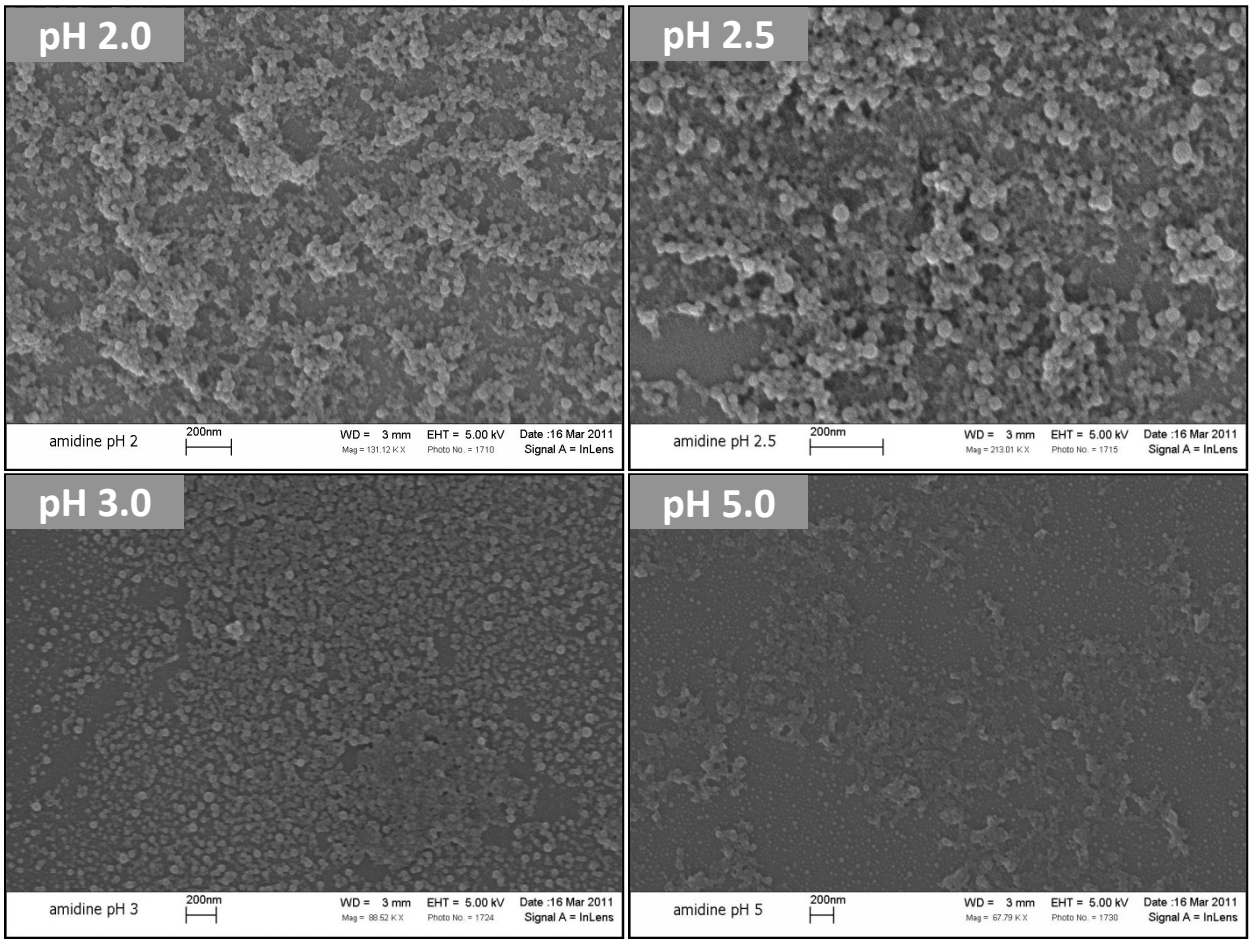

Figure 4-12: Silica surfaces with adsorbed amidine latex (0.5% vol. solution) at varying pH values.

A comparison of images between the sulfate and amidine nanoparticle systems at pH 2.0 is shown in Figure 4-13. Both images were done with 0.5% vol. nanoparticles. The amidine latex particles clearly have adsorbed in much larger quantities than the sulfate particles. Because of the large degree of adsorption, accurate estimates of the number density of nanoparticles were difficult. Our approach was to estimate the thickness of the adsorbed layer and then calculate the corresponding nanoparticle density. The estimation of the layer thickness was simply done visually; the layers were discontinuous over the surface, so the edges of the multi-layered regions were visible, so rough counts of the number of visible layers were made. For simplicity, it was assumed that the particles were adsorbed in discrete layers with the number of particles per layer equal to that of the visible surface layer, with the total particles per area being the visible particles multiplied by the number of layers in that region.

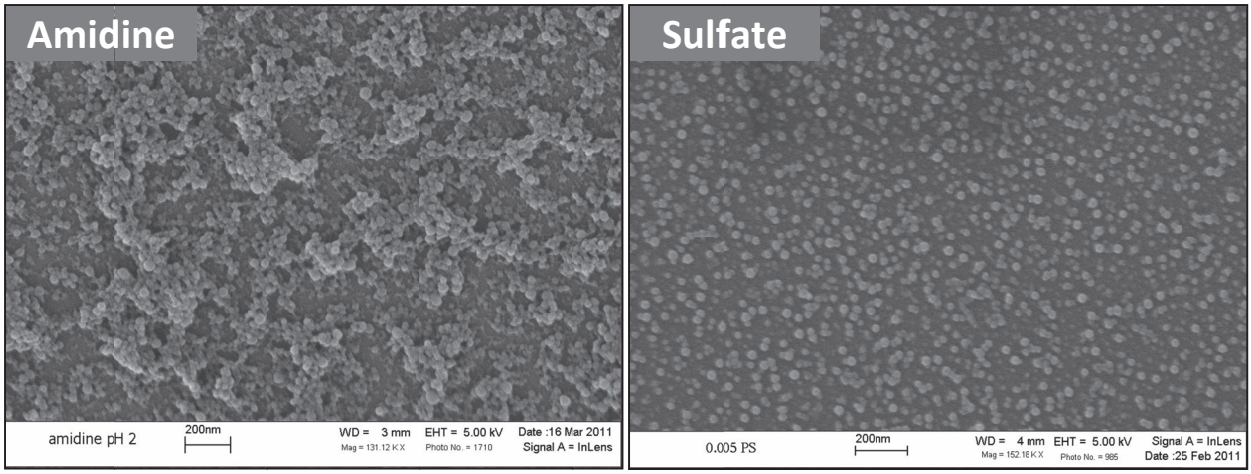

Figure 4-13: Comparison of amidine (left) and sulfate (right) latex adsorption at pH 2.0 on silica slides. Nanoparticle solution concentration was 0.5% vol. in both cases.

The approximate adsorbed particle densities for both amidine and sulfate latex particles at 0.5% vol. bulk concentration are shown in Figure 4-14 for various pH values. As seen, the amidine nanoparticles adsorb in substantially higher quantities at every observed pH, with at least three times more nanoparticles per unit area than with the sulfate nanoparticles. This is a key difference between the two systems, which can potentially explain the difference in stability of binary solutions using the different particles.

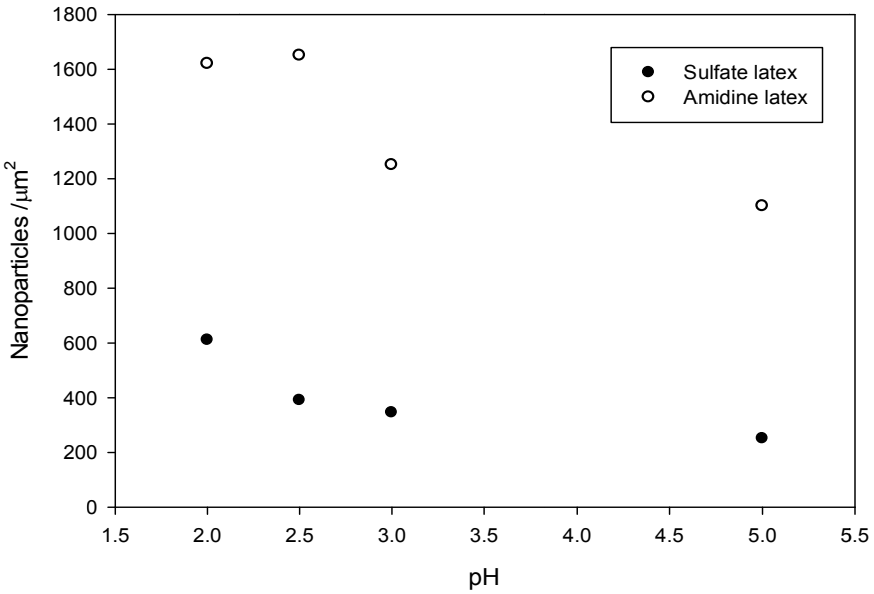

Figure 4-14: Comparison of approximate amidine latex and sulfate latex particle densities (both from 0.5% vol. nanoparticle solutions) on silica slides at varying pH.

4.4 Discussion

The results presented in the previous section can be summarized as follows:

1. Comparing the zeta potential data and flocculation experiments, we see that the silica begins to flocculate in solutions below a pH of about 4.5, where the microspheres had absolute zeta potentials below approximately 40 mV.
2. The binary solution zeta potential measurements all showed the effective zeta potential of the microspheres increase substantially upon the introduction of the nanoparticles. Specifically, adding 0.5% vol. of either sulfate or amidine nanoparticles increased the magnitude of the zeta potential to over 60 mV, which is significantly higher than the zeta potential at which bare silica microspheres remained stable.
3. Addition of the sulfate nanoparticles to the silica microspheres had no noticeable effect of the stability of dispersion. While some increased stability was noticed at pH 2.0, the improvement was not consistent in all samples.
4. The amidine latex nanoparticles produced drastically different results for the binary solutions, most notably in that they prevented flocculation of the silica at every pH value studied. These different stability behaviors indicate that zeta potential alone is not an accurate predictor of the stability of these binary dispersions.
5. The degree of adsorption of the sulfate and amidine nanoparticles onto a silica slide was substantially different. Specifically, as shown in Figure 4-14, the density of the amidine nanoparticles adsorbed on the silica slide was at least triple that of the sulfate nanoparticles at a given pH. In addition, in many regions, there appeared to be multiple layers of adsorbed amidine nanoparticles (perhaps 3 or 4 layers), while only single layers of adsorbed sulfate nanoparticles were observed.

One possible cause of the differences in adsorption is the size distribution of the two different types of nanoparticle. Both were specified by the manufacturer to be 0.02 μm in diameter, and the batch data that was provided gave an average size of 22-23 nm for the sulfate latex and 23 nm for the amidine. However, the coefficient of variation is 14.7% for the sulfate latex and 21.9% for the amidine latex. This difference in size distribution can be seen clearly in Figure 4-15, which shows SEM micrographs of silica surfaces with adsorbed sulfate and amidine nanoparticles (the amidine nanoparticle adsorption was performed using extremely dilute solutions to allow more easily viewing individual nanoparticles). As seen, for the amidine nanoparticles, particles smaller than 10 nm and larger than 50 nm in diameter are observed, which is not the case with the sulfate nanoparticles. It is possible that this wider range allows tighter packing of the nanoparticles on the surface and thus high coverage.

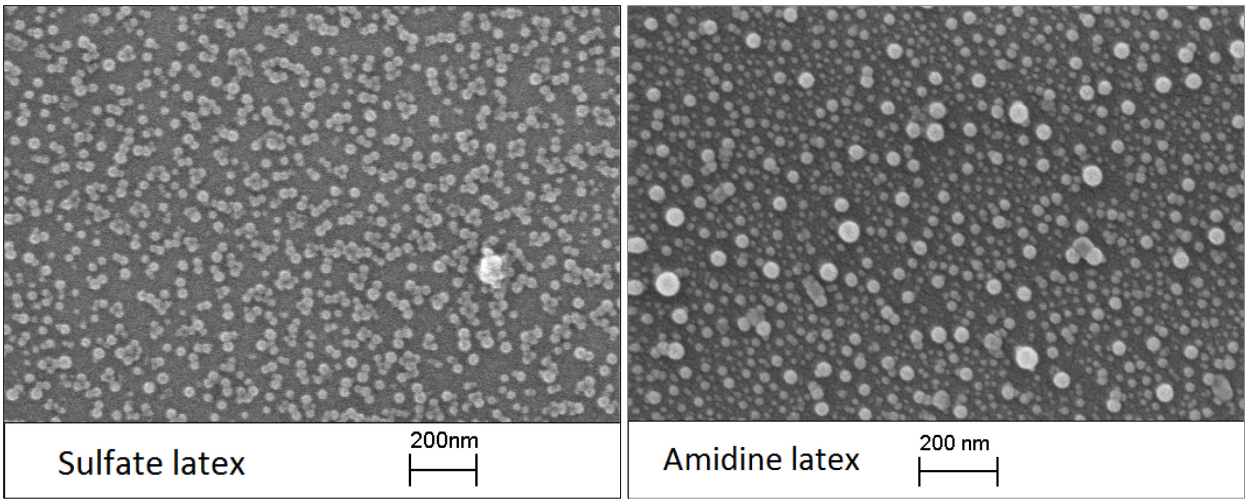

Figure 4-15: SEM micrographs showing differences in the size distribution of the latex nanoparticles.

In order to better understand these results, we developed a simple model to estimate the effect of the adsorbed nanoparticles on the van der Waals and electrostatic interaction energies between the silica microspheres. Our approach is to represent the layer of adsorbed nanoparticles as a continuous film with the charge located on the outer surface. A simple schematic is shown in Figure 4-16 (note that the silica surfaces, labeled 1 and 2, are identical in our system, however they are labeled distinctly to maintain consistency with the general form of the model equations).

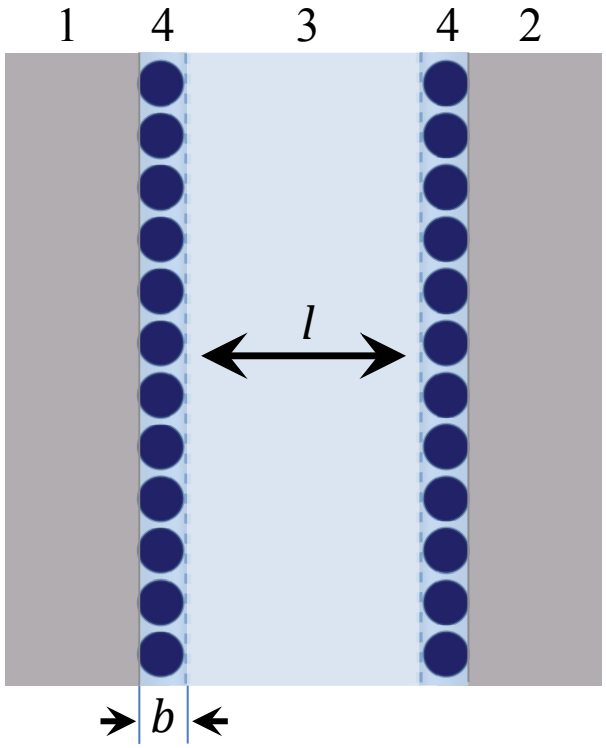

Figure 4-16: Schematic of the model system. The numbers correspond with the material subscripts of Eqs. (2) and (3). Specifically, the silica spheres are materials 1 and 2, the medium (water) is 3, and the

combined nanoparticle/water film is 4. The separation distance is designated by *l* and the film thickness as *b*.

We calculate the van der Waals interaction using the Lifshitz-based approach[24, 25], modified as described by Dagastine et al.[25] to include the presence of a film coating. In this approach, the dielectric properties of the film are assumed to be between those of the two constituents (i.e., polystyrene and water), which recognizes that the adsorbed nanoparticle layer is porous. In this approach, the Hamaker constant (including retardation effects) between two coated-planar half spaces is calculated using Equation 4.2.

$$A_{132}(l) = -\frac{3}{2}k_B T \sum_{n=0}^{\infty}{}' \int_{r_n}^{\infty} x \ln\{(1-\Delta_{31}^{*}\Delta_{32}^{*}e^{-x})(1-\bar{\Delta}_{31}\bar{\Delta}_{32}e^{-x})\}\,dx \tag{4.2}$$

where

$$\Delta_{jk}^{*} = \frac{\Delta_{j4}+\Delta_{4k}e^{-(bs_4/L)}}{1+\Delta_{j4}\Delta_{4k}e^{-(bs_4/L)}} \quad \Delta_{jk} = \frac{\varepsilon_j s_k - \varepsilon_k s_j}{\varepsilon_j s_k + \varepsilon_k s_j} \quad \bar{\Delta}_{jk} = \frac{s_k - s_j}{s_k + s_j}$$

$$s_k^2 = x^2 + \left(\frac{2\xi_n l}{c}\right)^2 (\varepsilon_k - \varepsilon_3) \quad r_n = \frac{2l\xi_n\sqrt{\varepsilon_3}}{c} \quad \xi_n = \frac{2\pi n k_B T}{\hbar} \quad \varepsilon_k = \varepsilon(i\xi_n)$$

Here, *c* is the speed of light in a vacuum, k_B is the Boltzmann constant, *T* is temperature, $\hbar$ is Planck's constant divided by 2π, and ε_k is the dielectric permittivity function evaluated at frequency ξ_n. (Again, in our system the properties of materials 1 and 2, referring to the silica spheres, are equal.) The Δ* term is the modified term introduced to the standard Hamaker constant to account for the properties of the coating layer (of thickness *b*).

Once the Hamaker constant is known, the van der Waals interaction between the two microspheres is calculated using the general expression

$$V_{132}(l) = -\frac{A_{132}(l)}{6}\left[\frac{2a_1a_2}{R^2-(a_1+a_2)^2} + \frac{2a_1a_2}{R^2-(a_1-a_2)^2} + \ln\left(\frac{R^2-(a_1+a_2)^2}{R^2-(a_1-a_2)^2}\right)\right] \tag{4.3}$$

where *R* is the center-center distance between the two microspheres of radii a_1 and a_2.[15]

The dielectric properties of the nanoparticle 'film' were calculated using the following two mixing rules taken from Dagastine, et al., in which the weighting variable is nanoparticle volume fraction. Note that different expressions are used for zero and non-zero frequency terms in the dielectric spectra.[25] In these equations, $\varepsilon(\omega)_i$ is the frequency-dependent dielectric permittivity of material *i* at frequency ω and ϕ_i is the volume fraction of component *i* (in this system either polystyrene or water) in the film. For the nanoparticle coating, $\varepsilon_{mixture}$ is equal to ε_4 in the Hamaker expression of Equation 4.2.

$$\varepsilon(0)_{mixture} = \sum_{i=1}^{k} \phi_i \varepsilon(0)_i \tag{4.4}$$

$$\left(\frac{\varepsilon(\omega)-1}{\varepsilon(\omega)+2}\right)_{mixture} = \sum_i \phi_i \left(\frac{\varepsilon(\omega)-1}{\varepsilon(\omega)+2}\right)_i \tag{4.5}$$

We assumed that the film thickness, *b*, to be 23 nm for the sulfate latex particles (the diameter of a single nanoparticle) and the volume fraction of nanoparticles used was based on the observed number density of adsorbed nanoparticles observed at each given pH value. Specifically, these are 0.15 at pH 2.0 and 0.1 at pH 3.0. The amidine latex nanoparticle films were estimated to be 90 nm in thickness (approximately four nanoparticle diameters), based on approximations from the SEM images, with a volume fraction of 0.6 (assuming the spheres were nearly uniform and approximately random close-packed).

The electrostatic interaction energy between the two microspheres is calculated using the following expression of Bell et al. which is based on a linear superposition of potentials.[108] Although strictly valid for gap widths greater than several Debye lengths, Bell et al. state that the error in the predicted energy at a separation of one Debye length for cases where the absolute surface potentials are less than 100 mV does not exceed 10%, which is sufficiently accurate for our purposes.[63, 108]

$$E_{132}(l) = 4\pi\varepsilon\varepsilon_0 \left(\frac{k_B T}{e}\right)^2 Y_1 Y_2 \frac{a_1 a_2}{(l + a_1 + a_2)} e^{-\kappa l} \tag{4.6}$$

For the electrostatic equation, $\varepsilon\varepsilon_0$ is the dielectric constant of the medium, Y_i is the effective dimensionless surface potential of sphere *i* (expressions provided by Bell et al.[30]) *l* is the distance of closest approach between the two spheres, and κ is the inverse Debye length.[63] We assume the surface potentials of the microspheres to be equal to the zeta potentials reported in Table 1.

Shown in Figure 4-17 is the distance-dependent Hamaker 'constant', $A_{132}(l)$, calculated between two planar silica half-spaces in water at pH 2.0 and coated with the sulfate nanoparticles. It is interesting that unlike a monotonically decreasing function, as normally arises from retardation effects, the film actually cause a peak in the Hamaker constant. Similar results were also observed by Dagastine et al. when the volume fraction of the solids the film was small.[25]

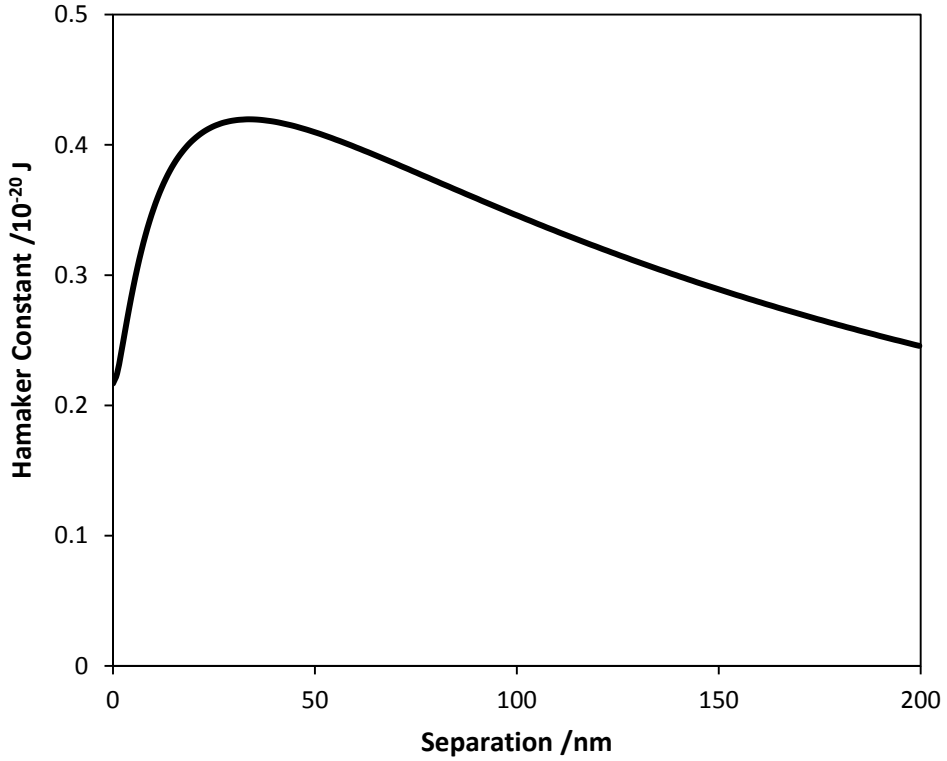

Figure 4-17: Hamaker constant vs. separation distance for two silica microspheres coated with a layer of sulfate latex nanoparticles, at pH 2.0.

The DLVO interactions between two 1.0 μm silica microspheres, uncoated as well as with sulfate latex or amidine latex, are shown in Figure 4-18 for pH 2.0 and 3.0. The plots of the interaction energy are in units of k_BT versus the separation distance. In each plot, zero separation is defined as the point of closest possible approach between the particles.

For the uncoated spheres, no repulsion is predicted at either pH, which is fully consistent with the stability behavior presented in the Results section. By comparison, for both the amidine and sulfate nanoparticles, the interaction is mainly repulsive and strong at both pH values. (For the sulfate nanoparticles, a peak in the repulsive energy is predicted very close to contact.) While these profiles are clearly consistent with the stability observed with the amidine nanoparticles, they cannot explain the flocculation that was observed with the sulfate nanoparticles.

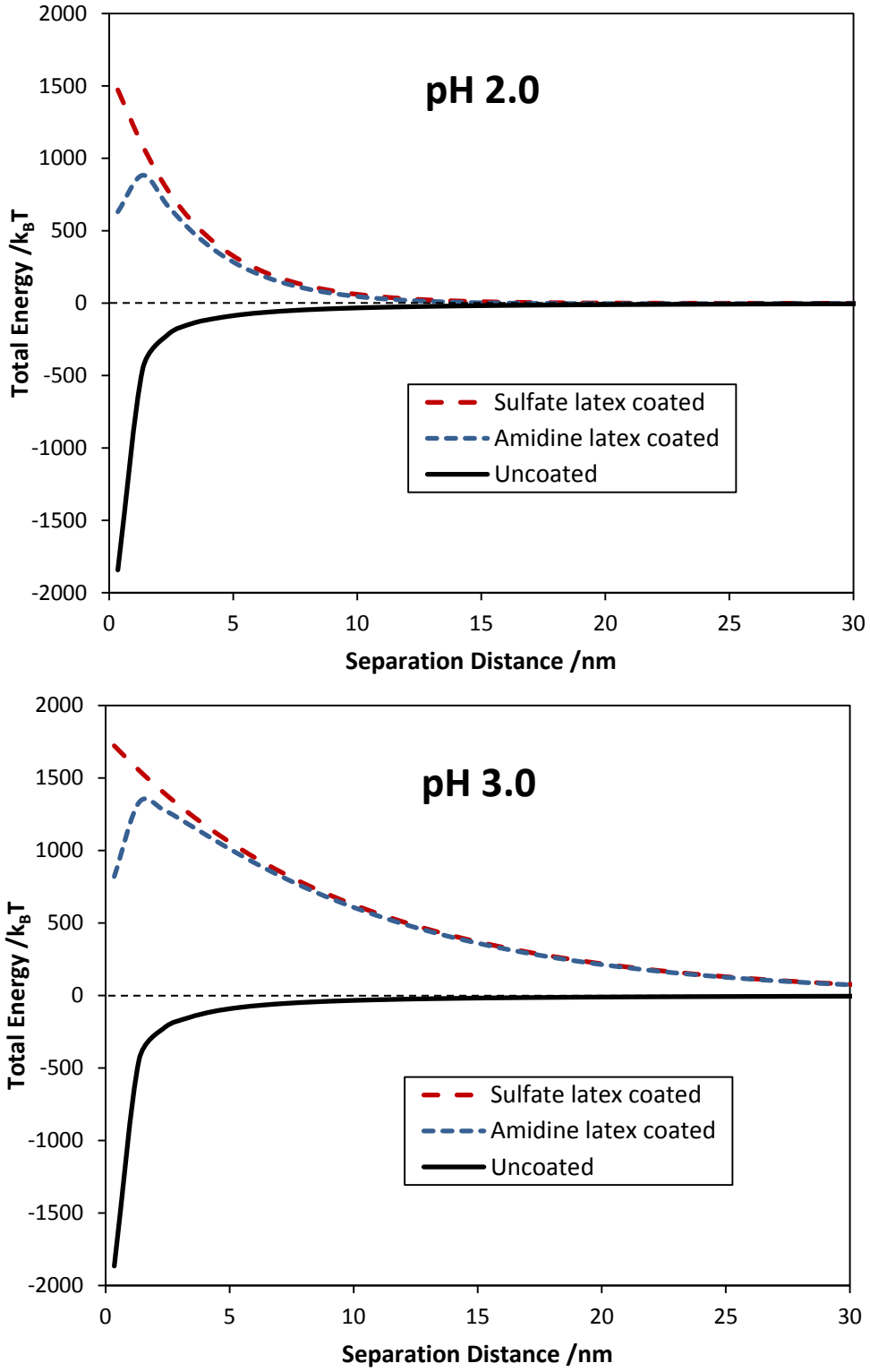

Figure 4-18: Interaction energy between 1.0 µm silica spheres at pH 2.0 and 3.0.

These model results clearly indicate that treating the adsorbed layer of nanoparticles as a continuous film is not appropriate, at least not for the sulfate system. Specifically, for both the

sulfate and amidine systems, having the charge distributed evenly over the outer surface of the coating creates a strong electrostatic repulsion that would effectively prevent aggregation. In other words, while the stabilizing effect of the amidine particles is correctly predicted, the unstable nature of the sulfate nanoparticle-coated microspheres is not.

One possible reason for this model fails for the sulfate system is the patchiness of the nanoparticle layer. As shown in Figure 4-14, even at pH 2.0, the surface coverage by the nanoparticles was only roughly 24%. Thus it is possible, even likely, that relatively 'bare' spots of could exist on each microsphere (similar to the micrographs in Figure 4-10 and Figure 4-13) and that the random Brownian motion of the microspheres would allow such spots to eventually align, leading to flocculation.

The interaction of heterogeneous surfaces has been studied previously by several different researchers. In systems where the average surface or zeta potential over the whole surface of a colloidal particle would indicate a sufficiently repulsive force to prevent aggregation or deposition, it has been shown that attraction and deposition still occurs.[109-112] This is typically attributed to heterogeneities in the surface charge, with surface patches that exist where attractive forces dominate over the surface-average repulsion, leading to particle deposition, as the local surface forces can vary greatly from attractive to repulsive depending on the orientation of the interacting surfaces.[109, 113]

Song et al. has shown theoretical colloid deposition rates in relation to the ionic strength of solution and the standard deviation of the local surface potential over a surface. At an ionic strength of 10 mM, the deposition rate on a surface with a standard deviation of 5.0 mV is over an order of magnitude greater than a homogeneously charged surface, and increasing the deviation to 12.5 mV increased the rate to over two orders of magnitude greater than the homogeneous surface.[114]

This influence of the charge distribution has been developed into analytical equations to calculate electrostatic interaction potentials while accounting for non-uniform charge distribution.[115] Subsequent force measurements by Thwar and Velegol indicated a significant reduction in the attractive force between latex microspheres with the addition of the polyelectrolyte NaPSS.[116] This reduced attraction was attributed to adsorption of NaPSS onto weakly-charged regions of the latex surfaces (which had been determined to have a degree of charge nonuniformity). Stability curves (using transmittance data from UV/Vis spectroscopy) for latex microspheres shown by Feick et al. indicate a strong dependence on the surface charge heterogeneity of the behavior of the suspended microspheres. The bare latex particles had highly negative zeta potentials (-123±2 mV) with large standard deviations (103±39 mV), yet were unstable.[21] The addition of NaPSS to the solution yielded far more stable particles, with the stability of the particles being orders of magnitude greater than the bare latex over the same period of time. There, the zeta potential remained highly negative (-113±3 mV) while the standard deviation was greatly reduced (21±17 mV).[21]

Model calculations have shown that planar surfaces[117] and spheres[113] with heterogeneous surface charge distributions can exhibit substantial attraction, even when the net surface charge would otherwise indicate strong repulsion. In the case of spheres, the modeling of Holt and Chan demonstrated that, depending on the orientation of the heterogeneities of one sphere relative to another, attractions can develop over effective ranges greater than that of the van der Waals force. In particular, a system with a net surface charge of 25 mV and a heterogeneous charge distribution would exhibit an energy barrier on the order of 1000 kT. By changing the distribution to a heterogeneous periodic form, this energy barrier could be almost completely eliminated.[113]

Still, the distribution of charge on spheres due to nanoparticle adsorption would not be a regular periodic pattern. It has been demonstrated experimentally that similar long range attractions can be produced with net neutral charged spheres, which have an irregular, disordered distribution of charge.[118] Silbert et al. showed that a relatively small percentage of charge domains contributing to the interaction, as low as 5%, was required to produce the observed attractions. Clearly, there is a strong dependence of surface interactions on the distribution of charge, and in comparison of the sulfate latex and amidine latex adsorption experiments, the sphere charge distribution with sulfate latex nanoparticles on the surface would be significantly more heterogeneous.

With respect to particle adsorption, the work of Santore and coworkers has shown that even comparatively small densities of heterogeneous surface patches can lead to large degrees of particle adsorption on surfaces.[110, 111] In these experiments, cationic patches 10 nm in size were placed on negatively charged silica substrates, producing a surface that was negatively-charged on average but containing randomly distributed attractive patches. When a solution containing negatively-charged silica microspheres was flowed over the surface, deposition occurred as long as the density of attractive patches on the surface exceeded a critical value. The magnitude of this critical patch density decreased with increasing Debye length, and could be as low as that corresponding to 10% coverage.[110, 111]

With the amidine nanoparticles, because the degree of surface coverage was so much larger, it is postulated that the number of bare patches present was much smaller than with the sulfate nanoparticles (see Figure 4-13). In addition, the multilayer coverage by the amidine nanoparticles would further inhibit any bare patches that were present from actually coming into contact.

4.5 Conclusions

An experimental study was performed to understand the ability of highly-charged nanoparticles to stabilize weakly-charged microspheres. It was found that both positively-charged amidine latex nanoparticles and negatively-charged sulfate latex nanoparticles significantly increase the magnitude of the zeta potential of weakly-charge silica microspheres at

low pH (i.e., near the IEP of silica). Specifically, with both nanoparticles, the magnitude of the zeta potentials was above 40 mV, which was the critical value needed to stabilize bare silica microspheres. Nonetheless, while addition of the amidine nanoparticles produced stable silica dispersions at all pH values studies, addition of the sulfate nanoparticles resulted in no noticeable change in stability. This finding clearly indicated that zeta potential alone is not sufficient for predicting stability.

Adsorption tests showed that the amidine nanoparticles adsorbed at a substantially higher degree than the sulfate ones. Specifically, the amidine nanoparticles produced multilayer coverage with adsorbed densities (# particles/area) that were roughly three times that of the sulfate nanoparticles. While the cause of this difference in adsorption behavior is not completely understood, the much larger polydispersity of the amidine nanoparticles could be a contributing cause.

A simplified model calculating the electrostatic and van der Waals forces between the nanoparticle-coated microspheres in which the adsorbed layer was treated as a continuous film could not explain the stability behavior, as the predicted electrostatic barrier to aggregation was orders-of-magnitude too large to allow aggregation. Instead, it is speculated that the relatively low level of surface coverage by the sulfate nanoparticles (about 24%) could allow uncoated patches to exist on the surfaces, which would align during random encounters.

These results indicate that highly-charged nanoparticles are capable of stabilizing weakly-charged microspheres provided the degree of adsorption is sufficiently large that uncoated patches are eliminated.

Chapter 5: Adsorption and Stabilizing Effects of Highly-Charged Latex Nanoparticles in Dispersions of Weakly-Charged Silica Colloids

This chapter consists of work that has been published. Reprinted with permission from: D. Herman, J. Y. Walz, Adsorption and Stabilizing Effects of Highly-Charged Latex Nanoparticles in Dispersions of Weakly-Charged Silica Colloids, J. Colloid Interface Sci., 2014, DOI: 10.1016/j.jcis.2014.11.022.

An experimental study was undertaken to determine the effectiveness of using highly charged nanoparticles as stabilizers for colloidal dispersions. The specific systems used here involved cationic (amidine) and anionic (sulfate) polystyrene latex nanoparticles with an approximate diameter of 20 nm and silica microparticles of diameter 1.0 μm, and experiments were conducted at the isoelectric point of the silica. It was found that while both types of nanoparticles adsorbed to the silica microparticles and increased the zeta potential to values where stability was expected, long term stability was not achieved, even at bulk nanoparticle concentrations as high as 0.5% vol. It is theorized that the incomplete coverage of the microparticles by the nanoparticles (i.e., surface coverage never exceeded 50%) allowed either direct contact between bare patches of the underlying microparticles or, alternatively, for nanoparticles adsorbed on one microparticle to bridge to bare spots on a neighboring microparticle.

5.1 Introduction and background

Control of the stability of colloidal dispersions, such as through the addition of electrolytes or polymeric stabilizers, remains a topic of great practical importance. As such, developing novel types of stabilizers and flocculants that allow fine tuning stability, or even reversibly controlling stability, is still of interest in many fields.[31-34]

Over the past 20 years or so, control of stability using highly charged nanoparticles has received growing interest. For example, numerous researchers have shown that otherwise stable dispersions of micron-sized particles can be flocculated using the depletion interaction that arises upon the addition of highly-charged, negatively-adsorbing nanoparticles.[39, 47, 119-121] One attractive feature of this approach is that because the nanoparticles do not deposit onto the surface of the microparticles, and furthermore because this depletion flocculation primarily occurs in shallow, secondary energy wells, the flocculation is potentially reversible upon dilution.

More recently, various researchers have investigated a phenomenon termed nanoparticle haloing in which highly-charged nanoparticles weakly adsorb to microparticles that are near their isoelectric point (IEP).[8, 53, 55, 56] The additional repulsive force produced by this haloing

effect has been predicted to be strong enough to stabilize dispersions of such microparticles.[35, 59, 60, 102, 122] Other researchers have shown that in some systems, the repulsive force actually arises from strong, irreversible deposition of the nanoparticles as opposed to the weak adsorption suggested in the nanoparticle haloing phenomenon.[63, 84]

In previous work, the authors of this paper investigated the ability of polystyrene latex nanoparticles that were either positively (amidine) or negatively (sulfate) charged to stabilize dispersions of weakly-charged silica microparticles.[123] The results indicated that both nanoparticle types adsorbed to the surface (the amidine in greater quantities than the sulfate latex), and significantly increased the effective zeta potential of the microparticles beyond the point where the silica alone would be electrostatically stable. In suspensions containing the amidine latex nanoparticles, the silica suspensions were quite stable. However, the experiments also showed that the sulfate latex nanoparticles could not reproducibly stabilize the same suspensions at any of the concentrations used (up to 0.5% vol.). The authors concluded that though the sulfate latex provided a net increase in the zeta potential, the lower degree of adsorption led to a patchy surface that was ineffective in preventing flocculation of the Brownian particles.

While this prior work clearly demonstrated the possibility of stabilizing weakly-charged microparticles using highly-charged nanoparticles, there were nonetheless numerous issues that remained unresolved. For example, in the previous work, while adsorption of both the amidine and sulfate nanoparticles resulted in significant increases in the zeta potential of the silica microparticles, only with the amidine nanoparticles was stability achieved. Furthermore, the degree of adsorption of the amidine nanoparticles, as judged by adsorption onto flat silica slides, appeared to be substantially greater than that of the sulfate nanoparticles, even though the absolute magnitude of the zeta potentials of the two types of nanoparticles in the bulk were similar and the adsorption tests were performed at the IEP of the silica slides.

The goal of this present work was to address some of these unresolved issues in order to definitively answer the question of whether relatively low concentrations of highly-charged latex nanoparticles can serve as effective stabilizers of weakly-charged silica microparticles. In the present study, measurements of zeta potential, degree of adsorption, and dispersion stability were performed using amidine and sulfate nanoparticles that had been thoroughly cleaned using dialysis with an ion exchange resin. The purpose of the cleaning step was to ensure that any observed stabilizing effects arose from the nanoparticles themselves and not any surfactants or other additives that could be present in the suspension.

In addition, adsorption measurements of the amidine and sulfate nanoparticles were performed using the silica particles themselves at the same solution conditions, specifically pH, as those used in the stability tests. This was done to avoid possible effects of differences in geometry or IEP resulting from the use of flat silica slides, as was used in the prior work

5.2 Materials and methods

5.2.1 Overview of experiments

Three different types of experiments were performed in this study to better understand the impact of the amidine and sulfate nanoparticles on both the interparticle forces and the stability behavior of the silica microparticles. First, a set of stability tests were performed over a range of nanoparticle concentrations, ranging up to 0.5% vol. The experiments with suspensions containing both silica microparticles and polystyrene nanoparticles were carried out at the isoelectric point of the silica microparticles such that the microparticles were inherently unstable due to insufficient net surface charge. Second, zeta potential measurements were performed to understand how the adsorption of nanoparticles changes the surface charge of the silica microparticles as a function of nanoparticle concentration. Finally, adsorption experiments were performed to determine the degree of adsorption of the nanoparticles on the silica microparticles at the silica IEP.

5.2.2 Materials

All the experimental solutions were prepared using water that had a resistivity of 18.2 MΩ-cm. The water was filtered by a RiOs 8 reverse osmosis system (Millipore, catalog #ZR0S6008Y) and subsequently treated by a Barnstead EASYpure II UV Ultrapure water system (Thermo Scientific, catalog #D7401). Fused silica slides (Corning 7980 fused quartz silica, item #3x1x1mm) were obtained from TGP (Technical Glass Products, Inc., Painesville, OH). The silica microparticles used were supplied at a concentration of 10% w/v in water with a specified average diameter of 1.0 μm (Polysciences, Inc., Warrington, PA, catalog #24326-15). IDC brand polystyrene latex nanoparticles (Life Technologies, Carlsbad, CA) were used. The particles had a specified diameter of 0.02 μm, and experiments were done with both sulfate and amidine latex (catalog #S37200, and catalog #A37309, respectively). The titrants used were hydrochloric acid (Optima grade, Fisher Scientific, catalog #A466-250) and sodium hydroxide (1.0 N Mallinckrodt Standard grade, catalog #4693-60), each diluted to 0.1 M using pure water.

5.2.3 Nanoparticle solution preparation

The nanoparticle suspensions used in these experiments were dialyzed to remove any excess ions from the solution. The suspensions were made by diluting the stock solution with the purified, deionized water to a concentration of 0.5% vol. The solutions were prepared in 20 ml scintillation vials (Wheaton Science Products Inc., catalog #986540), which had been rinsed with ethanol and deionized water. Dialysis of the suspensions was performed by adding ion-exchange resin (Bio-Rad, catalog #143-7425) to each vial to the manufacturer specification of 5 g resin per 100 mL of solution. The vials were gently mixed for 4 hours using a continuous sample rotator that was operating at 4 rpm to slowly invert the samples and redistribute the resin. At the end of the dialysis period, the nanoparticle solutions were decanted from the resin into clean vials.

5.2.4 Zeta potential measurements

Measurements of the zeta potential of silica microparticles and the two types of latex nanoparticles (separately) were obtained using a Zetasizer Nano ZS (Malvern Instruments Ltd, Worcestershire, UK), with measurements performed in disposable folded capillary cells (catalog #DTS1060C). Prior to the measurements, the cells were rinsed first with pure ethanol, then DI water, before being dried with ultra-high purity nitrogen. The measurements on the latex nanoparticles were performed as single measurements at a given pH. For the silica microparticles, multiple measurements were taken across a large pH range in a single experiment in order to determine the IEP. In this experiment, the Malvern MPT-2 Autotitrator was used to automatically adjust the pH of the sample.

A Micro-Electrophoresis Apparatus Mk II (Rank Brothers Ltd., Cambridge, England) was used to measure the effective zeta potential of the silica microparticles in suspensions of nanoparticles. Nanoparticle concentrations used for these measurements were equal to those used in the stability measurements, while the microparticle concentration was more dilute (approximately 0.01% vol.) in order to observe individual silica particles in the cell. The zeta potential was determined from the electrophoretic mobility, which was calculated from the visually-measured particle velocity.

5.2.5 Stability

The stability of the silica microparticle dispersions was determined from visual observation. Suspensions of the desired concentrations of latex nanoparticles (0-0.1% vol. of either amidine or sulfate) were prepared and titrated to the desired pH of 3.5 (the IEP of the SiO_2) using 0.1 M HCl before being transferred to the cuvettes. A quantity of silica microparticles was then added to the suspensions to reach 0.1% vol. microparticles. The cuvettes were capped, inverted to evenly distribute the particles, and briefly sonicated before beginning the experiment. Photographs of the set of samples (placed against a black background for maximum contrast) were taken at regular intervals over a total observation period of six hours.

5.2.6 Nanoparticle adsorption and size distribution

In order to better understand the adsorption behavior of the latex nanoparticle on silica microparticles, experiments were performed to directly visualize the adsorbed particles using scanning electron microscopy (SEM). An approximately 0.01% vol. suspension of 1.0 μm silica microparticles was prepared and titrated to pH 3. Droplets of the suspension were spread on the surface of cleaned silica slides and were allowed to dry thoroughly. This provided a thin layer of microparticles (a monolayer or less over most of the surface) on the surface which were sufficiently attached as to remain in place through gentle soaking and rinsing in nanoparticle suspensions.

Dispersions of nanoparticles, made using the nanoparticles that had been cleaned using ion exchange resin, were prepared at the desired concentrations (0.5% vol. and lower), and briefly sonicated. The nanoparticle solutions were titrated to the desired pH of 3.5 using 0.1 M

HCl, as was a blank (nanoparticle-free) solution that was used as a rinse solution. The prepared microparticle-coated slides were gently rinsed with the particle-free solution before being immersed in the nanoparticle suspensions for 20 minutes. The slides were then removed from the nanoparticles and once again very gently dipped in the pH-adjusted rinse solution to rinse away any excess particles that had not adsorbed to the surface. The slides were allowed to air dry, after which the surfaces were sputter-coated with a 1-2 nm layer of gold before being imaged using SEM.

A separate set of adsorption studies were performed to determine the size distribution of the adsorbed latex nanoparticles. For these measurements, the adsorption was done onto flat silica slides to permit ease of viewing. In addition, the nanoparticle concentrations were low enough (0.01% vol. for sulfate, 0.0005% vol. for amidine) that there was sufficient space between adsorbed particles to easily distinguish the particles and evaluate the sizes. Plain silica slides were sonicated in ethanol, rinsed clean with pure water, dried with compressed ultra-high purity nitrogen, and then immersed in the nanoparticle solutions for 15 min before being rinsed with the blank solution.

To determine the size distribution of the adsorbed nanoparticles, the resulting SEM images were processed using the open source ImageJ software[124]. Each image was loaded into the software and the contrast threshold was adjusted to produce a binary black and white image of the particles. The black and white was inverted so that the particles would show as black on a white background. The particle analysis function was used to evaluate the area of each particle in the image. Each measured particle area was assumed to be the cross-sectional area of a spherical particle, from which the particle diameter could be calculated.[*]

5.3 Results

5.3.1 Zeta potential

Figure 5-1 shows the zeta potential for the 1.0 μm SiO_2 spheres used in the stability experiments as a function of pH. The spheres are highly negatively charged above approximately pH 4.0. The IEP was determined to be approximately pH 3.5, which was the pH used in the stability experiments. Below the IEP, the particles acquire a weak positive charge.

[*] See Appendix B1 for more information.

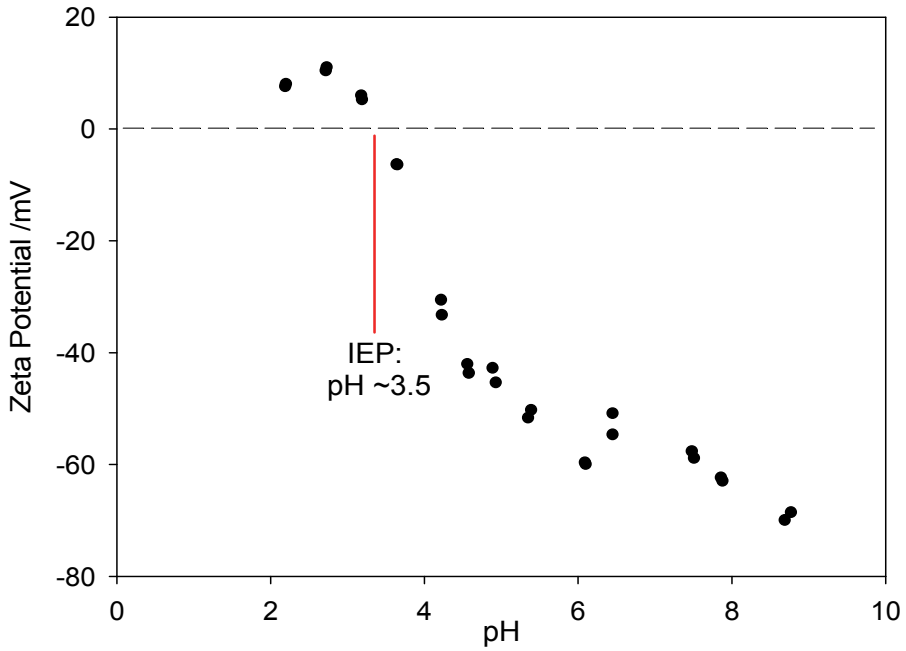

Figure 5-1: Zeta potential as a function of pH for the 1.0 μm silica microparticles. The ionic strength of the dispersions was not fixed.

Zeta potential measurements of the nanoparticles themselves at pH 3.5 gave values of -40.5±16 mV for the sulfate nanoparticles and +47.2±18.6 mV for the amidine nanoparticles, where the variability values are the standard deviations obtained using a minimum of 12 individual measurements.

5.3.2 Stability

Figure 5-2 shows the stable and unstable pH ranges for these silica microparticles. With no added nanoparticles, the dispersion is unstable from pH 3.4 to pH 3.6, which is in agreement with the zeta potential results presented in Figure 5-1 in which the IEP was determined to be approximately pH 3.5. As with the zeta potential measurements, the ionic strength of the dispersions was not fixed in these samples. Below pH 3.3 the microparticles were stable, presumably because of the small but finite positive charged observed in the zeta potential results. Though not shown, the microparticles remained stable until the pH was below approximately pH 2.5, at which point flocculation occurred, presumably because the ionic strength became sufficiently large to screen the electrostatic repulsion between the particles. It is also important to note that the silica microparticles do sediment slowly even when stable. As seen in Figure 5-2, the stable suspensions exhibit a very sharp boundary between the settling particles and the clear supernatant, while the unstable suspensions have no such boundary.

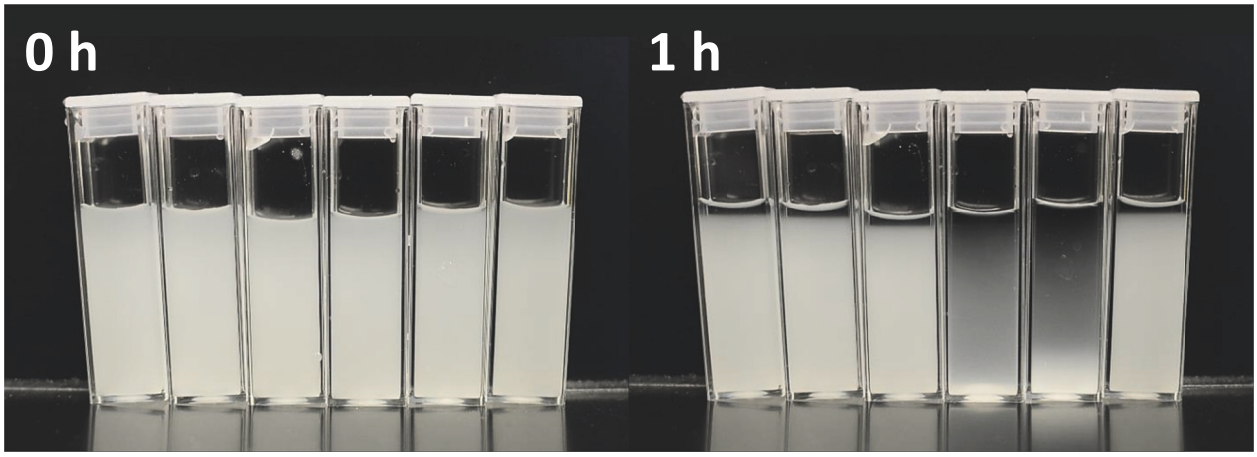

Figure 5-2: Flocculation of 1.0 μm silica spheres. Samples (L to R): pH 2.9, 3.1, 3.2, 3.4, 3.6, 3.9. The unstable range is approximately pH 3.4 to 3.6.

The images in Figure 5-3 show 0.1% vol. silica suspensions with added amidine latex nanoparticles at concentrations ranging from 0 to 0.5% vol. over the course of 6 hours. All the samples were at the IEP of the microparticles, pH 3.5. The higher concentrations of nanoparticles give the solution a blue color, which is unrelated to the stability of the microparticles in the suspension. The 0% and 0.001% vol. samples were clearly unstable and began flocculating in a time of less than one hour and the microparticles completely settled out of the suspension within two hours. At concentrations of 0.01% vol. and greater the flocculation proceeded much more slowly, such that complete sedimentation was not achieved until six hours.

These experiments clearly indicate that while the amidine nanoparticles may be capable of slowing the flocculation, they were nonetheless incapable of stabilizing the suspension, even at nanoparticle concentrations as high as 0.5% vol. This is a significant difference compared to previous work which showed that amidine nanoparticles at a concentration of 0.5% vol. were capable of providing long-term stability to similar dispersions.[123] This difference is addressed further in the Discussion section.

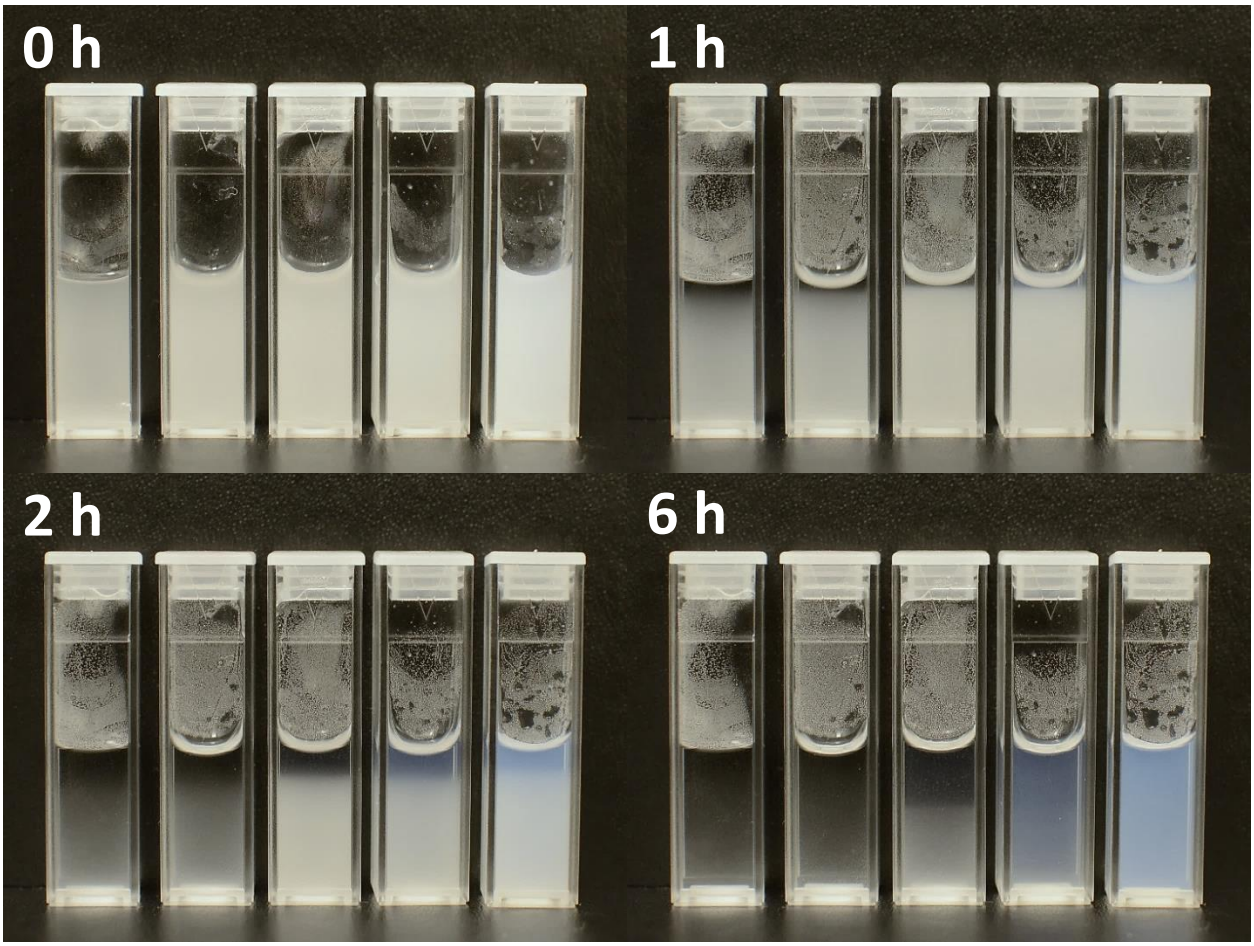

Figure 5-3: Stability of 0.1% vol. 1.0 µm silica microparticle dispersions in increasing concentrations of amidine latex nanoparticles (20 nm diameter). Samples were at pH 3.5 (SiO_2 IEP). Nanoparticle concentrations by volume were (L to R): 0%, 0.001%, 0.01%, 0.1%, 0.5%.

For completeness, these stability tests were repeated using sulfate nanoparticles at the same concentrations used with the amidine nanoparticles. Having not observed any stability in previous work using sulfate nanoparticle concentrations of 0.1, 0.5 and 1.0% vol.[123], there was no expectation of stability with these dialyzed nanoparticles. Figure 5-4 shows photographs of the silica dispersions with added sulfate latex nanoparticles at concentrations ranging from 0 to 0.5% vol. As expected, all samples with sulfate latex concentrations below 0.5% vol. flocculated in less than two hours, while the 0.5% vol. dispersion completely flocculated and sedimented within three hours.

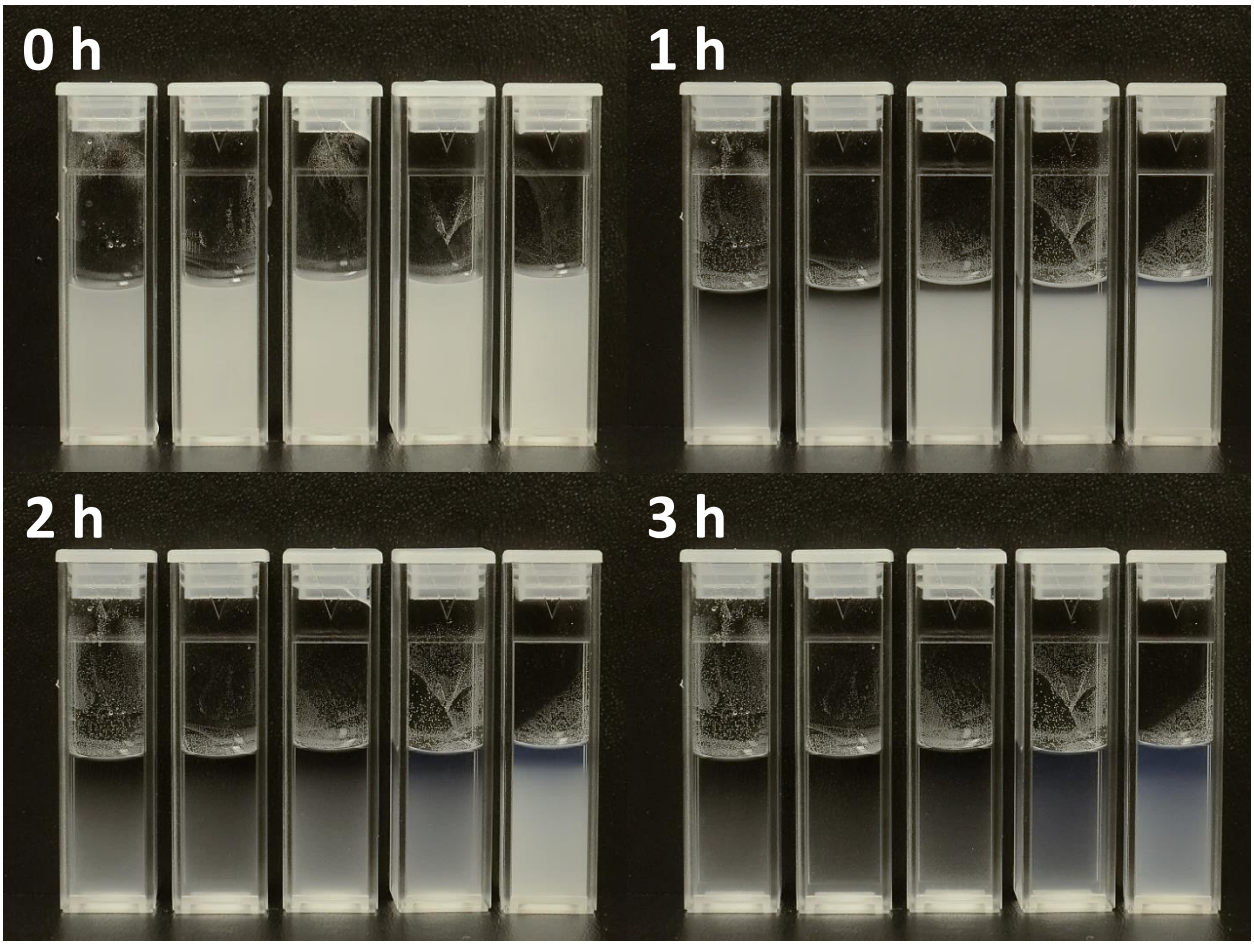

Figure 5-4: Stability of 0.1% vol. 1.0 μm silica microparticles with sulfate latex nanoparticles. Nanoparticle concentrations by volume were (L to R): 0%, 0.001%, 0.01%, 0.1%, 0.5%.

To determine how the zeta potential of the microparticles changes as the concentration of nanoparticles increases, electrophoresis measurements were performed using the Rank Bros. Microelectrophoresis Apparatus MKII. Table 5-1 shows the zeta potentials of the 1.0 μm silica spheres at a range of concentrations of added sulfate and amidine nanoparticles. As with the flocculation experiments in Figure 5-3 and Figure 5-4, the zeta potential measurements were carried out at pH 3.5, the IEP of the microparticles. Both the amidine latex and sulfate latex nanoparticles show a steady increase in the absolute zeta potential with increasing nanoparticle concentration.

Table 5-1: Zeta potentials (mV) for 1.0 μm silica microparticles in increasing concentrations of latex nanoparticles at pH 3.5 (SiO_2 IEP). The error values reported are the standard deviation of each measurement. Note that the value reported for the 0% vol. sample was measured using the Zetasizer Nano ZS, while the other values were measured using the Rank Brothers Mk II Micro-Electrophoresis apparatus.

Bulk nanoparticle conc., % vol.	Amidine	Sulfate
0%	+3.2±4.0	+3.2±4.0
0.001%	+9.2±2.5	-4.1±0.7
0.01%	+29.0±20.8	-17.4±10.1
0.1%	+37.6±16.1	-23.0±5.8
0.5%	+47.6±13.7	-40.8±21.0

Although there is significant variability in the data, it does appear that the amidine nanoparticles lead to larger absolute zeta potentials, on average, than the sulfate nanoparticles. For example, a sulfate latex concentration greater than 0.1% vol. is necessary to exceed the magnitude of the zeta potential observed with the 0.01% vol. amidine suspensions. This observation may explain the behavior observed in the flocculation experiments. Specifically, though no stability was achieved with either nanoparticle type, the dispersions containing amidine nanoparticles at or above 0.01% vol. showed a much lower flocculation rate, as did dispersions containing sulfate nanoparticles at 0.5% vol.

It is important to note that the magnitude of the zeta potentials reported in Table 1 greatly exceed those necessary for stability in the dispersions containing only microparticles. Specifically, looking at the results presented in Figure 5-1 and Figure 5-2, it is seen that dispersions containing positive zeta potentials as low as +10 mV were stable. By comparison, the dispersion containing 0.5% vol. amidine nanoparticles at the IEP of the silica, which had a measured zeta potential of +47.6±13.7 mV, was unstable. This result confirms the conclusion from our earlier paper that with these systems containing added nanoparticles, the zeta potential is not a reliable predictor of dispersion stability.

5.3.3 Nanoparticle adsorption and particle size

The images in Figure 5-5 show the characteristics of the nanoparticle adsorption of amidine latex nanoparticles directly on the silica microparticles that were used in the stability experiments. The bulk nanoparticle concentrations in the adsorption experiments are 0.001%, 0.01%, 0.1%, and 0.5% vol. (identical to the concentrations used in Figure 5-3). As the nanoparticle concentration of the suspension increases, we see a clear increase in the number of particles that are adsorbed to the silica microparticles. There is some noticeable variation between individual microparticles, even in a single image. This is most visible at the lower concentrations, particularly in areas where there are multiple layers of silica spheres, as well as

locations where the microparticles are in close contact with each other. This could result from the fact that the microparticles were dried onto a slide surface rather than having been freely dispersed in a nanoparticle suspension. Any underlying spheres would therefore be less exposed to the nanoparticles.

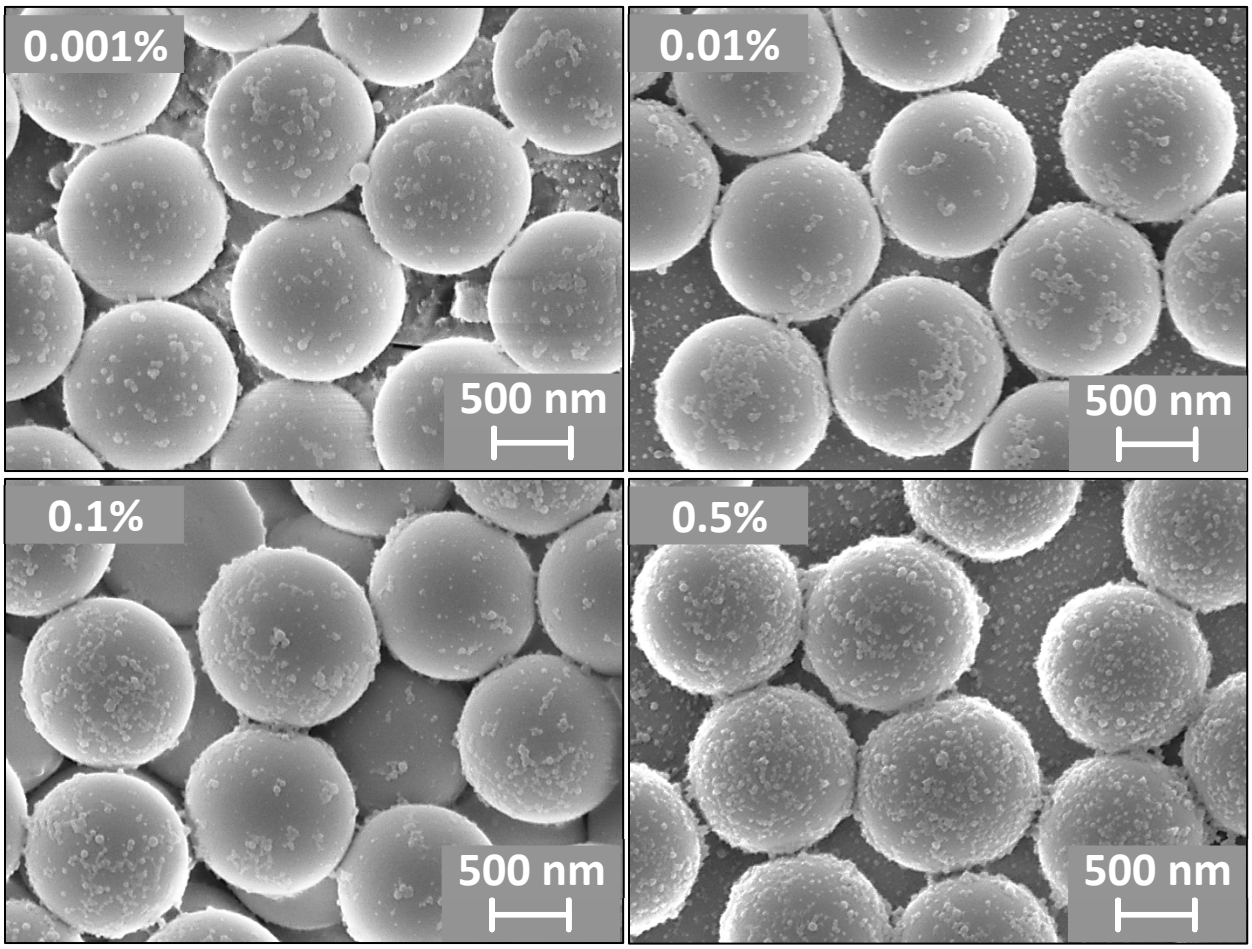

Figure 5-5: SEM micrographs of 1.0 μm silica microparticles with adsorbed amidine latex nanoparticles. The degree of adsorption increases with increasing bulk nanoparticle concentration.

Overall, the adsorption experiments are consistent with the zeta potential measurements in Table 5-1. Even at the lowest measured concentration (0.001% vol.) there is a very noticeable amount of nanoparticles adsorbed onto the silica, enough to give the almost negligibly charged silica microparticles (zeta potential of +3.2 mV at pH 3.5 with no added nanoparticles) a weak positive zeta potential (+9.2 mV). Both the zeta potential and number of adsorbed particles increase with the overall nanoparticle concentration. However, it is important to note that even at the highest bulk concentration of nanoparticles (0.5% vol.), the surface coverage is far from complete. Specifically, based on simply counting the number of nanoparticles in a given area and

assuming that each nanoparticle covers an area equal to its cross sectional area, we roughly estimate the fractional surface coverage to be less than 50%.

Similar adsorption tests were performed using the sulfate nanoparticles and the results are shown in Figure 5-6. As with the amidine nanoparticles, there is a clear increase in density of adsorbed nanoparticles, though the total number of adsorbed nanoparticles is somewhat less. For example, with the 0.5% vol. bulk concentration of sulfate nanoparticles, we estimate the fractional surface coverage to be less than 30%. This is consistent with the zeta potential measurements which showed lower absolute zeta potentials with the sulfate nanoparticles compared to the amidine nanoparticles at equal bulk concentrations. Furthermore, as with the amidine nanoparticles, there are significant gaps between adsorbed particles, with exposed patches of the silica surface in between.

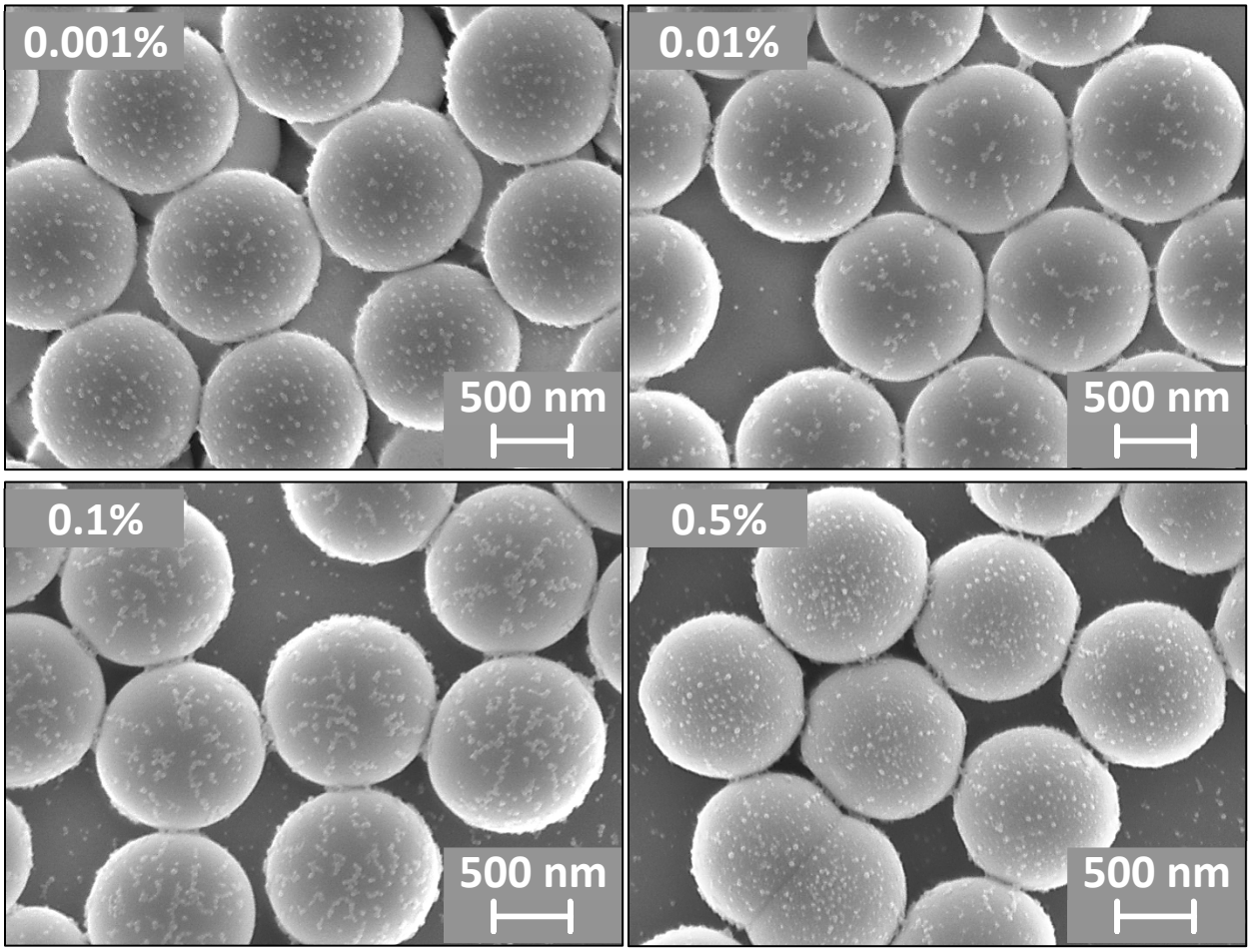

Figure 5-6: SEM micrographs of 1.0 μm silica microparticles with adsorbed sulfate latex nanoparticles. As with the amidine nanoparticles, the degree of adsorption increases with increasing bulk concentration.

The difference between the degree of sulfate and amidine latex nanoparticle adsorption is most apparent at the highest bulk nanoparticle concentration. A higher magnification comparison

between the two (at 0.5% vol.) is shown in Figure 5-7. In both cases, the adsorption is relatively uniform over the microparticle surfaces, but there is a much greater quantity of adsorbed amidine latex particles. In addition, the amidine latex particles appear much more likely to adsorb in clusters, while the sulfate latex largely remain adsorbed as individual particles. This difference is discussed further below in the Discussion section.

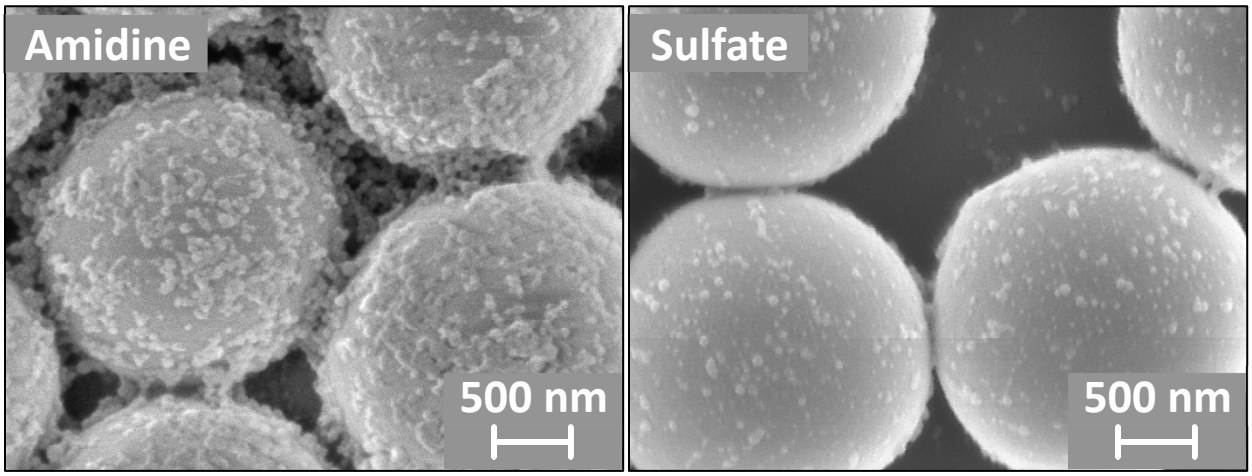

Figure 5-7: Comparison of the degree of adsorption of amidine latex (left) and sulfate latex nanoparticles (right), both at a bulk nanoparticle concentration of 0.5% vol.

5.4 Discussion

The findings presented in the previous section are summarized below.

1. The amidine latex nanoparticles are capable of slowing the flocculation and sedimentation of unstable silica microparticles using nanoparticle concentrations of 0.01% vol. and greater. However, even at the highest nanoparticle concentration used (0.5% vol.), the sample flocculated within six hours.
2. Sulfate nanoparticles were also incapable of stabilizing the silica microparticles at any of the concentrations tested, though the 0.5% vol. sample displayed a lower rate of flocculation
3. The absolute magnitude of the zeta potential of negligibly charged silica microparticles increased steadily with increasing concentrations of added latex nanoparticles. The maximum values observed at 0.5% vol. was +47.6 mV for the amidine latex and -40.8 mV for the sulfate latex.
4. SEM micrographs of silica microparticles which had been exposed to nanoparticle suspensions (at the silica IEP of 3.5) showed increasing levels of adsorption as the bulk nanoparticle concentration increased. The samples in which a reduction in flocculation rate was observed had relatively high nanoparticle coverage, though not high enough to eliminate exposed patches of silica (i.e., surface coverage never exceeded 50%).

5. The amidine latex nanoparticles adsorbed in greater quantities than the sulfate latex and appeared more likely to adsorb in groups or clusters.

The differing degrees of adsorption of the sulfate and amidine nanoparticles is difficult to understand, specifically because, as explained above, differences in the magnitude of the electrostatic interaction are not expected to be a significant factor. One explanation considered was that differences in the degree of polydispersity in the size distribution of the sulfate and amidine latex particles could be a cause. The reported mean diameter of the amidine and sulfate nanoparticles are roughly the same, however previous SEM images suggested that the standard deviation of the size distribution for the amidine nanoparticles is larger. For example, could different size fractions show a greater tendency to adsorb?

To test this hypothesis, adsorption tests onto a flat silica slide were performed at the IEP of the slide, which was found to be approximately pH = 2.55. Performing these tests onto a flat slide facilitated ease of viewing and allowed for more accurate size determination. The bulk concentrations of the nanoparticles were adjusted independently to obtain adsorbed nanoparticle densities that allowed easy size determination.

SEM images of the adsorbed sulfate and amidine nanoparticles are shown in Figure 5-8 and show a noticeable difference in size distribution, with the adsorbed amidine nanoparticles appearing to be significantly more polydisperse than the sulfate nanoparticles. It should be noted that the actual number density of adsorbed nanoparticles is not important here, as the bulk concentration of each nanoparticle type has been adjusted to yield adsorbed densities that allow accurate size determination of individual nanoparticles.

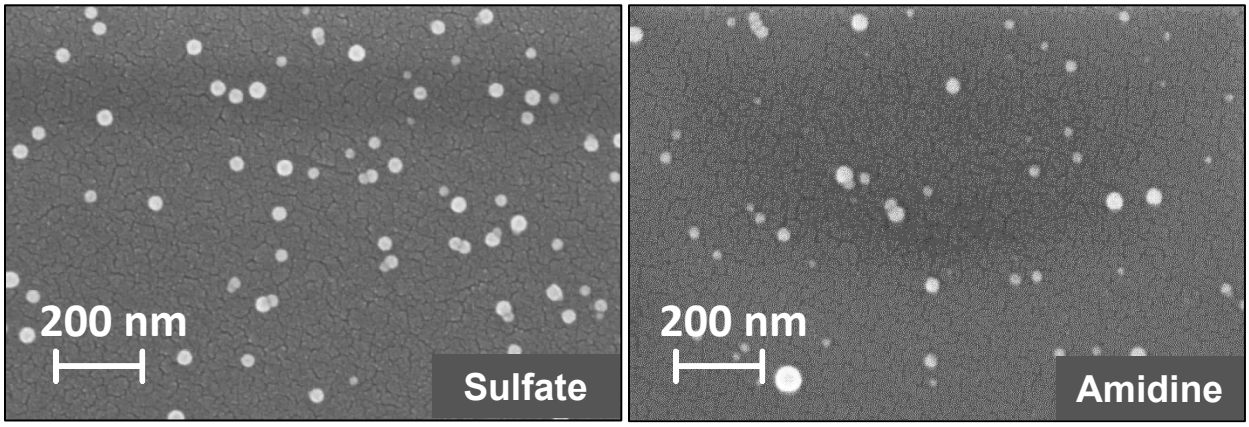

Figure 5-8: Example images used in determining the particle size distribution of adsorbed polystyrene nanoparticles. The nanoparticles were adsorbed onto a silica slide from a solution at a bulk pH of 2.5, which was the measured IEP of the slide.

From these images, histograms of the size distribution of the adsorbed nanoparticles were constructed and are shown in Figure 5-9. In both cases, the average diameters of adsorbed particles were close to the specified diameter for the bulk solution. Specifically, the mean

diameter for the adsorbed sulfate nanoparticles was approximately 24 nm with a standard deviation of 10 nm, while the mean diameter of the adsorbed amidine nanoparticles was 22 nm with a mean diameter of 12 nm. While these values are similar, it is clear that the shape and width of the distributions are notably different, with the sulfate having a more symmetric distribution and the amidine being much more skewed toward smaller sizes, more akin to a log normal distribution. (It should be noted that particles with a diameter less than 5 nm could also be present, however such particles could not be reliably imaged.)

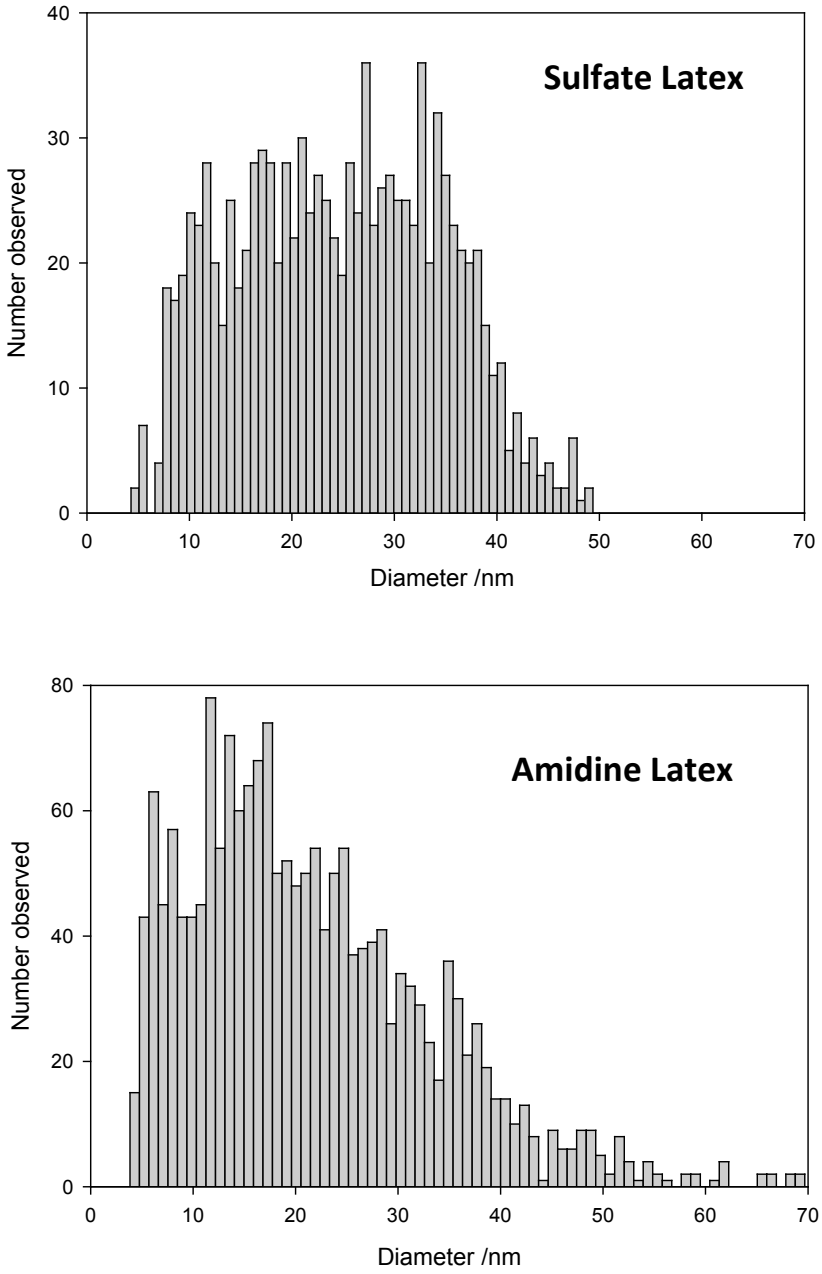

Figure 5-9: Particle size histograms for adsorbed sulfate latex (top) and amidine latex (bottom).

One additional contributing factor related to polydispersity that should be mentioned is that the broader size distribution measured for the amidine nanoparticles allows a greater degree of surface coverage at the jamming limit. Specifically, in the random sequential adsorption (RSA) model, a jamming limit exists were the gaps between adsorbed particles are too small to allow further adsorption.[125] This RSA model assumes that the particles adsorb sequentially and irreversibly, and overlap of adsorbed particles is not allowed. In the case of monodisperse hard spheres, the RSA jamming limit is approximately 55% surface coverage.[126] With charged particles, the maximum surface coverage of the particles depends on the ionic strength of the solution. Specifically, decreasing the ionic strength increases the thickness of the electric double layer and lowers the jamming limit. As an example, experiments by Ko et al. showed that the jamming limit can drop to as low as 10% coverage at ionic strengths below 10^{-5} M.[127]

It has also been shown that a polydisperse size distribution allows for a greater degree of surface coverage, beyond 55%, and even small differences in the size distribution can yield significant changes in the distribution of the adsorbed particles.[128-130] The reason for this increase is that smaller particles are better able to fill in the gaps between larger adsorbed particles, improving the total coverage of the surface. Numerical values from Monte Carlo simulations of polydisperse suspensions showed that for uniform distributions of hard particles, the jamming limit increases to about 60% when the particle radii have a normalized standard deviation, $\bar{\sigma}$ (where $\bar{\sigma}$ is the standard deviation of the size distribution normalized by the mean) of 10%, and a limit of 65% for $\bar{\sigma}$ = 20%. In cases where the particles can interact, the maximum coverage can exceed 70%.[128] Furthermore, the shape of the particle size distribution (e.g. Gaussian, uniform, etc.) can affect the adsorbed coverage, particularly at long time scales.[128] As shown in Figure 5-9, the sulfate and amidine latex distributions show a notably different shape, which could be a contributing factor in the different degrees of adsorption.

Additionally, polydisperse particle systems often lead to differences in the distribution of adsorbed particles versus the bulk suspension. In particular, the smaller particles adsorb preferentially over the larger particles as the jamming limit is approached, leading to an adsorbed layer containing a higher percentage of small particles than that which is present in the bulk.[128-130] In charged particle systems, this preferential adsorption is most significant at high ionic strengths, where the Debye length is significantly shorter and the effective radius of the particle (physical radius plus the effective interaction distance of the charged surface) approaches that of the physical radius. Since the histograms in Figure 5-9 were generated with adsorption layers far less dense than the jamming limit (the samples were made using low concentrations for ease of imaging and analysis), it is likely that the actual distribution of the adsorbed amidine latex nanoparticles is even more skewed towards the smallest particles, which could further explain the different levels of adsorption at the concentrations used in Figure 5-5, Figure 5-6, and Figure 5-7.

It should finally be mentioned that differences in specific chemical interactions between the latex and silica surfaces also contributes to the different degrees of adsorption observed. One

example would be hydrogen bonding between surface groups. However, additional study would be required to determine the exact nature of these interactions.*

Perhaps the most surprising finding of this work is the inability of either type of nanoparticle to stabilize the microparticle dispersions, especially considering the zeta potential values reported in Table 1 and the SEM images shown in Figure 5-5 and Figure 5-6. The fact that flocculation was observed even with zeta potential as large as 40 mV confirms the conclusion made in our earlier paper that with these nanoparticle-covered microparticles, the zeta potential is not a reliable predictor of stability. A similar conclusion has been reached by previous researchers, namely that a nonuniform distribution of surface charge can lead to instability of a dispersion, even when the measured zeta potential is sufficiently high.[117, 131]

It is clear from the SEM images in Figure 5-5, Figure 5-6, and Figure 5-7 that even at the highest nanoparticle coverages (i.e., 0.5% vol. amidine nanoparticles), there is still significant patches of uncoated silica, and it is likely that this patchiness plays a key role in explaining the stability results observed here, especially at the lower nanoparticle concentrations where the surface coverage is relatively small. Specifically, in the aggregation of two microparticles, two possible mechanisms are proposed. In the first, the adsorbed nanoparticles are either mobile or are weakly adsorbed such that the presence or approach of another nanoparticle-coated microparticle results in the creation of larger patches of bare silica that permit aggregation, due to rearrangement of the nanoparticles. In the second mechanism, aggregation occurs via adsorbed nanoparticles on one microparticle essentially bridging to bare spots on a nearby microparticle. It should be noted that these mechanisms are clearly not mutually exclusive, as it is possible that both phenomena occur to some degree.

The fact that the rate of aggregation slows noticeably at the higher concentrations of sulfate and amidine nanoparticles indicates that degree of surface coverage is important. This suggests that desorption of the nanoparticles during interaction of two microparticles is not a significant factor, since such desorption could occur at any degree of surface coverage.

In previous work Ji et al. used colloidal probe atomic force microscopy to measure the interaction force between a silica particle and silica plate in solutions of highly charged sulfate latex nanoparticles as a function of pH and nanoparticle concentration[63]. At pH values near the silica IEP, these authors found that deposition of the sulfate nanoparticles occurred and that this deposition led to repulsive forces between the silica particle and plate that continually increased as the bulk nanoparticle concentration increased. Furthermore, the characteristic decay length of this repulsion was found to be in very good agreement with the Debye length of the solution, meaning that the repulsion arose from electrostatic repulsive forces between the charged surfaces. This result suggests that at least some of the adsorbed nanoparticles were remaining within the interaction region, leading to an increased electrostatic repulsion. This result suggests that mobility of the polystyrene nanoparticles on the silica is also not significant, since such

* See Appendix D for more information

mobility would not result in such large increases in the magnitude of repulsion, especially at the lower nanoparticle concentration where the surface was sparsely covered

It is thus our hypothesis that the flocculation that is observed in the experiments described here results from the presence of the nonuniform distribution of nanoparticles on the surface. This flocculation could involve either direct silica-to-silica contact, which would be more likely to occur at the lowest nanoparticle coverages, or nanoparticles adsorbed on one silica particle bridging to a bare spot on a neighboring silica particle, which would be more likely at the higher nanoparticle coverages.

At the same time, it should be noted that if the jamming limit of adsorption had indeed been reached in some of the stability measurements described above, then bridging of nanoparticles from one region to another would require either some nanoparticle desorption or translation, as otherwise there would not be sufficient space for such bridging to occur. If this were indeed the case, it would mean that neither the sulfate nor amidine nanoparticles would be effective stabilizers for these silica dispersions, as the energy of adsorption would be too small to keep the nanoparticles fixed in place during interaction of two silica microparticles.

One remaining issue that needs to be addressed is the finding in our earlier work that long-term of the silica microparticles could be achieved with amidine nanoparticles, specifically at a concentration of 0.5% vol. [123] As mentioned previously, one of the major differences between the earlier experiments and those described in this current paper is that the nanoparticles used in these current experiments were ion exchanged prior to use. It is possible that the stock amidine solutions contained a cationic, molecular additive, possibly a surfactant of some type, which was co-adsorbing to the silica microparticles contributing to their stability. We thus believe that these current experiments are a better test of the ability of charged nanoparticles to stabilize these weakly-charged silica particles.

5.5 Conclusions

This work has shown that low concentrations (i.e., ≤0.5% vol.) of highly-charged cationic and anionic polystyrene nanoparticles are, in general, not effective stabilizers for dispersions of charged silica microparticles. Although the nanoparticles clearly adsorb to the weakly-charged silica particles and, by doing so, increase the zeta potential of the microparticles to values that would appear to be sufficient to prevent flocculation, the surfaces nonetheless remain only partially covered (i.e., coverage ≤50%) and contain relatively large patches of the underlying microparticle surface. Such patches would either allow the microparticles to contact directly, which would be expected at low nanoparticle coverages, or alternatively allow nanoparticles adsorbed on one microparticle to bridge to a patch on a neighboring microparticle.

Note that while these results clearly demonstrate the challenges associated with using charged nanoparticles as effective stabilizers, they do not preclude their potential use. Specifically, if the energy of adsorption were relatively low (which could be the case for these

experiments) the nanoparticles could either desorb or translate on the surface, creating a bare patch of the underlying microparticle. On the other hand, in systems where the energy of adsorption was sufficiently high, such that nanoparticle desorption or migration was unlikely, then stabilization should occur, especially once the jamming limit of surface coverage has been reached. Thus experiments involving a broader range of both micro- and nanoparticles are needed before a more definitive statement about the stabilizing ability charged nanoparticles can be made.

Chapter 6: Effects of Metal Oxide Nanoparticles on the Stability of a Colloidal Dispersion

6.1 Introduction

The effects of adding charged nanoparticles on the interparticle forces and stability of colloidal systems has been the subject of numerous studies.[48, 99, 100] In systems where the nanoparticles are repelled from the colloids, such as through repulsive electrostatic forces, attractive depletion forces arise that can be sufficient to induce flocculation of an otherwise-stable dispersion.[39, 105, 132] As the nanoparticle concentration increase, long-range structural forces arise due to ordering of the nanoparticles in the interparticle gap region that can actually halt the depletion flocculation.[97]

Recently, various authors have become interested in the impact of adsorbing nanoparticles. Lewis and co-workers studied the impact of highly-charged zirconia nanoparticles on the gelation behavior of a system of silica particles that were very weakly charged (i.e., near the silica IEP). It was found that at low nanoparticle concentrations, the zirconia arrested the gelation, which the authors attributed to the formation of a halo of nanoparticles around the silica particles.[8, 60] A key feature of this nanoparticle haloing phenomenon was that the nanoparticles were trapped in weak energy wells near the surface of the silica particles.

In subsequent studies, Walz and co-workers studied the impact of highly-charged zirconia and polystyrene nanoparticles on the interparticle forces between a silica probe particle and silica plate, measured with colloid probe atomic force microscopy (CP-AFM).[63, 84] These authors measured strong increased electrostatic repulsive forces between the probe particle and plate resulting from adsorption of the nanoparticles. Unlike the nanoparticle haloing phenomenon, these authors found that the nanoparticles were irreversibly bound to the surface of the silica, as the additional repulsion did not disappear upon flushing the bulk nanoparticles from the system.

Recently, the authors of this paper have become interested in the potential use of highly-charged nanoparticles to stabilize an otherwise unstable dispersion of micron-sized colloidal particles against flocculation. Experiments to-date have focused on anionic (sulfate) and cationic (amidine) latex nanoparticles added to dispersions of micron-sized silica particles.[123, 133] The pH of the dispersions was maintained at the silica IEP such that flocculation of the dispersion occurred rapidly. While both the sulfate and amidine nanoparticles adsorbed to the silica and increased the measured zeta potential of the silica particles to values where stability would have been expected, neither type of nanoparticle was able to halt flocculation, even at bulk nanoparticle concentrations as high as 1.0% vol. Two possible explanations offered for this lack of stabilization were (1) the incomplete coverage of the silica surfaces by the nanoparticles left gaps where flocculation could occur, or (2) the adsorbed nanoparticles either desorbed or translated upon interaction of the silica particles, creating bare spots for flocculation to occur.

As a follow-up to this earlier work with polystyrene, we describe in this present paper similar experiments to those of Herman and Walz conducted with two different type of metal oxide nanoparticles – aluminum oxide (alumina) and zirconium oxide (zirconia). The reasoning here is that because of the stronger attractive van der Waals forces between these metal oxide nanoparticles and silica compared to the polystyrene nanoparticles and silica, these particles may not be displaced upon interaction of the silica colloids and thus stability could potentially be achieved. Additionally, the particles do not require any surface modifications to maintain a large positive surface charge (e.g. amidine groups on polystyrene).

6.2 Materials and methods

6.2.1 Overview of experiments

The experiments in this study were performed to determine the adsorption and stabilizing properties of different metal oxide nanoparticles on systems of weakly charged, unstable silica colloids. First, stability experiments were carried out at the isoelectric point of the silica with nanoparticle concentrations ranging from $1x10^{-5}$% to 1.0% vol. Second, zeta potential measurements were performed to understand the effect of the added nanoparticles on the surface charge of the silica microparticles. Additionally, adsorption experiments were performed to observe the degree of adsorption and surface coverage of the nanoparticles on the silica microparticles. Finally, a set of colloid probe AFM force measurements were used to confirm that any observed repulsion was due to electrostatic forces, as well as to determine whether the effects of the nanoparticles was reversible.

6.2.2 Materials

Deionized water was filtered by a Barnstead EASYpure II UV Ultrapure water system (Thermo Scientific, catalog #D7401), which provided water with a resistivity of 18.2 MΩ-cm. Fused silica slides (Corning 7980 fused quartz silica, item #3x1x1mm) from Technical Glass Products (Painesville, OH) were used as substrates. Silica microparticles with a 1.0 μm average diameter were used, and were supplied at a concentration of 10% w/v in water (Polysciences, Inc., Warrington, PA, catalog #24326-15). Zirconia (ZrO_2) nanoparticles (product #ZR10/20) were supplied by Nyacol (Ashland, MA) at 20% by weight. The average diameter of the nanoparticles was specified to be 5-10 nm. Alumina (Al_2O_3) nanoparticles (Nanostructured & Amorphous Materials, Inc., Houston TX, stock #7016WJWG) had a specified diameter of 10±5 nm, and were supplied at 20% by weight. Hydrochloric acid (Optima grade, Fisher Scientific, catalog #A466-250) was used as a titrant.

For the CP-AFM force measurements, 30 μm silica spheres (Microsphere-Nanosphere, Cold Spring, NY) were used as colloid probes. The AFM cantilevers used were the D-Lever on ORC8-10 model cantilevers (Bruker AFM Probes, Camarillo, CA). The glue used to mount the spheres was a thermoplastic epoxy (EPON 1004F Resin, Momentive, Columbus, OH).

6.2.3 Preparation of nanoparticle dispersions and stability measurements

In order to remove any unknown ions that were present in the bulk suspension, the nanoparticle dispersions used in these experiments were dialyzed before being used. The bulk suspensions were supplied as aqueous suspensions that were free of any surfactants and were supplied at pH values of either 1.5 (for the zirconia nanoparticles) or 4.0 (for the zirconia nanoparticles). The experimental suspensions were prepared by diluting the stock dispersions of zirconia and alumina particles with purified, deionized water to 0.1% vol. The suspensions were dialyzed using ion-exchange resin (Bio-Rad, Hercules, CA, catalog #143-7425) in clean scintillation vials at the manufacturer-specified ratio of 5 g resin per 100 mL of solution. The resin removed both cations and anions. Using a continuous sample rotator, the filled vials were gently mixed for 4 hours in order to keep the resin well-distributed throughout the suspensions. Once the ion-exchange step was finished, the 0.1% vol. samples were further diluted to the lower concentrations and titrated to the desired pH value.

Additionally, the 1% vol. zirconia suspension required separate dialysis using dialysis tubing (Sigma Aldrich, #D9652). At that concentration, the ionic strength was too great for the ion-exchange resin to completely remove the excess ions. Instead, the 1.0% dispersion was suspended in the dialysis tubing in a column of pure water, which was replaced periodically over approximately three days, until the pH and conductivity of the suspension were relatively constant.

In the case of the alumina nanoparticles, the dialyzed suspensions were placed in an ultrasonicator for 8 hours in order to better disperse the particles which were aggregated in the bulk supply. Even with the sonication procedure, it was not possible to fully disaggregate the alumina nanoparticles. Sizing measurements were performed using dynamic light scattering (DLS), with an approximate number weighted mean diameter of 99 nm and volume weighted mean of 1337 nm (in contrast to the specified 10-15 nm). This indicates that there is significant aggregation present in the samples, and based on the difference between the number and volume means there is a very large range of particle sizes present in solution. In contrast, DLS measurements of the zirconia nanoparticles gave particle diameters of approximately 4.9 nm and 5.6 nm for the number and volume weighted means, respectively, indicating a relatively uniform size distribution.

The stability of the silica microparticle suspensions was monitored through visual observation. Silica microparticles were added to suspensions of nanoparticles (which were at concentrations ranging from 0 to 0.1% vol.) until a final silica concentration of 0.1% vol. was reached Final adjustments to the pH were made in order to insure that the suspensions were at the silica IEP (previously determined to be approximately pH 3.5[133]). The suspensions were added to cuvettes and briefly sonicated; the stability was then recorded photographically. The suspensions were all observed for a minimum of 12 hours.

6.2.4 Zeta potential measurements

The zeta potentials of the oxide nanoparticles alone were measured by dynamic light scattering using a Zetasizer Nano ZS (Malvern Instruments Ltd, Worcestershire, UK), in the folded capillary cells (catalog #DTS1060C). Prior to the measurements, the cells were rinsed with pure ethanol, followed by DI water, and then dried with ultra-high purity nitrogen. The measurements were performed once the suspensions had been titrated to pH 3.5.

The effective zeta potential of the silica microparticles in suspensions of the oxide nanoparticles was measured using a Micro-Electrophoresis Apparatus Mk II (Rank Brothers Ltd., Cambridge, England), configured with a rectangular cell. The nanoparticle concentrations used in these measurements matched those that were used for the stability measurements (0-0.1% vol.), while the concentration of silica was more dilute (approximately 0.01% vol.) to allow clearly viewing of the individual microparticles within the microelectrophoresis cell. The velocity of individual silica microparticles was measured and used to determine the electrophoretic mobility, from which the zeta potential could be calculated

6.2.5 Nanoparticle adsorption on silica microparticles

Adsorption experiments were performed in order to directly visualize any adsorbed nanoparticles and to approximate the adsorption behavior of the oxide nanoparticles that occurs in the silica microparticles suspensions. A suspension of 1.0 μm silica microparticles (approximately 0.01% vol.) was prepared and titrated to pH 3.0. Droplets of the silica suspensions were spread on the surfaces of clean silica slides and allowed to completely dry. This produced a thin layer of microparticles (approximately a monolayer or less in most locations) on the slide surface which, upon drying, were sufficiently attached as to remain on the surface even after gentle soaking and rinsing in the various nanoparticle suspensions.

Nanoparticle dispersions, created using the ion-exchange treated oxide nanoparticles, were prepared by diluting the stock to concentrations ranging from 10^{-5}% to 10^{-1}% vol., and then briefly sonicated. The nanoparticle solutions were titrated to the IEP of the silica microparticles, pH 3.5, with 0.1 M HCl. A nanoparticle-free solution at the same pH was also prepared for use as a rinse solution. The prepared slides (with the adsorbed 1.0 μm silica microparticles) were gently rinsed with the blank solution before being immersed in the nanoparticle suspensions for 20 minutes. The slides were then removed from the nanoparticle suspensions and very gently rinsed in the blank solution to remove any excess particles that were not adsorbed to the microparticle surfaces. The slides were air dried and the samples sputter-coated with a 1-2 nm layer of gold before being imaged with SEM.

6.2.6 Colloidal probe AFM

Force measurements were performed using CP-AFM, which measured the force between a probe sphere that is attached to the tip of an AFM cantilever and a flat slide. The silica spheres were mounted on the cantilever chip (with a nominal spring constant of k=0.05 N/m) using a probe mounting microscope and translating stage with a cantilever holder, and then cleaned

using a UV/Ozone treatment (BioForce Nanosciences, Inc., Ames, IA) for 20 min. The final spring constant for the cantilever (with attached silica sphere) was calculated using the method of Hutter and Bechhoefer.[96] The CP-AFM force measurements were conducted using an Asylum Research MFP-3D AFM with the closed fluid cell (model #CCELL). The silica substrates were cleaned by ultrasonication in 100% ethanol before being rinsed and dried with ultra-high purity nitrogen, then glued to the base plate of the AFM fluid cell with epoxy. The disassembled fluid cell components were sonicated in pure ethanol for 1 hour before being rinsed with ultrapure water and dried. The cell was then assembled and filled with the desired solution. Solution exchange was performed to introduce and later flush the nanoparticles from the cell. This was accomplished by slowly flowing 20 mL of solution through the fluid cell (volume <5 mL) to ensure complete exchange of solutions.

The force measurements were performed at a 100 nm/s scan rate to avoid hydrodynamic forces, with the scan range starting at 1.0 μm separation. The data was recorded as cantilever deflection versus distance and converted to force versus separation curves via the analysis methods of Ducker et al.[94] Approximately 30 curves per sample were averaged into a single curve to reduce noise and irregularities.

6.3 Results

6.3.1 Stability

The images in Figure 6-1 show the initial stability measurements of silica microparticles with added zirconia nanoparticles. The suspensions all contained 0.1% vol. silica microparticles and these first set of experiments used concentrations of zirconia nanoparticles ranging from 10^{-2}% to 1.0% vol. The images shown are from the beginning of the experiment and at the 6 hour mark. The suspension with only silica microparticles actually flocculated within approximately 1 hour, while all three suspensions containing zirconia nanoparticles were fully stable for the entire observation period, which extended beyond 12 hours.

It is important to note that in these experiments the 1.0 μm silica microparticles slowly sediment on their own, even when the suspension is completely stable, due to the size and density of the particles. It was found that with these systems, the stable silica particles will sediment to the bottom of the cuvette in approximately 14 to 15 hours and exhibit sharply-defined sedimentation boundaries consisting of a clear supernatant over an opaque layer of silica microparticles. Unstable suspensions will show a visible reduction in turbidity and increasingly unclear boundary between the supernatant and silica until the suspension has completely aggregated and settled, leaving an effectively transparent cuvette.

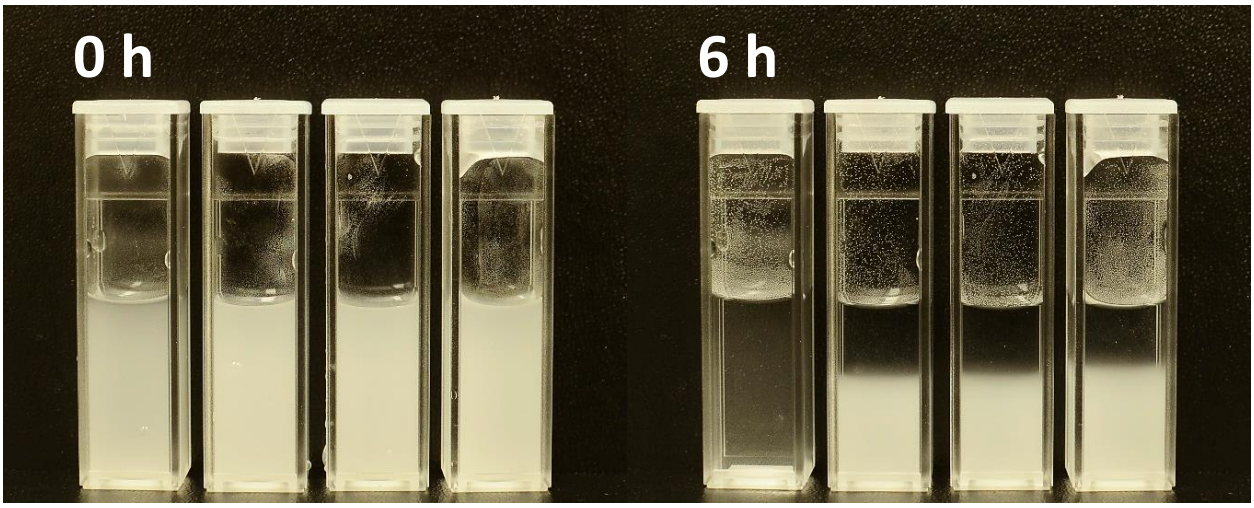

Figure 6-1: Stability of 0.1% vol. suspensions 1.0 μm silica microparticles with increasing zirconia nanoparticle concentrations. Suspensions are at pH 3.5 (silica IEP). L to R: 0%, 10^{-2}%, 10^{-1}%, 1.0% vol. zirconia nanoparticles.

As all the silica/zirconia suspensions in Figure 6-1 were stable, further measurements were done to determine the threshold concentration of zirconia nanoparticles needed to completely stabilize the silica dispersions. Figure 6-2 shows the stability with much lower concentrations of zirconia nanoparticles, from 10^{-6}% to 10^{-3}% vol. Here, we do find that the lowest concentrations of zirconia do no stabilize the suspension. Specifically, the 10^{-6}% vol. sample flocculates as rapidly as the silica-only sample (i.e., less than one hour). The 10^{-5}% vol. sample aggregates more slowly than the two lower concentrations but is still clearly unstable, as it flocculates and settles significantly in less than 2 hours. The two remaining suspensions, 10^{-4}% and 10^{-3}% vol., are visibly stable, and the samples remained so for the full observation period (>12 h). From this we can conclude that in order to stabilize a 0.1% vol. suspension of the silica microparticles, a minimum concentration of 10^{-4}% vol. of the zirconia nanoparticles is required.

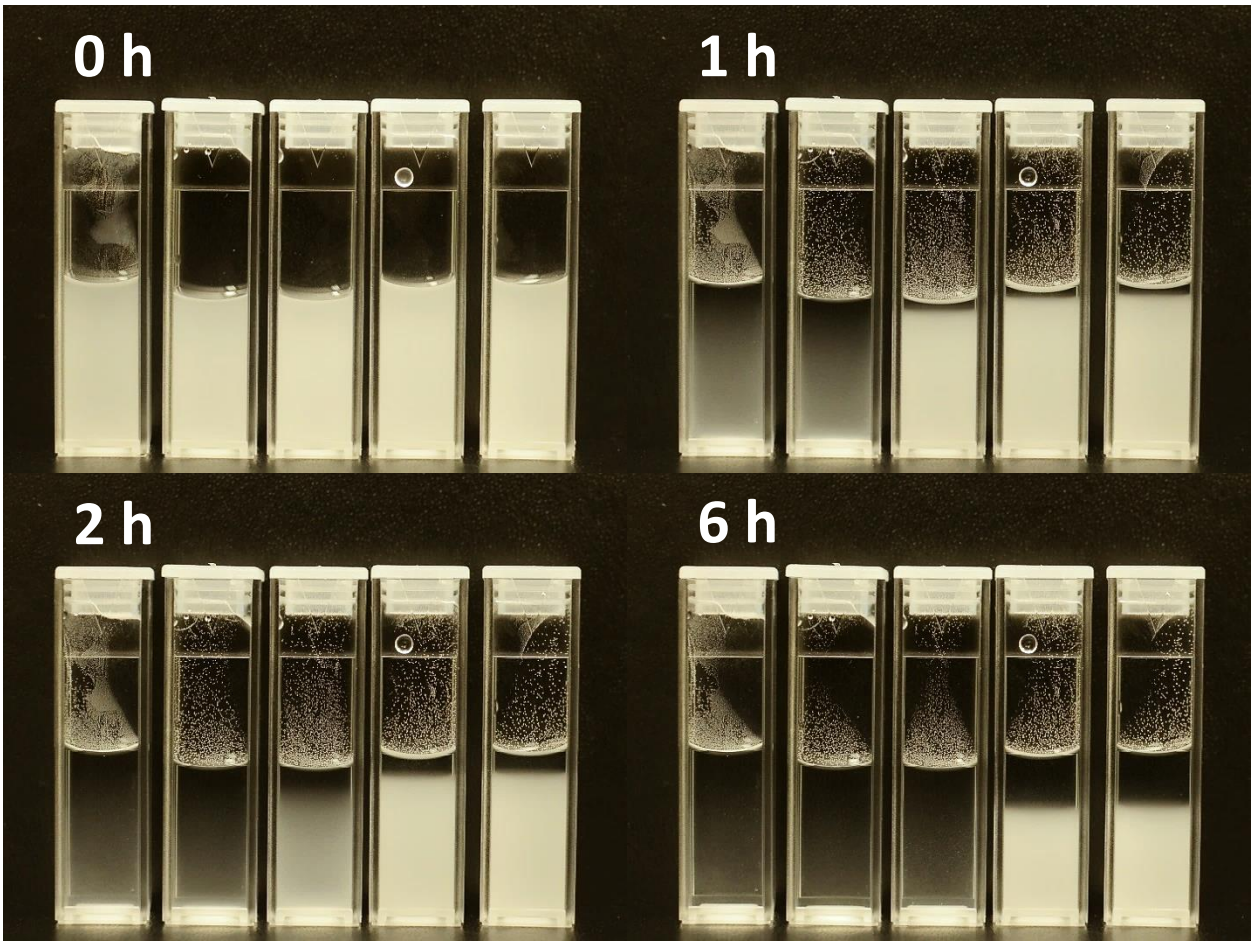

Figure 6-2: Stability of 0.1% vol. suspensions 1.0 μm silica microparticles with increasing zirconia nanoparticle concentrations. Suspensions are at pH 3.5 (silica IEP). L to R: 0%, 10^{-6}%, 10^{-5}%, 10^{-4}%, 10^{-3}% vol. zirconia nanoparticles.

Similar stability experiments were performed with the alumina nanoparticles. The images shown in Figure 6-3 include 10^{-4}%, 10^{-3}%, and 10^{-2}% vol. alumina suspensions, along with a silica-only suspension (all at pH 3.5 and with 0.1% vol. silica microparticles). Here we see that the addition of 10^{-2}% vol. alumina nanoparticles to the silica suspension results in a stable suspension, which was fully stable for the entire observation period of more than 12 hours (as with Figure 6-1 and 2, there were no observable changes after 6 hours, which is the last image shown for each experiment). The two lower concentrations appear to slow the rate of flocculation; however it was only slowed by 1-2 hours. The critical alumina concentration required to stabilize the silica (10^{-2}% vol.) is approximately 2 orders of magnitude greater than the zirconia. However, because of the larger size of the nanoparticles (approximately 10-15 nm), the bulk number density at this concentration was only 5 to 10 times that of the zirconia nanoparticles (approximately 5 nm) at its critical stabilization concentration (10^{-4}% vol.).

It is necessary to note that the highest concentration of alumina nanoparticles (10^{-2}% vol.) exhibits a bluish coloration. This actually arises from the alumina nanoparticles and is unrelated

to the stability of the silica suspension. Additionally, in contrast to the zirconia, 10^{-2}% was the highest alumina concentration that was used, as the higher concentrations became too opaque to sufficiently observe the stability behavior of the silica microparticles.

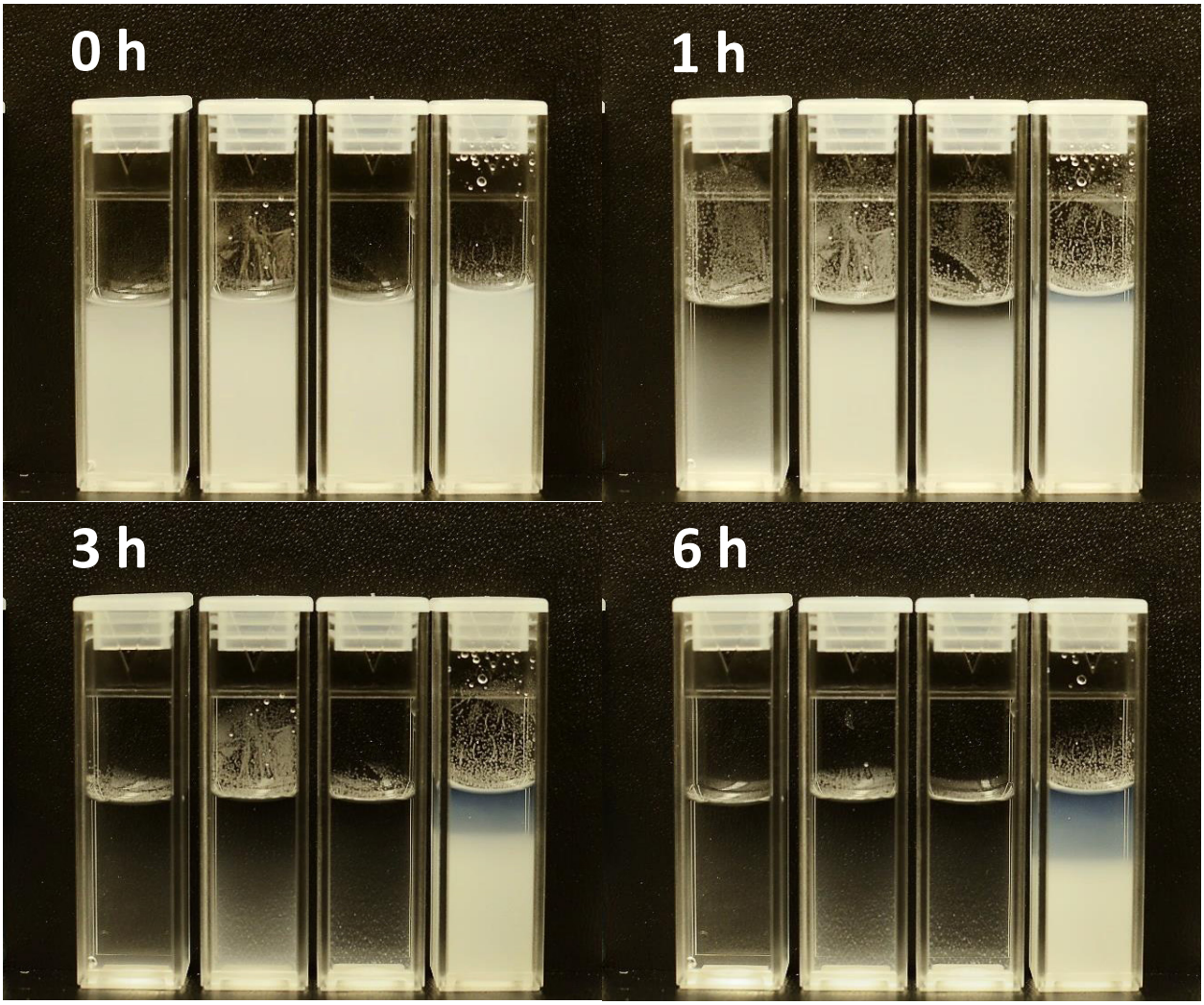

Figure 6-3: Stability of 0.1% vol. suspensions 1.0 μm silica microparticles with increasing alumina nanoparticle concentrations. Suspensions are at pH 3.5 (silica IEP). Left to right: 0%, 10^{-4}%, 10^{-3}%, 10^{-2}% vol. zirconia nanoparticles.

6.3.2 Zeta potential

The zeta potential measurements reported in Table 5-1 were all measured at pH 3.5. The nanoparticles alone were each highly and positively charged, with average zeta potentials of 44.3 and 56.2 mV for the zirconia and alumina nanoparticles, respectively. This was expected as both oxides have significantly higher isoelectric points than silica. The silica microparticles alone were nearly uncharged, with a zeta potential of only 3.1 mV.

The addition of zirconia nanoparticles to the silica dispersions effectively increased the zeta potential of the microparticles at concentrations of 10^{-4}% vol. and higher (10^{-5}% was within one standard deviation of zeta measured with no added nanoparticles). The zeta potential increased consistently with zirconia concentration to approximately 42.1 mV at 10^{-2}%. Further increasing the zirconia nanoparticle concentration to 10^{-1}% resulted in no further increase in the zeta potential. The zeta potential at the critical stabilization concentration (10^{-4}% vol.) was 12.9 mV, which is reasonable based on previous stability measurements which showed that the silica dispersions alone were stable with a zeta potentials as low as roughly +10 mV (pH below the IEP).[133]

Table 6-1: Measured zeta potentials for 1.0 μm silica microparticles in suspensions with increasing concentrations of oxide nanoparticles (along with the nanoparticles alone, which were measured using DLS). The zeta potentials for silica were determined using micro-electrophoresis at pH 3.5 (the IEP of the SiO_2 microparticles). The standard deviation is used for the reported error values.

Bulk nanoparticle conc., % vol.	ζ Zirconia (mV)	ζ Alumina (mV)
Nanoparticles only	44.3±8.9	56.2±9.9
0	3.1±2.1	3.1±2.1
10^{-5}	3.2±0.9	---[a]
10^{-4}	12.9±5.8**	9.9±1.2
10^{-3}	30.4±11.2	14.8±2.4
10^{-2}	42.1±7.3	22.8±6.4**
10^{-1}	42.6±4.4	---[a]

[a] Alumina zeta potential was not measured at these concentrations

**Lowest concentration where stability was observed

The addition of alumina nanoparticles had a similar effect, with increasing concentrations resulting in higher effective zeta potentials for the silica. In comparison to the zirconia, however, the zeta potential was lower at equivalent bulk volume concentrations. The maximum measured zeta potential, 22.8 mV, occurred at 10^{-2}% vol., which was the concentration needed to stabilize the suspension. While this zeta potential was higher than that found necessary to stabilize the suspension using the zirconia nanoparticles, because measurement were only performed at factor of 10 intervals of concentration, an precise statement about the zeta potential needed for stabilization is difficult. It seems clear that with either nanoparticle, an effective zeta potential of 20 – 25 mV would be sufficient for stability.

6.3.3 Nanoparticle adsorption on silica microparticles

Figure 6-4 shows five SEM micrographs of 1.0 μm silica microparticles that had been immersed in zirconia nanoparticles suspensions ranging from 10^{-5}% to 10^{-1}% vol. at pH 3.5. As with the zeta potential measurements, there is a visible increase in the quantity of adsorbed nanoparticles with increasing concentrations of nanoparticles in the suspension. With suspension concentrations of 10^{-3}%, 10^{-2}%,and 10^{-1}% vol., there are clearly visible layers of adsorbed nanoparticles and possibly multi-layer converage at the highest two nanopaticle concentrations. At the lower two concentrations, while there clearly appears to be nanoparticles present on the surface, their density is markedly lower. (It should be mentioned that because of the small average diameter of the zirconia nanoparticles – about 4.9 nm – discerning individual nanoparticles with the SEM is difficult.)

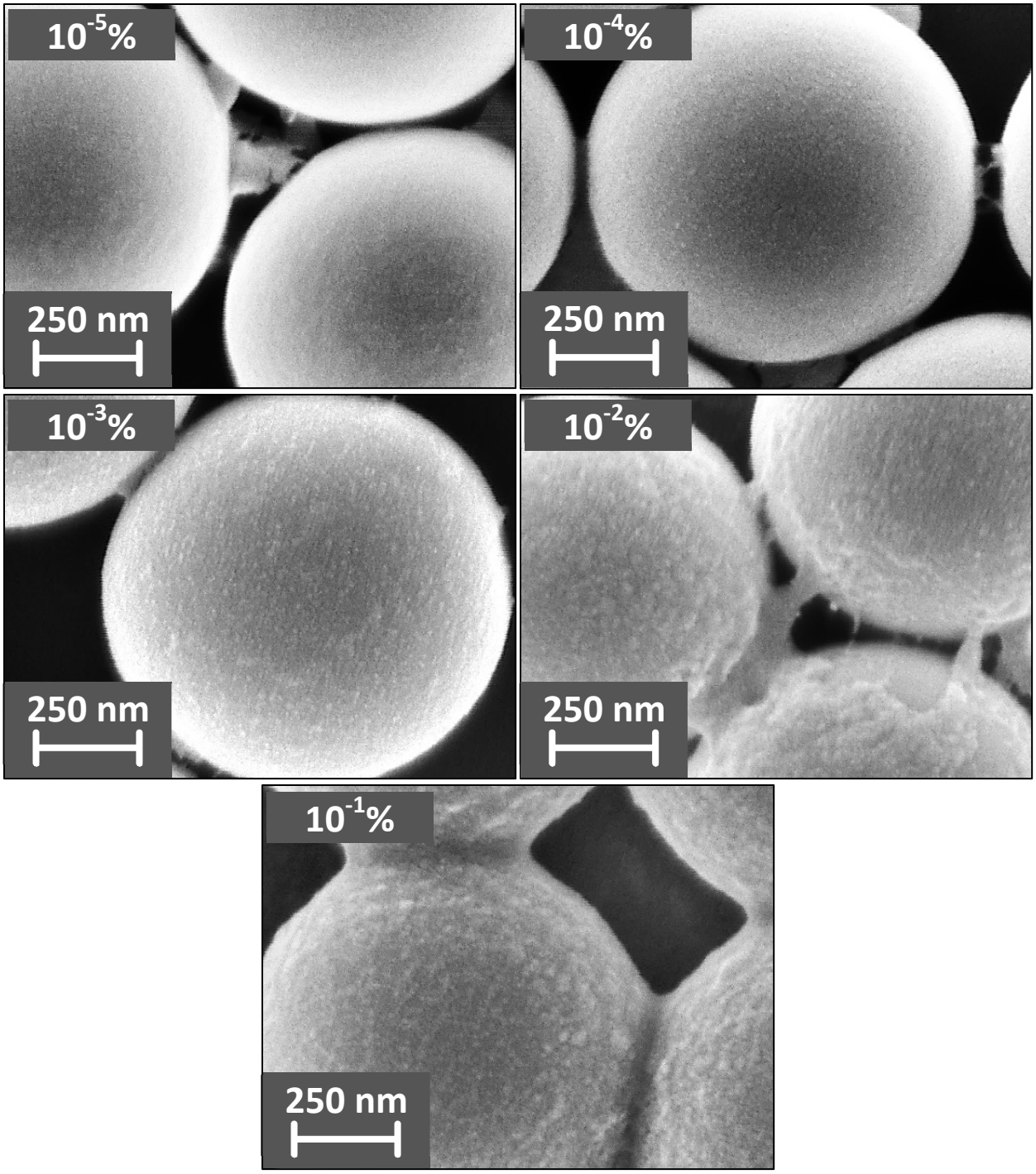

Figure 6-4: SEM micrographs showing the adsorption of zirconia nanoparticles on 1.0 μm silica spheres. Zirconia concentrations range from 10^{-5}% to 10^{-1}% vol.

SEM micrographs of alumina nanoparticle adsorption on the silica microparticles are shown in Figure 6-5. Again, the number density clearly increases with increasing bulk concentration of nanoparticles. The sample from the suspension with the lowest bulk concentration (10^{-4}% vol.) has very few particles visible on the silica surface; however by 10^{-2}%

(the concentration that successfully stabilized the silica suspension) there is a substantially greater degree of adsorption.

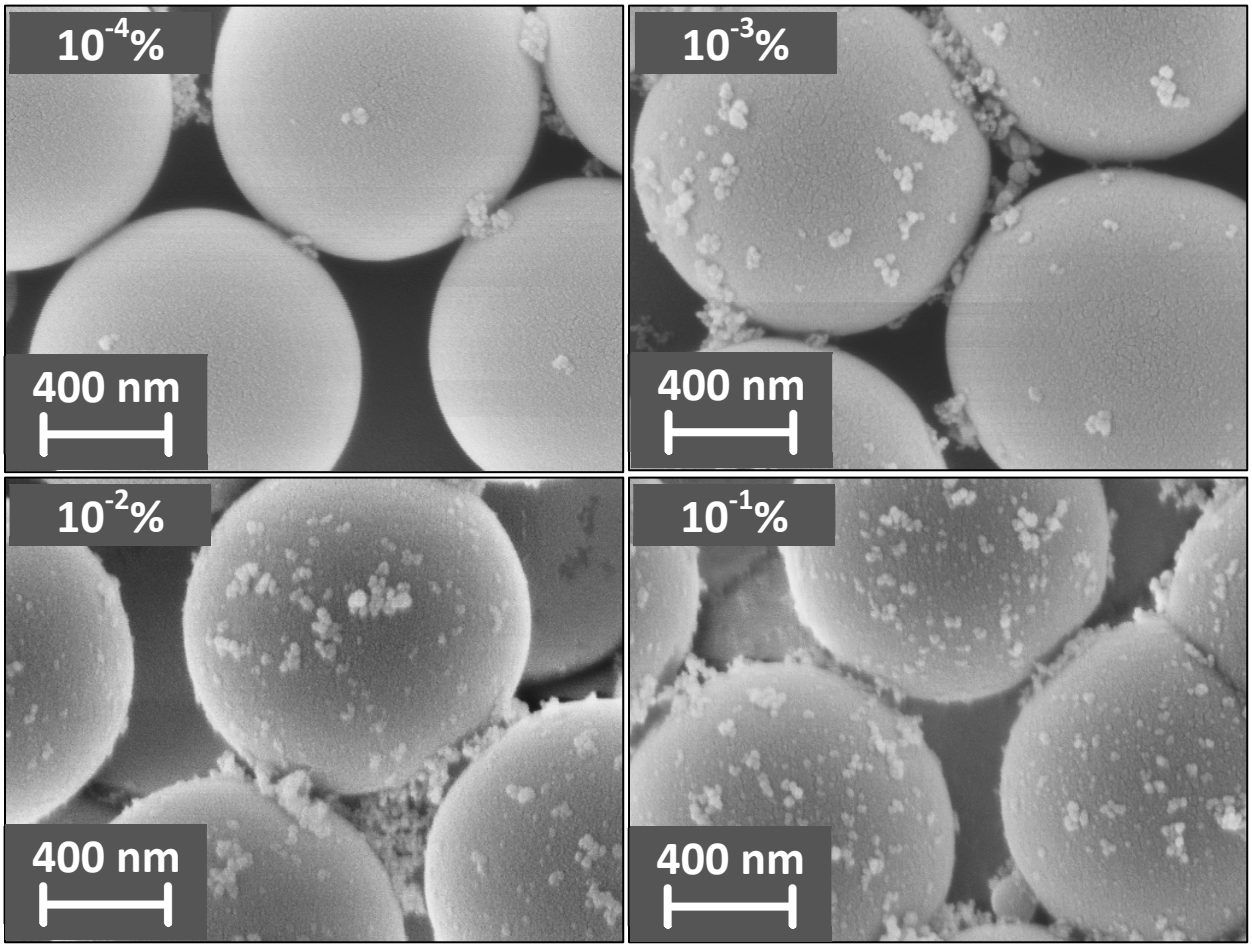

Figure 6-5: SEM micrographs showing the adsorption of alumina nanoparticles on 1.0 μm silica spheres. Alumina concentrations range from 10^{-4}% to 10^{-1}% vol.

The alumina nanoparticles are slightly easier to image than the zirconia particles as they are somewhat larger. Size measurements of individual alumina particles from the SEM images indicate that most of the particles are 12 to 15 nm in diameter, which is close to the manufacturer-specified average of 10±5 nm. However, size measurements conducted with dynamic light scattering indicated that there was a very large amount of aggregated nanoparticles in the suspension. The alumina obtained from the manufacturer was actually in a gel state and even upon dilution, the observed high turbidity suggested significant aggregation. After dilution and multiple attempts to re-disperse the nanoparticles using ultrasonication, the measured average was still greater than 90 nm. This is likely the reason that the particles appear in clusters in Figure 6-5, even at the lowest concentrations. Additionally, they appear more susceptible to the effects of drying the sample prior to imaging, as in each sample the particles have

accumulated between the silica microparticles in significantly greater quantities than what is present on the exposed surfaces. As a result, it is not completely clear if the images in Figure 6-5 are a true representation of the degree of coverage of the silica particles in the bulk suspension.

6.3.4 CP-AFM and reversibility

A set of colloid probe force measurements were performed to investigate the forces between the silica surfaces in the presence of nanoparticles at the silica IEP. The AFM system had a lower IEP than that of the microparticle suspensions used for the stability tests. Since 30 μm silica spheres were used as the colloidal probes, they sedimented too quickly to obtain a zeta potential and directly determine the IEP. Instead, the effective IEP of the silica system was determined in the AFM, by reducing the pH until the repulsive forces were essentially eliminated. This occurred at a pH of 2.55. The measurement was performed with both zirconia and alumina nanoparticles (separately). Figure 6-6 shows the effects of added nanoparticles on the forces between silica surfaces at the silica IEP. In each experiment, the interaction was measured with water only (at the same pH as the nanoparticle solutions), after which the nanoparticle solution was introduced and the force measured again. The nanoparticle solution was then flushed from the cell using the pure water before the final measurement (all solutions were titrated to pH 2.55). The final rinse step was measured after approximately one hour of equilibration time, to allow any potential desorption to occur.

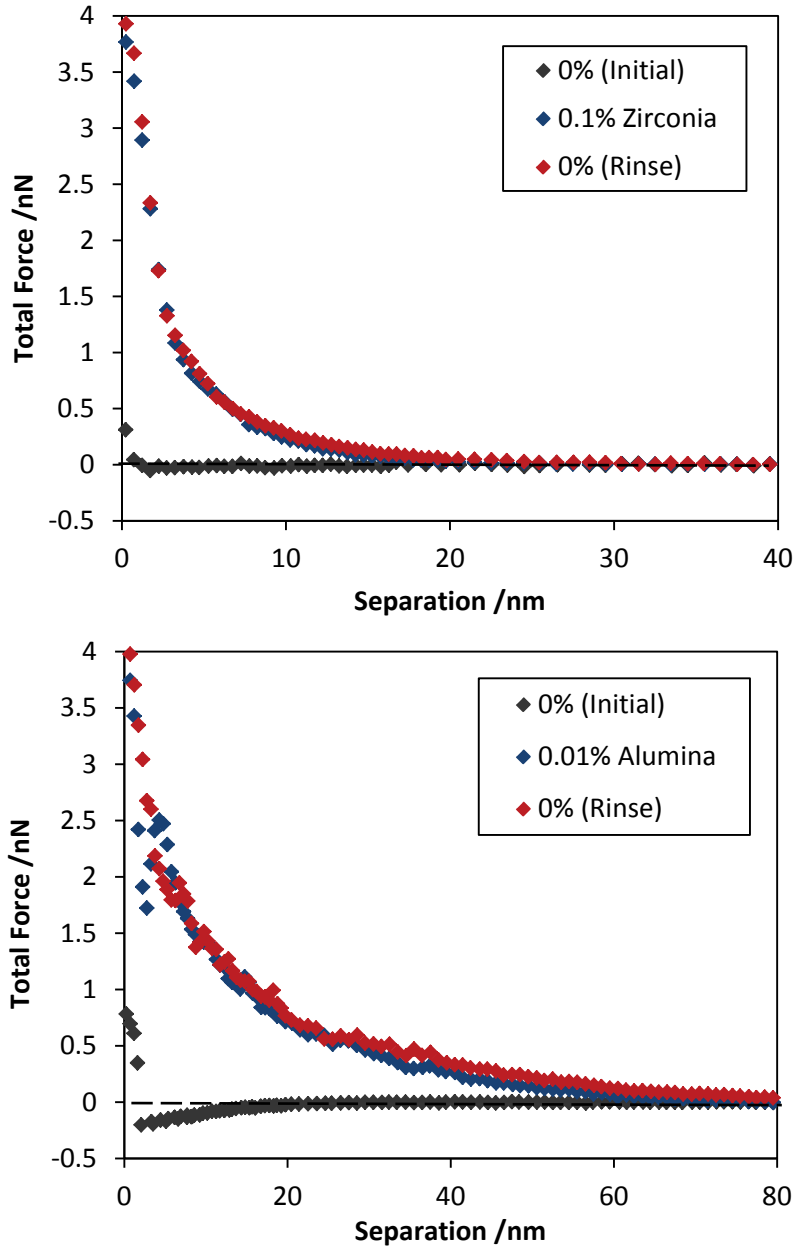

Figure 6-6: Force measurements (using CP-AFM) showing the increase in electrostatic force between a silica sphere and plate in water only (0% Initial), upon introduction of the nanoparticles, as well as the irreversibility of the force after flushing the system with water (0% Rinse). Measurements performed at the silica IEP (pH 2.55). Top: Zirconia. Bottom: Alumina. *Note the difference in scales on the x-axis.*

With the first solution exchange, it is clear that the introduction of nanoparticles produces a significant repulsive force between silica surfaces, both with zirconia and alumina, compared to the initial nanoparticle-free measurement. The forces between the zirconia have a significantly shorter range than the alumina (the two graphs have different x-axis scales in order to better show the shape of each curve), and the force curve in the alumni systems was more noisy, resulting from greater variability in the individual force curves obtained in the alumni system.

Once the nanoparticle suspension has been flushed from the fluid cell and replaced with nanoparticle-free water of identical pH, we clearly see that the repulsive force remains. Not only that, but the forces after the rinse are effectively identical to those measured in the nanoparticle suspensions, with the two curves overlapping almost completely. This indicates that the nanoparticles are quite strongly adsorbed to the silica surfaces, and is consistent with previous reversibility studies using polystyrene latex particles.[63, 84] It is possible that there may be some long term desorption, since this rinse curve was only measured 1 hour after the flushing of the nanoparticles from the system, however for moderate time scales, the adsorbed particles should be expected to remain on the surfaces.

If the force curves are purely electrostatic, the forces follow an exponential decay that is dependent on the Debye length (κ^{-1}).[11] From a semi-log plot (ln(*force*) versus separation) we can calculate a decay length of the curves and compare it to the theoretical Debye length of the solution, which is dependent on the ionic strength (in this case we assume that the ionic strength is equal to the concentration of titrant required to reach the experimental pH). The semi-log plot of a purely electrostatic should yield a straight line, the slope of which is equal to the negative inverse Debye length ($-\kappa$). The semi-log plots for the nanoparticle solution curves (Figure 6-6) are shown in Figure 6-7.

The theoretical Debye length for the solutions is approximately 5.7 nm.[14] From the fit of the slopes, we find that the zirconia measurements have decay lengths of approximately 4.8 nm and 5.5 nm (0.1% zirconia and 0% rinse, respectively). These values are sufficiently close enough to the calculated Debye length to indicate that the repulsion in the zirconia system arises primarily from electrostatics. Furthermore, it is reasonable for the decay length for the solution containing nanoparticles to be somewhat shorter than the theoretical κ^{-1}, since the nanoparticles themselves release counterions into the system.[122]

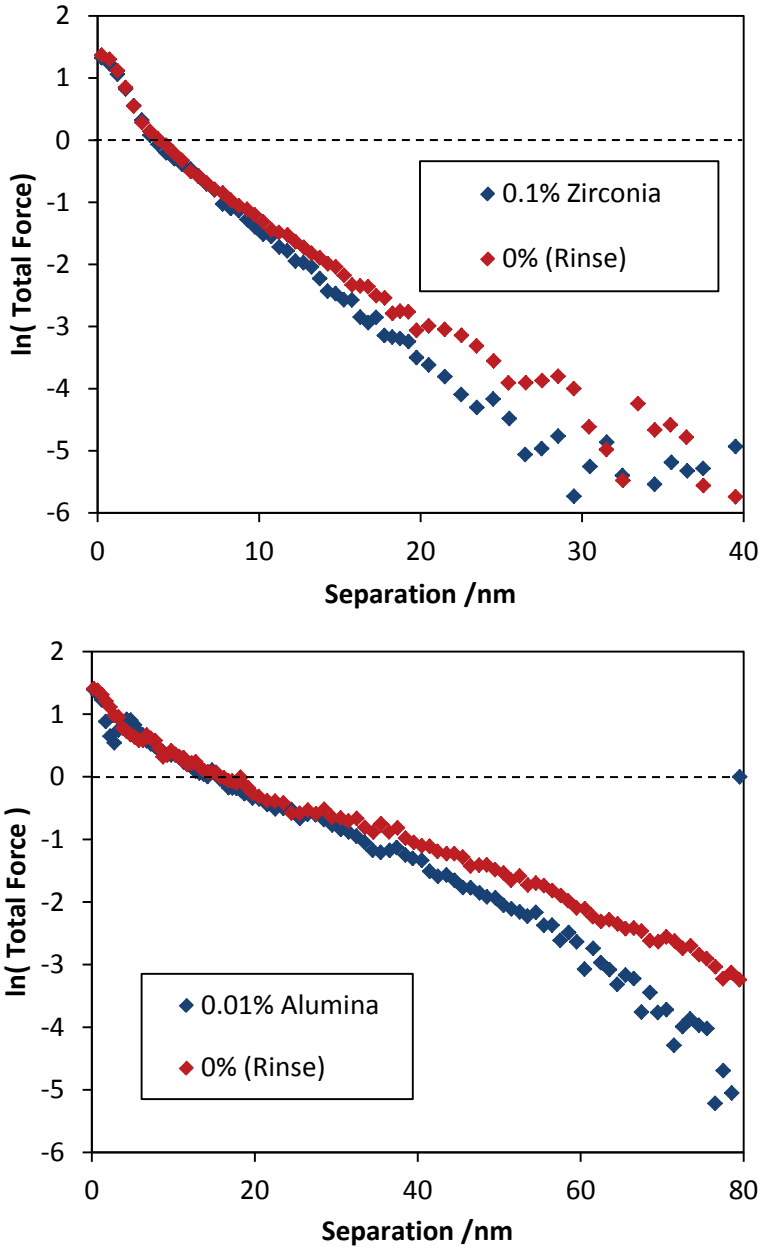

Figure 6-7: Semi-log plots of the measured force curves in the nanoparticle solutions. Top: Zirconia. Bottom: Alumina.

The repulsive forces (Figure 6-6) for the alumina nanoparticles system show a longer range of interaction compared to the zirconia, with decay lengths of approximately 16.2 nm and 19.3 nm for the 0.01% alumina and 0% rinse, respectively. Given that the decay lengths are substantially larger than the Debye length of the system, these results suggest that there is an additional, most likely steric, component to the repulsive interactions. Steric forces arise in systems where the surface layer or features extend outward and physically interact with other approaching surfaces.

While we can see from the SEM images (Figure 6-5) that the alumina particles used in the stability tests are not fully covered with nanoparticles, there are a significant number of nanoparticle aggregates in the system (as previously mentioned, while the individual nanoparticles were 10-15 nm, the measured average diameter was about 90 nm, indicating aggregation of the nanoparticles in the bulk). Although it is possible that the level of coverage is higher in the AFM system, coverage similar to that of Figure 6-5 could still result in a steric force component. In the individual force curves (prior to averaging), there were typically small peaks in the force before reaching full contact, which would occur if the adsorbed particles and aggregates shifted during approach.

6.4 Discussion

The presented results can be summarized by the following points:

1. The flocculation of silica microparticle dispersions (at the IEP) can be prevented with the addition of charged metal oxide nanoparticles. Zirconia and alumina nanoparticles were both found to be effective stabilizers of a 0.1% suspension of 1 μm diameter silica particles at critical stabilization concentrations of 10^{-4}% vol. (zirconia) and 10^{-2}% vol. (alumina). At and above these concentrations, the silica microparticles remained stable for the entire observation period (>12 h).
2. The added nanoparticles were highly positively charged, and the measured zeta potential of the silica microparticles in suspension with the nanoparticles increased with increasing nanoparticle concentration. The silica had a zeta potential of 12.9±5.8 mV in 10^{-4}% zirconia and reached a maximum potential of approximately 42 mV at 10^{-2}%, after which no further increase was observed with increase zirconia concentrations. Using alumina nanoparticles, the silica had a potential of 22.8±6.4 mV at 10^{-2}% vol.
3. Both types of nanoparticles adsorbed on the silica microparticles at the stable concentrations, as imaged by SEM. The zirconia showed significantly higher levels of coverage (though due to particle size were more difficult to image at lower concentrations). The alumina had significant adsorption at the lowest stable concentration however there were still substantial gaps between adsorbed particles.
4. CP-AFM measurements showed that the adsorbed charged nanoparticles provide significant repulsion between silica surfaces, though it appears that while the forces in the zirconia system are only electrostatic, the alumina system may exhibit steric forces as well.
5. After flushing the nanoparticle solution from the fluid cell, the repulsive forces persisted, nearly unchanged from the measurements with nanoparticles. The adsorption is effectively irreversible (at constant solution conditions), with no change in the forces after being exposed to nanoparticle-free water at the same pH for 1 hour.

These results clearly show that complete stabilization of unstable colloids is achievable using adsorbing, highly-charged nanoparticles. This finding is in contrast to previous studies

conducted by these authors using both sulfate and amidine polystyrene particles.[123, 133] Although zeta potential measurements conducted with these latex nanoparticles indicated that the silica microparticles should be stable (i.e., zeta potentials as large as 47.6 mV were obtained), long-term stability was never achieved.

One motivation for choosing the new nanoparticles for this study was to try particles with a smaller diameter. The expectation was that for a given volume fraction, the smaller nanoparticles would have a comparatively greater number density, potentially increasing the degree of adsorption. The smaller nanoparticle size would also more effectively distribute the charge across the surface of the microparticles and thus better approximate a uniform coating on the sphere. This would be an improvement over the polystyrene particles, which had diameters greater than 20 nm (compared to the 5 to 15 nm of the zirconia and alumina).

However, as seen in Figure 6-5, the alumina adsorption is still quite patchy, with significant space between particles or aggregates. This adsorption behavior is very similar to what was seen with polystyrene nanoparticles, in particular the negatively charged sulfate latex.[133] Given that the silica microparticles with adsorbed polystyrene nanoparticles remained unstable, even with bulk nanoparticle concentrations as high as 0.5% vol., the adsorbed coverage is clearly not the determining factor controlling stability.

A second factor that needs to be considered is the strength to which the nanoparticles are bound to the silica surface. Specifically, if the nanoparticles either desorb or laterally migrate on the surface upon interaction of two silica particles, then bare silica particles would be created that allow aggregation. Such desorption or migration would occur if the energy barrier preventing nanoparticle motion were sufficiently small. Assuming that the electrostatic interactions in the various systems were all approximately similar, then primary force holding the nanoparticles in place would be the attractive van der Waals force.

According to Lifshitz theory, the van der Waals interaction energy per unit area, E_{vdW}, between two half spaces separated by distance l is given by the expression[24]

$$E_{vdW} = -\frac{A(l)}{12\pi l^2} \tag{7.1}$$

where $A(l)$ is the distance-dependent Hamaker 'constant'. This constant can be calculated using the dielectric response functions for the two half-spaces, along with that of the intervening medium.

Using dielectric spectra data taken from the literature[26-28], Hamaker constants as a function of separation distance for various materials interacting with silica were calculated and are plotted in Figure 6-8. It can be clearly seen that at contact (as well as larger separations) the Hamaker constant is greater for the oxides than it is for polystyrene, which has a value of approximately 0.99×10^{-20} J at contact. Zirconia is more than twice that of polystyrene, with a value of approximately 2.1×10^{-20} J, and alumina is approximately 1.7×10^{-20} J. Since the van der Waals interaction is directly proportional to the Hamaker constant (Equation 7.1), the attractive

component of the total interaction between microparticle and nanoparticle can be more than twice as large with zirconia than with polystyrene latex, which would result in a much lower tendency to desorb or migrate.[133]

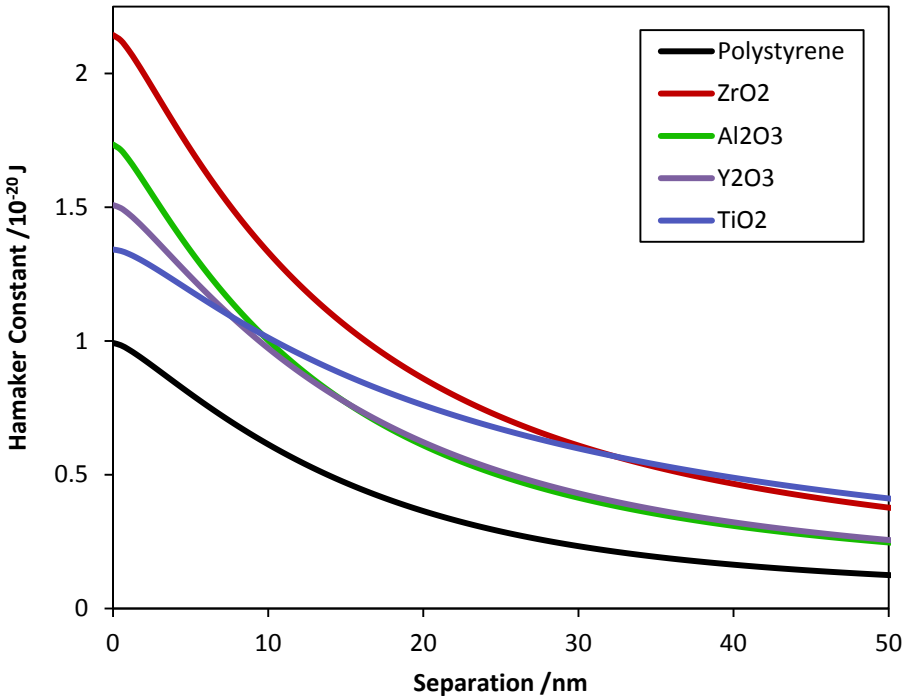

Figure 6-8: Calculated Hamaker constants, *A(l)*, for the interaction between silica and other materials (polystyrene, zirconia, alumina, yttria, titania) at separation distances less than 50 nm.

It should be mentioned that there could, of course, be other short-range contributions to the adhesion force holding the nanoparticles in place other than simply the van der Waals force. Furthermore, recent work has questioned the validity of using the Lifshitz theory, which is based on interacting half-spaces, for particles of nanometer size.[134] In calculations for two identical 5.88 nm spheres, the Lifshitz approach (compared to the alternative "coupled dipole method") underestimated the van der Waals force by about 10% at separations greater than 2 nm, while at near-contact, the forces were overestimated by more than 20%.[135] Nonetheless, these results do support the idea that strength of adhesion could be an important factor in determining whether a specific type of nanoparticle would be an effective stabilizer.

6.5 Conclusions

The experiments in this study have demonstrated that stabilization of weakly charged silica microparticles (which, at the IEP, flocculate out of suspension in less than 1 hour) can be effectively stabilized with both positively-charged zirconia and alumina nanoparticles. The zirconia nanoparticles successfully stabilized suspensions of 0.1% vol. silica microparticles using

a wide range of concentrations, from 1.0% to as low as 10^{-4}% vol., while the alumina nanoparticles stabilized the silica at 0.01% vol. The suspensions were stable for the entire observation period of more than 12 hours.

For both nanoparticle types, the nanoparticles directly adsorbed to the microparticles, as observed using SEM imaging. The adsorption led to increasing zeta potentials with increasing nanoparticle concentration. Additionally, significant repulsive forces were measured in the nanoparticle systems that were not present with the silica surfaces alone. The nature of the zirconia induced forces was electrostatic; however the forces produced by these particular alumina nanoparticles were too long ranged to be purely electrostatic. It is suggested that aggregation of the nanoparticles, in the bulk and adsorbed to the silica surface, led to significant steric repulsion. Furthermore, with both the silica and zirconia, the forces were determined to be effectively irreversible, as there was no detectible difference in the repulsion 1 hour after flushing the fluid cell with particle-free water at the same pH.

It is theorized that the stabilizing ability of these metal oxide nanoparticles arises in part from their stronger degree of adhesion to the silica surfaces, specifically as compared to polystyrene latex nanoparticles which were previously shown to be unable to stabilize similar silica suspensions. This increased strength of adhesion could result from a stronger attractive van der Waals force, as the Hamaker constant for both the zirconia/silica and alumina/silica systems was roughly twice that of the polystyrene/silica system. While additional studies with a broader range of nanoparticles are clearly warranted, it seems clear that the strength of adhesion could be an important factor in assessing the effectiveness of charged nanoparticles as colloidal stabilizers.

Chapter 7: Forces and Force-scaling in Systems of Adsorbing Nanoparticles as Measured using Colloidal-Probe Atomic Force Microscopy

7.1 Introduction

The forces between colloidal particles is not only fundamental interest, but of practical importance in understanding and controlling suspension properties, including rheology, aggregation, and colloidal stability.[136] While research into the nature and behavior of colloidal suspensions has been conducted since the late 19th century, only within the last few decades have instruments and techniques been created which allow for directly measuring forces between individual particles, which has allowed for improved understanding of colloidal interactions and related phenomena. The development of devices such as the osmotic stress device (interactions macromolecules and semi-permeable interfaces) and the surface force apparatus (interactions between smooth cylindrical surfaces) allow measuring interaction forces between specific surfaces at angstrom-scale resolution at small separation distances.[67, 70, 75, 77] Another technique, total internal reflection microscopy (TIRM), provides a noninvasive method of measuring colloidal interactions on a single particle immersed in a liquid with sensitivity to forces as small as 0.01 pN.[71, 72]

The development of atomic force microscopy (AFM) has led to the ability to measure forces between a wide variety of surfaces and particles, down to the molecular level.[94] Initially, colloidal force measurements were performed using sharp cantilever tips; however in 1991 the colloid probe AFM (CP-AFM) technique was developed, which provided a method for measuring the forces between a micron-sized sphere and a flat substrate.[80, 94, 137] This technique utilizes a colloidal microsphere with a known radius attached to the tip of an AFM cantilever. CP-AFM allows for a wide selection of materials for the probe particle and substrate, as well as significant modifications to the surfaces that are not possible with other techniques. Furthermore, the signal-to-noise ratio in the measurements is improved due to the larger total force exerted on the probe particle compared to a sharp tip [95].

With many of these techniques, including CP-AFM, the force can be easily scaled to different particle sizes and shapes using the Derjaguin approximation, which provides a simple algebraic expression relating the force between a spherical particle and plate to the interaction energy per unit area between two infinite plates.[138] The Derjaguin approximation requires making some assumptions about the geometry, primarily that the radii of curvature of the interacting surfaces is much greater than both the separation distance and the characteristic length scale of the force.[14, 136, 139] At common colloidal probe sizes, however, it has been shown to be an accurate technique for predicting equilibrium surface forces. For the electrostatic interaction between two charged surfaces, the accuracy of the approximation has been shown to

improve with increasing electrostatic surface potentials.[140, 141] More details about the Derjaguin approximation will be provided in the Theory section.

Recently, many research groups, including this one, have used CP-AFM to measure forces between colloidal particles in suspensions of nanoparticles.[61-63, 84] In many cases, the focus was on negatively-adsorbing nanoparticles, such that a depletion interaction was produced at short ranges due to exclusion of the nanoparticles from the gap region.[48, 49] In other cases the focus was on adsorbing nanoparticle systems, such as systems containing weakly-charged micron-sized particles in a suspension of highly-charged nanoparticles.[17,18,23,24] In these systems, adsorption of the nanoparticles creates strong electrostatic repulsive forces between the micron-sized particles at short separations that can be sufficient to stabilize them against flocculation.

In experiments involving CP-AFM, the Derjaguin approximation is typically used to analyze the measured force profiles. Specifically, the measured forces are frequetly normalized by the radius of the probe particle, since the Derjaguin approximation predicts that the force scales linearly with particle radius. Recent measurements from our group, however, have called into question the validity of this assumption. This manuscript reports on a comprehensive study focused on understanding the validity of the Derjaguin approximation in systems of adsorbing nanoparticles. CP-AFM was used to measure the force profile between a micron-sized, spherical, silica particles and silica plate in in nanoparticle suspensions at and above the pH value of the silica isoelectric point (IEP). The nanoparticles used were either negatively-charged polystyrene latex nanoparticles (sulfate surface groups) or positively-charged zirconia (zirconium dioxide, ZrO_2) nanoparticles. In addition to the force measurements, adsorption experiments were used to characterize the degree of nanoparticle adsorption at different solution conditions.

7.2 Theory

The Derjaguin approximation was first presented in 1934.[138] In general, the approximation involves approximating the shape of a curved surface using a set of concentric rings. Figure 7-1 shows a simple schematic of two spherical particles, each of equal radius R, which have been approximated by a set of parallel rings, each at distance Z from the opposing surface. For very thin rings (thickness much smaller than radius), the area each ring can be approximated as $(2\pi x)\mathrm{d}x$, where x is the inner radius of a ring of thickness dx. The force between the two spheres can then be described by Equation 6.1, where $f(Z)$ is the normal force per area between two planar surfaces and D is the distance of closest approach between the two surfaces. The upper integration limit of infinity is based on the assumption that the characteristic length scale of the force is much smaller than the particle radii.

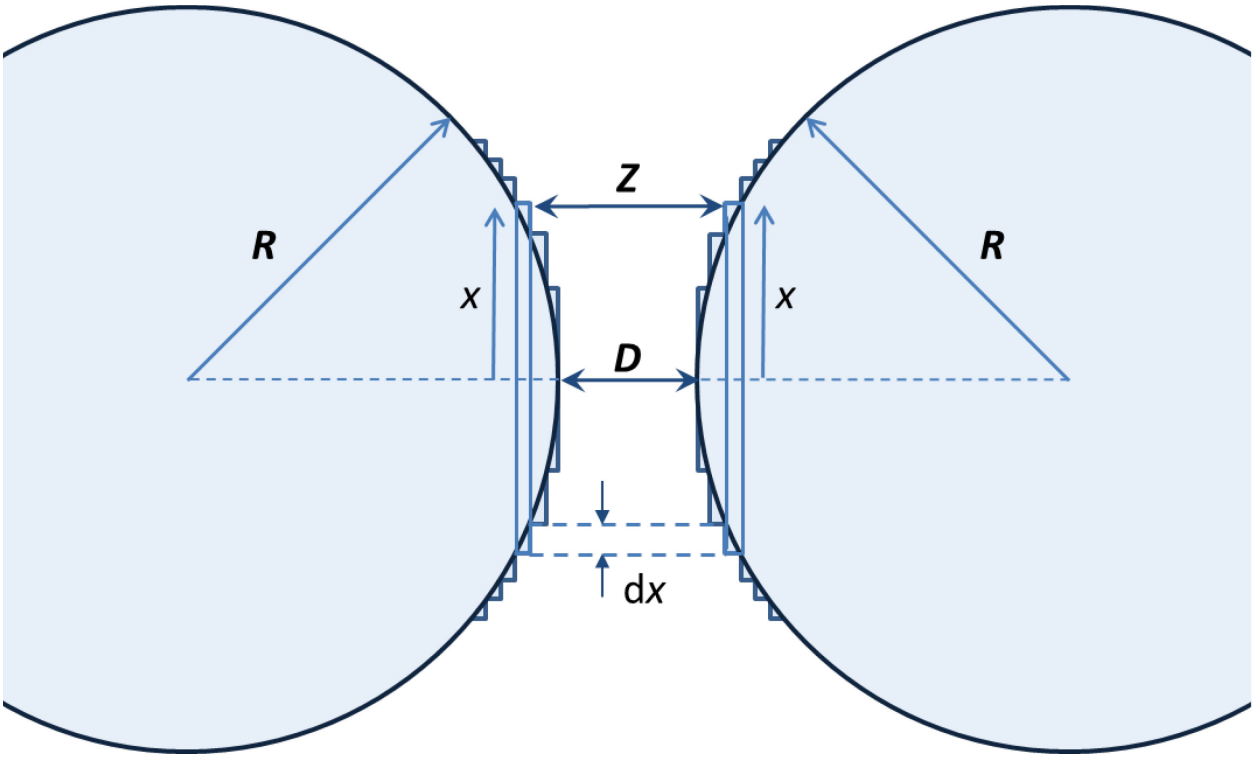

Figure 7-1: Schematic of two interacting spherical particles, with a visual representation of the Derjaguin approximation.

$$F(D) = 2\pi \int_{Z=D}^{Z=\infty} f(Z) x \, \mathrm{d}x \tag{6.1}$$

Because of the assumption that the range of the interaction is much smaller than the radii of the interacting particles, the interaction region will be confined to the area around the point of closest approach between the particles. In this area, the distance between two opposing points on the surfaces, Z, can be approximated as [14]

$$Z \approx D + \frac{x^2}{R} \tag{6.2}$$

yielding

$$\mathrm{d}Z \approx \frac{2}{R} x \, \mathrm{d}x \tag{6.3}$$

Inserting the relationship for $x\mathrm{d}x$ obtained from this equation into Equation 6.1 and integrating yields Equation 6.4, which is the general Derjaguin approximation for the force between two spherical particles. As explained above, the equation assumes that the separation distance, D, and length scale of the interaction are smaller than the particle radii.[14]

$$F(D) = \pi R \int_{Z=D}^{Z=\infty} f(Z) \mathrm{d}Z \tag{6.4}$$

For the case of a spherical particle of radius R interacting with a flat plate, a similar derivation shows that the force is simply that predicted by Equation 6.4 multiplied by 2. Finally, using the fact that interaction force is simply the negative derivative of the interaction energy, the following relationship can be derived relating the force between s colloidal particle and plate, $F(D)$, to the energy per unit area between two infinite plates, $W(D)$

$$F(D) = 2\pi R\, W(D) \tag{6.5}$$

The important point of this equation is that for equal surface conditions and separation distances, the force between a particle and plate should scale linearly with the particle radius.

The Derjaguin approximation has been shown to be accurate for a variety of colloidal interactions, including electrostatic forces, the non-retarded van der Waals force, polymer induced forces, adhesion, and depletion forces.[11, 14, 136, 142, 143] Various modification to the approach, such as the surface element integration (SEI) technique, provide a wider range of applicability (e.g., smaller particles), but typically at the expense of mathematical simplicity.[139] As an example, Todd and Eppell showed that the SEI technique was better than the Derjaguin approximation at predicting the electrostatic interaction between a 7 nm AFM cantilever tip and flat substrate in a solution with a Debye length of 9.6 nm.[144] However, in the vast majority of the measurements of colloidal forces using techniques such as CP-AFM and TIRM, the system parameters are such that the assumptions inherent in the Derjaguin approximation are easily met and the technique is thus applicable.

7.3 Materials and methods

7.3.1 Materials

The various solutions were prepared using water that had a resistivity of 18.2 MΩ-cm, produced by a Barnstead EASYpure II UV Ultrapure water system (Thermo Scientific, catalog #D7401) that was fed by the in-house DI water. Fused silica slides (Corning 7980 fused quartz silica, item #3x1x1mm) were supplied from TGP (Technical Glass Products, Inc., Painesville, OH). Two types of nanoparticles were used: sulfate latex (catalog #S37200, Life Technologies, Carlsbad, CA) with a specified diameter of 0.02 μm, and zirconia (product #ZR10/20, Nyacol, Ashland, MA) which had a specified diameter of 5-10 nm. To adjust the solution pH, hydrochloric acid (Optima grade, Fisher Scientific, catalog #A466-250) and sodium hydroxide (1.0 N Mallinckrodt Standard grade, catalog #4693-60) were used, each diluted to 0.1 M using ultrapure water.

For the CP-AFM force measurements, two sizes of silica spheres, 5 μm (Polysciences, Inc., Warrington, PA) and 30 μm (Microsphere-Nanosphere, Cold Spring, NY) were used as colloidal probes. The AFM cantilevers used for the force measurements were ORC8-10 model cantilevers (Bruker AFM Probes, Camarillo, CA). The glue used to mount the spheres was a thermoplastic epoxy (EPON 1004F Resin, Momentive, Columbus, OH).

7.3.2 Preparation of nanoparticle suspensions

The nanoparticle suspensions used in these experiments were prepared by diluting the supplied stock solution with the ultrapure deionized water to the desired concentration. The solutions were prepared in 20 mL scintillation vials (Wheaton Science Products Inc., catalog #986540), which had been cleaned with ethanol and rinsed with deionized water. In order to remove any excess ions, dialysis of the suspensions was performed by adding ion-exchange resin (Bio-Rad, catalog #143-7425) to each suspension at the manufacturer specified ratio of 5 g resin per 100 mL of solution. The nanoparticle suspensions were rotated for 4 hours using a continuous sample rotator (operating at 4 rpm) to slowly mix the samples and redistribute the resin throughout the suspension. Once the dialysis period had finished, the nanoparticle suspensions were decanted into clean scintillation vials. Each sample was then titrated to the desired pH value (either pH 2.5 or 9.0) immediately prior to each experiment.

7.3.3 Nanoparticle adsorption

Dialyzed nanoparticle solutions (1.0% and 0.1% vol.) were titrated to the desired pH (pH 2.5 or 9.0) using 0.1 M HCl and 0.1 M NaOH, as was a blank (nanoparticle-free) solution for use as a rinsing solution. Cleaned silica slides were submerged in the nanoparticle suspensions for 20 min. The slides were removed from the nanoparticles and lightly rinsed in the pH-adjusted blank solution in order to remove any non-adsorbed particles. The slides were left to air dry and then sputter-coated with gold (less than a 2 nm thick coating) before being imaged via scanning electron microscopy.

7.3.4 Colloid probe atomic force microscope measurements

Particle interactions and forces between silica surfaces in suspensions of the polystyrene latex nanoparticles were investigated using CP-AFM. For these experiments, the silica spheres to be used as colloidal probes were cleaned by diluting the stock solution with 100% ethanol and then shaken until the spheres were evenly distributed. The suspensions were centrifuged, the supernatant drawn off, and the spheres dried in a low temperature oven. The clean spheres were mounted on the D-lever (nominal spring constant k=0.05 N/m) of an ORC8 cantilever chip using a probe mounting microscope with translating stage and cantilever holder. As there was some variation in particle size, the exact particle diameter of the sphere was determined using a calibrated onscreen ruler before being cleaned in a UV/Ozone cleaner (BioForce Nanosciences, Inc., Ames, IA) for 20 min. An example of each sphere type is shown in Figure 7-2 (imaged via SEM). The contact surface of attached probes were imaged on a TGT01 ultra-sharp tip silicon grating (NT-MDT, Santa Clara, CA) using an Asylum Cypher AFM (Asylum Research, Santa Barbara, CA). Each sphere that was used in an experiment had an RMS surface roughness of less than 1.0 nm (typically less than 700 pm), which was calculated from a flattened image of the sphere surface. The precise spring constant of the cantilever (with mounted spherical probe) was determined via the method of Hutter and Bechhoefer[96].

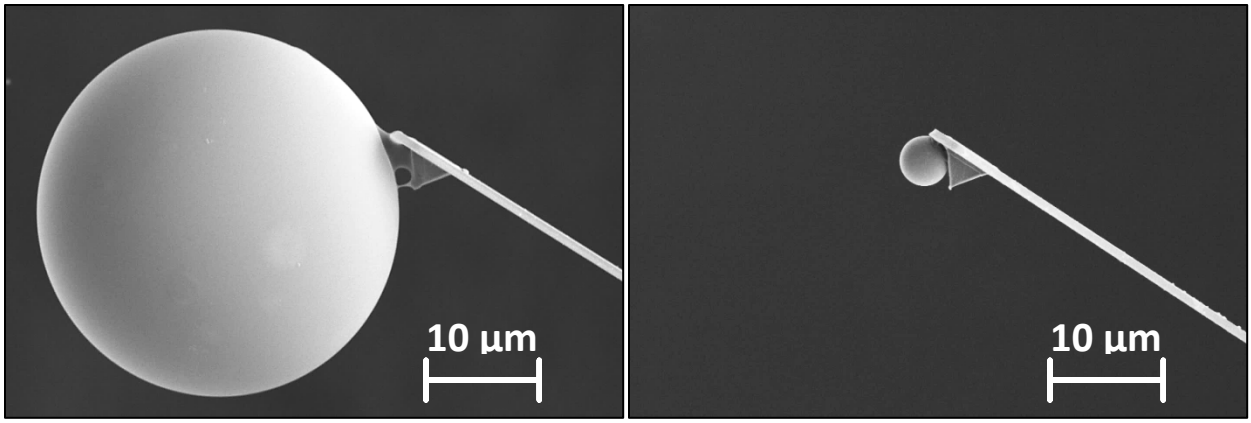

Figure 7-2: SEM micrographs of AFM cantilevers with attached probes: 30 µm (left) and 5 µm (right) diameter SiO_2 spheres.

The CP-AFM force profile experiments were performed using an Asylum Research MFP-3D AFM in a closed fluid cell environment (model #CCELL). The experiments utilized a sphere and plate geometry, with the forces being measured between the cantilever-mounted probe and a flat silica slide. The silica slide substrates were cleaned by ultrasonication in 100% ethanol before being rinsed and dried with ultra-high purity nitrogen, then glued to the base plate of the AFM fluid cell with epoxy. The disassembled fluid cell components were sonicated in pure ethanol for 1 hour before being rinsed with ultrapure water and dried. The cell was then assembled and filled with the desired solution.

The force measurements were performed at a 100 nm/s scan rate (slow enough to avoid hydrodynamic forces), with the scan range starting at 1.0 µm separation. The number of deflection-distance curves (approach and withdrawal) recorded ranged from 30-50 per sample, depending on the quality of the individual curves. The raw deflection data was converted to force versus separation curves via the analysis methods of Ducker et al.[94] and the individual curves were averaged into a single curve to reduce noise and other irregularities. All the force curves reported in this paper are the curves measured as the probe approaches the surface. For each experiment comparing two different probe sizes, the solution was withdrawn from the fluid cell, the cantilever was switched out for one with the other probe size, and the solution was replaced in the cell.

7.4 Results

7.4.1 Measured force profiles

The approach force curves in Figure 7-3 show the forces between a silica probe particle and silica plate without added nanoparticles in cases in which the silica surfaces are either highly charged (pH 9.0) or uncharged (at the IEP of pH 2.5). In the highly charged case at pH 9, the purely repulsive force results from the electrostatic repulsion between the negatively-charged

particle and plate, with the total force depending on the radius of the colloidal probe. The 30 µm probe experiences a greater force than the 5 µm by a factor of approximately 6 and, as shown in the adjacent graph, the two curves are nearly the identical when normalized by dividing each by $2\pi R$ as per the Derjaguin approximation. The small remaining difference likely arises from small differences in the zeta potential between the two silica particle sizes or slight inaccuracies in determining the exact sphere radius. At the IEP, by comparison, it is apparent that the electrostatic interaction has effectively been eliminated. (With the 30 µm probe particle, a small van der Waals attraction is measured at separations less than approximately 20 nm; this attraction is likely too small to be detected with the 5 µm probe particle.)

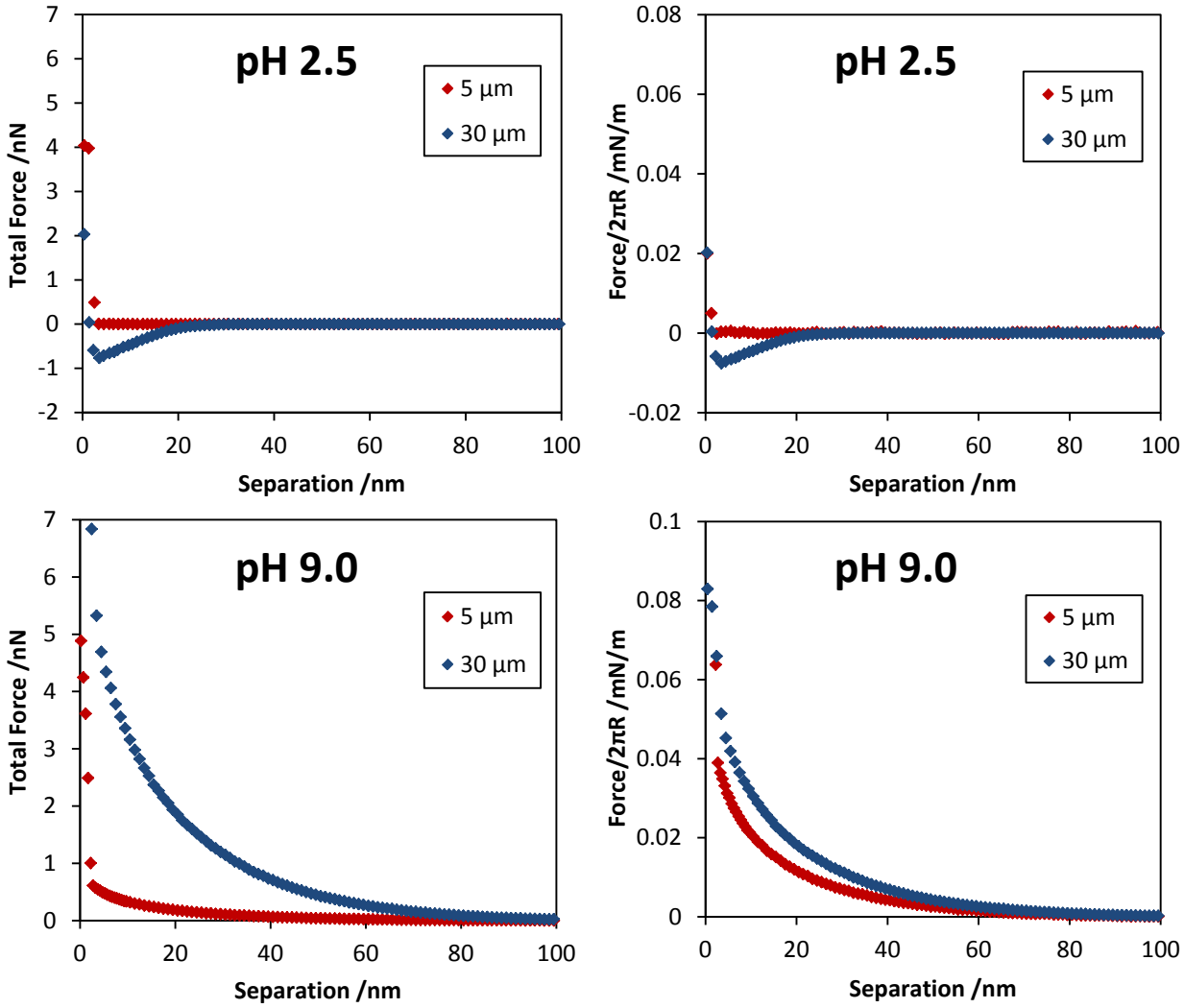

Figure 7-3: Forces between only silica surfaces at pH 2.5 (top) and pH 9.0 (bottom), for 5 and 30 µm colloidal probes. Left: Total force measured (nN). Right: Force scaled by $2\pi R$ (mN/m).

These experimental results shown in Figure 7-3 are the comparison basis for the results for the subsequent experiments performed in the presence of the nanoparticles. The experiments

performed at pH 2.5 charged such that there is a strong repulsion between the silica surfaces. Furthermore, the electrostatic repulsion scales linearly with the size of the probe particle.

Upon the introduction of charged nanoparticles to the system, a very clear repulsive force develops. Previous results from this group have shown that this repulsion arises from adsorption of the nanoparticles.[63, 84] Figure 7-4 shows the interaction between the 5 and 30 μm silica sphere and plate in the presence of the negatively charged sulfate latex nanoparticles. The experiment was carried out at bulk nanoparticle concentrations of 0.1% vol. as well as 1.0% vol. The force is very similar, in terms of both magnitude and range of interaction, to measurements that were previously reported by Ji, et al.[63] The magnitude of the force is slightly smaller in the 1.0% vol. nanoparticle solution, which likely arises from the higher ionic strength produced from the counterions of the charged nanoparticles.[122]

Surprisingly, however, the measured forces at both nanoparticle concentrations are found to be almost completely independent of the size of the probe particle. As a result, when the force curves are normalized by $2\pi R$, a significant difference is now observed.

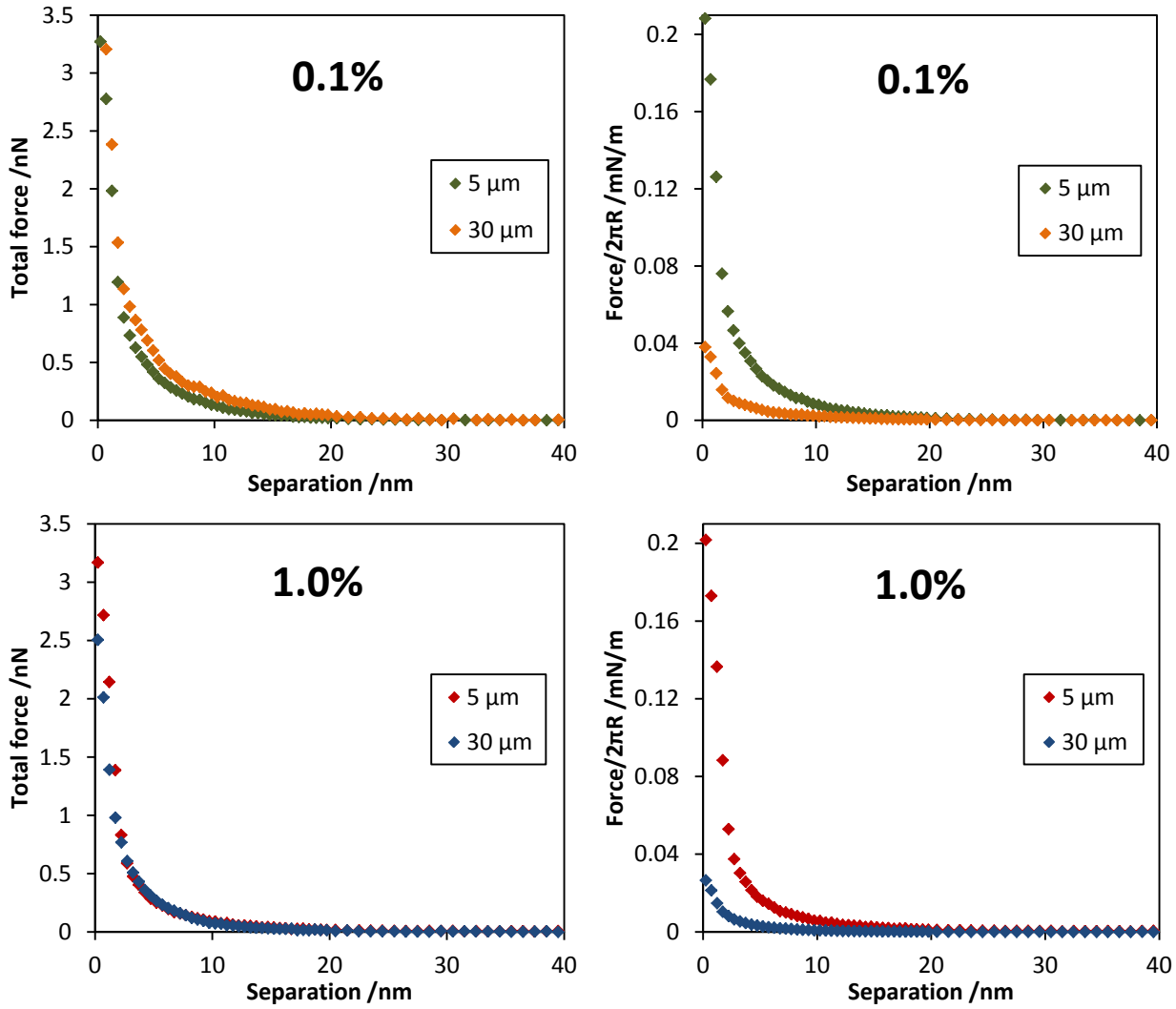

Figure 7-4: Approach force curves for two probe diameters (30 µm, 5 µm) at pH 2.5 (silica IEP) in solutions of sulfate latex nanoparticles. The graphs on the left show the total unscaled force (nN), while those on the right show the forces scaled by $2\pi R$ (mN/m).

As the repulsive forces observed in the experiments at the silica IEP (pH 2.5) arise due to the adsorption of nanoparticles, further experiments were done well above the IEP at pH 9.0 where the silica and sulfate latex are both strongly negatively charged in order to minimize the adsorption of the nanoparticles. At pH 9.0, the silica zeta potential would be approximately -70 mV [123, 133], while the zeta potential of the sulfate latex nanoparticles was measured using a Malvern Zetasizer to be -43.6±5 mV. As in the previous plots, Figure 7-5 shows the silica and sulfate latex systems (1.0% and 0.1% vol., using both 5 µm and 30 µm probes), but at the higher pH. Here we can see that the 0.1% vol. system effectively returns to the same relationship between the sphere size and interaction force as was in the system with no nanoparticles (Figure 7-3). Specifically, the force measured with the larger probe particle is higher than that obtained with the smaller particle, and when normalized by $2\pi R$ the two curves are nearly the same.

However, the 1.0% vol. system still exhibits the non-dependence on sphere size that occurs in the system at pH 2.5.

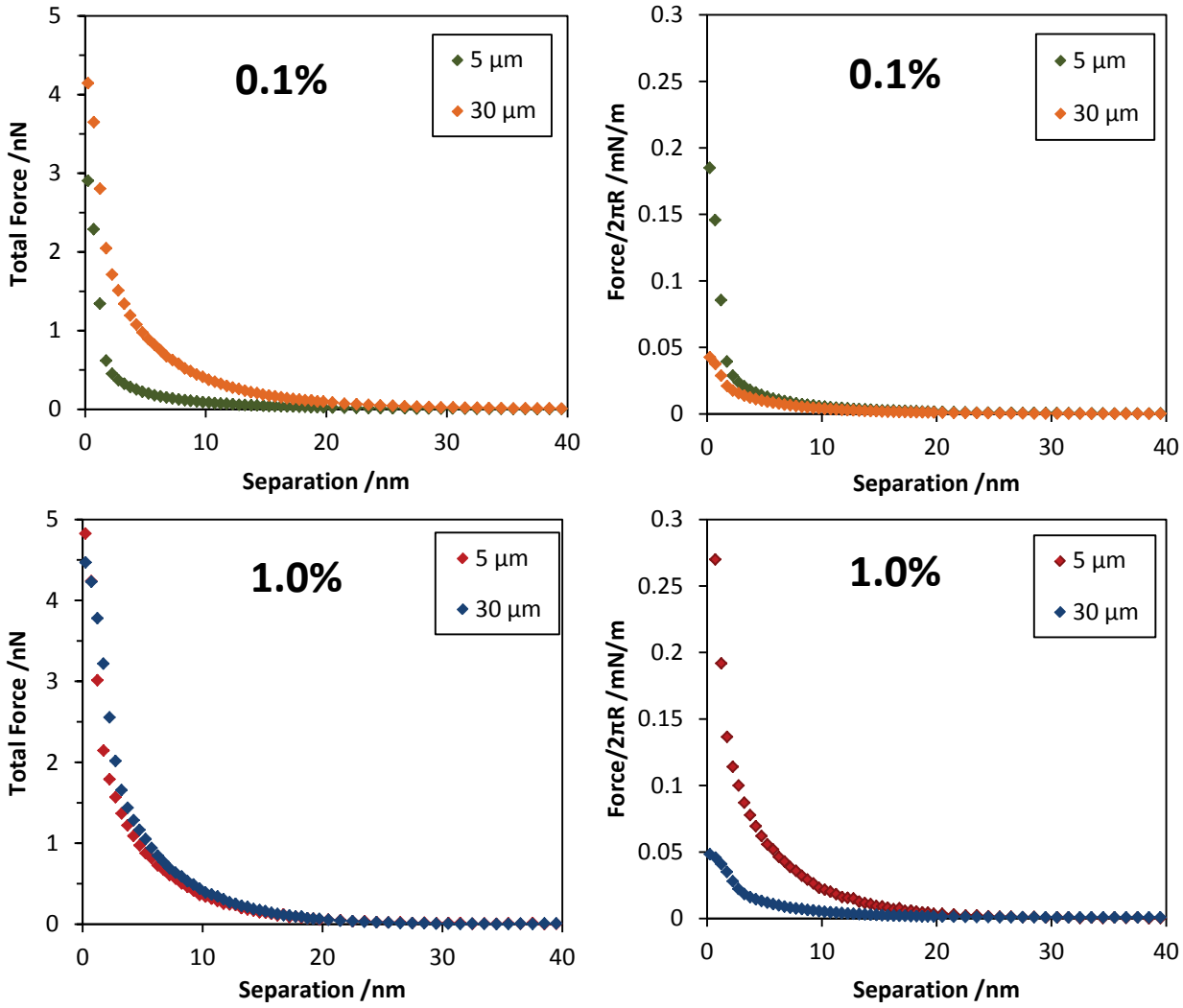

Figure 7-5: Approach force curves for two probe diameters (30 µm, 5 µm) at pH 9.0 (minimizing nanoparticle adsorption) in solutions of sulfate latex nanoparticles. Left column: Total unscaled force (nN). Right column: Force scaled by 2πR (mN/m). Top row: 1.0% vol., Bottom row: 0.1% vol.

It is interesting to note that at pH 9.0, the absolute value of the force measured in the presence of nanoparticles (Figure 7-5) is significantly less than that measured without the nanoparticles (Figure 7-3). As an example, with the 30 µm probe particle, the force at a separation distance of 10 nm in the system without nanoparticles was approximately 3 nN. By comparison, for the systems containing both 0.1% and 1.0% sulfate latex nanoparticles, the force at this separation was approximately 0.4 nN. While some of this difference could be due to the higher ionic strength arising from the nanoparticles, a more likely explanation is a different definition of separation distance. In the CP-AFM measurements, separation is measured relative

to the point of hard contact between the surfaces. With nanoparticles in solution, even a small amount of adsorbed nanoparticles would mean that hard contact would involve a layer of nanoparticles between the silica particle and plate. As a result, the distance between the actual silica surfaces would actually be larger than that reported in Figure 7-5, which would mean a weaker repulsive force.

Figure 7-6 shows the forces between different silica probes in systems of zirconia nanoparticles (0.01% and 0.1% vol.) at pH 2.5. The zirconia nanoparticles were chosen because they had a higher calculated Hamaker constant at contact with a silica surface and therefore would have a stronger van der Waals attraction, leading to enhanced adsorption. Using Lifshitz theory [24], the zirconia-silica system had a Hamaker constant of approximately 2.1×10^{-20} J, compared to 0.99×10^{-20} J for the polystyrene-silica system. One other difference is that at pH 2.5, the zirconia nanoparticles are positively charged, and have zeta potentials of approximately+43.3.±7.8 mV (also measured using Malvern Zetasizer).

Nonetheless, behavior similar to that observed with the latex particles is observed. The zirconia nanoparticles produce significant repulsion between the silica surfaces. The 0.1% system is slightly more repulsive than the 0.01% but the difference is relatively small. In addition, at equivalent volume fractions, the zirconia leads to a greater repulsive force than the sulfate latex nanoparticles. For example, the repulsive force with the zirconia nanoparticles is approximately twice that of the latex nanoparticles at separations of 5 – 10 nm and 0.1% vol. (seen in Figure 7-4). This could be explained in part by the slightly higher absolute zeta potential of the zirconia particles (+43.3±7.8 mV) relative to the latex (-35.1±5.3 mV), as well as an increased degree of adsorption. Regardless, no dependence on probe size is observed with the zirconia nanoparticles, indicating that this unusual behavior is not unique to the latex nanoparticles.

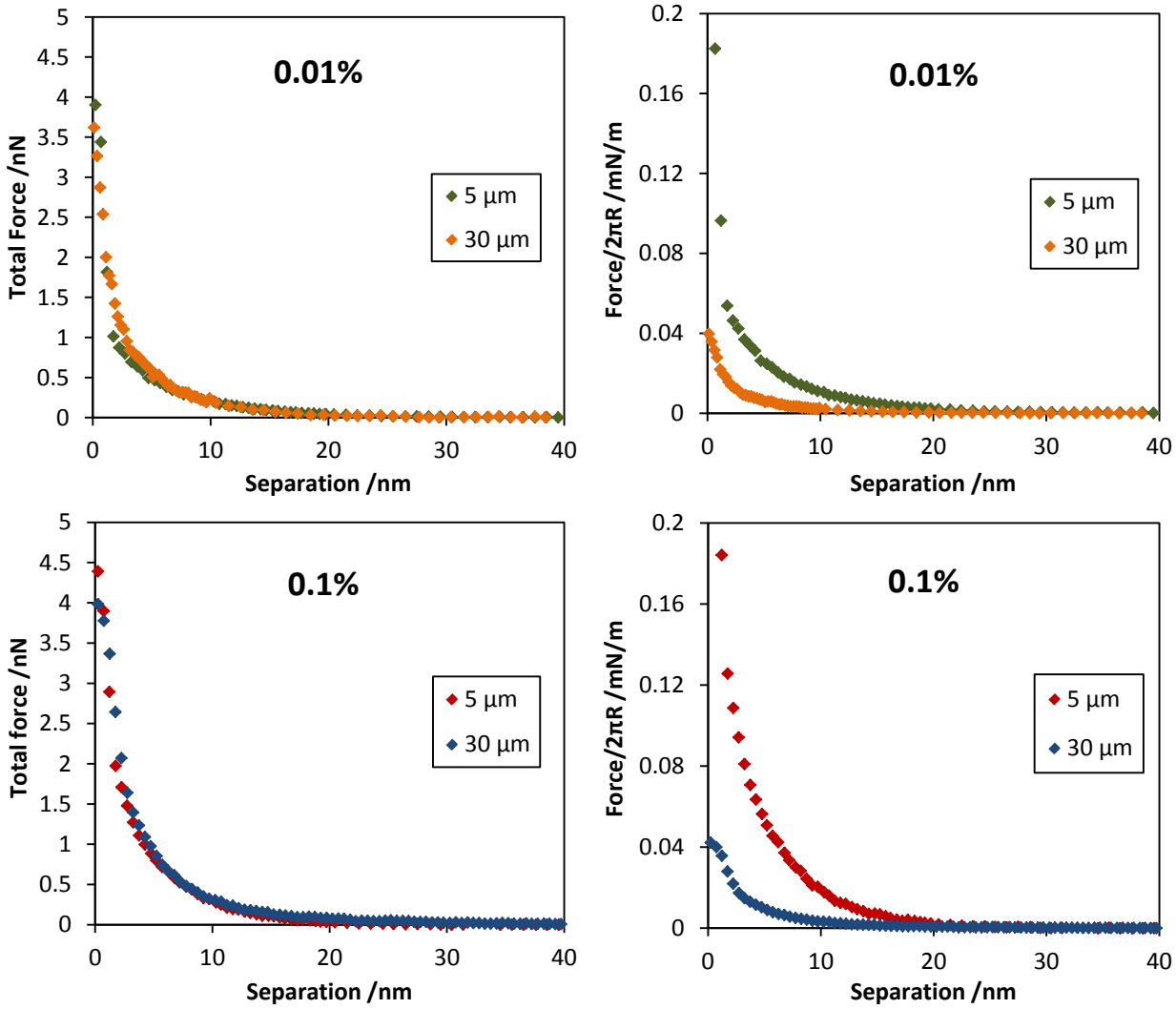

Figure 7-6: Approach force curves for two probe diameters (30 µm, 5 µm) at pH 2.5, in solutions of zirconia nanoparticles. The graphs on the left show the total, unscaled force (nN), while the force scaled by $2\pi R$ (mN/m) is shown in the graphs on the right.

From the plots in Figures 6-3 through 6-6, it is clear that while there are slight differences between each curve, they all appear to follow an approximate exponential decay. For a purely electrostatic repulsion, the repulsive force should decay roughly exponentially, especially at larger separations, and therefore a semi-log plot (natural log of the force versus separation distance) should yield a straight line with the slope of the line equal to the negative of the inverse Debye length, κ. Semi-log plots of the force for the systems containing latex nanoparticles are shown in Figure 7-7. The decay lengths, obtained from the slope of the linear region of each plot, are given in Table 7-1.

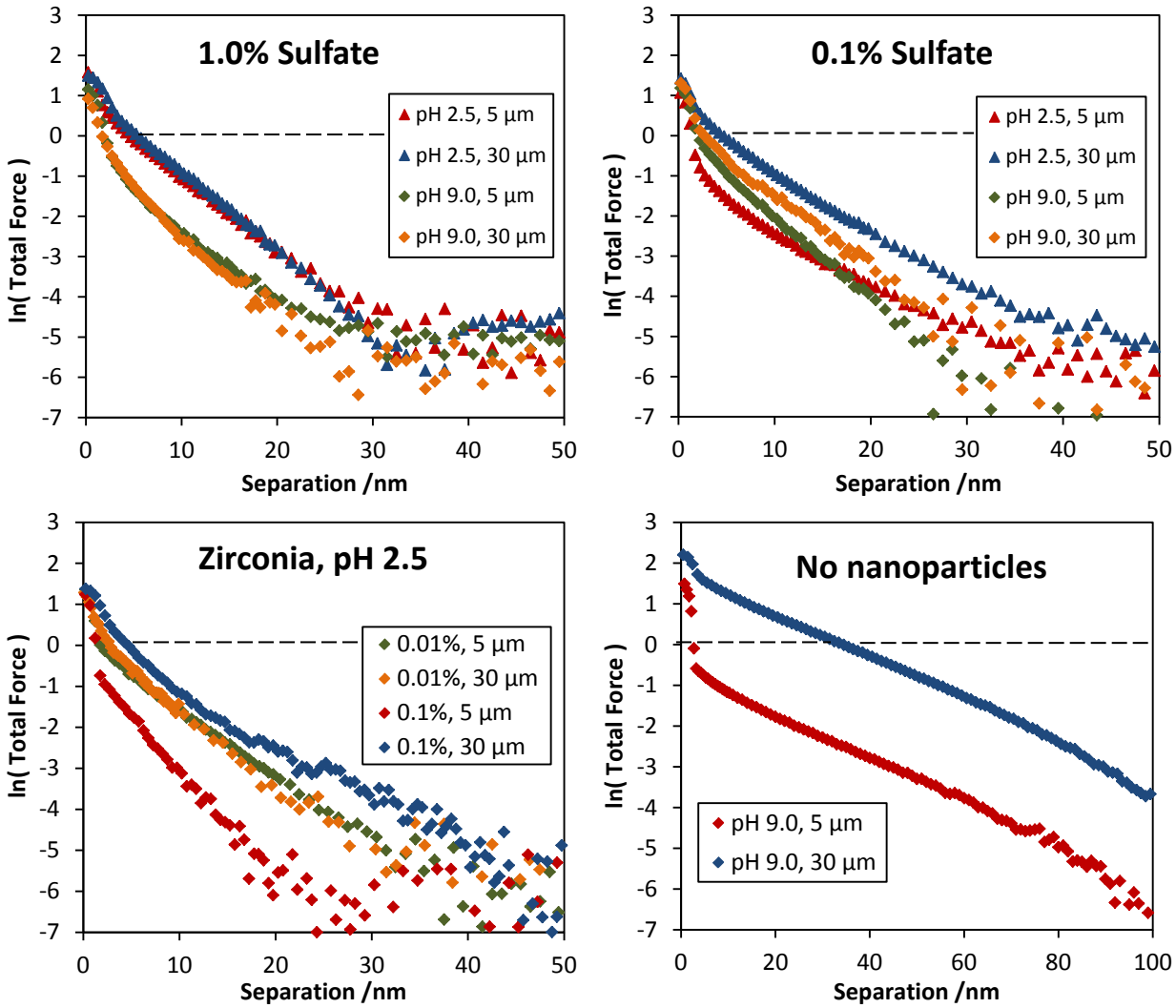

Figure 7-7: Graphs of the natural log of the total force as a function of separation distance; comparisons of different nanoparticle solutions with different colloidal probe sizes (5 µm and 30 µm). Top left: 1.0% vol. sulfate latex.

Also listed in Table 7-1 are the theoretical Debye lengths (κ^{-1}) which were calculated using an ionic strength determined from the known amount of titrant that was added to each solution to reach the desired pH. In the experiments utilizing the sulfate latex nanoparticles, each experiment results in an approximately linear plot at separation distances less than approximately 30 nm for the 1.0% vol. and less than 50 nm for the 0.1% vol. suspension (the region where the total force is non-zero). They also deviate slightly from linearity at very small separations (< 4-5 nm), which has been observed previously [63].

At pH 2.5, the calculated Debye lengths for the sulfate latex suspensions actually agree quite closely with the theoretical Debye length of 5.72 nm. The ionic strength is relatively high at this pH, resulting in small values; however each sample was within a few tenths of a nanometer

of the predicted Debye length (except the 0.1% sample using the 5 μm sphere, which was about 20% smaller). This indicates that the repulsive forces measured are electrostatic in nature.

Table 7-1: Comparison of the theoretical Debye length (κ^{-1}) with the decay length values calculated from the measured force curves. All units are in nanometers.

	pH 2.5 (5 μm)	pH 2.5 (30 μm)	pH 9.0 (5 μm)	pH 9.0 (30 μm)
Theoretical κ^{-1}	*5.72*	*5.72*	*28.22*	*28.22*
No nanoparticles	---[a]	---[a]	17.21	20.25
0.1% Sulfate	4.68	5.47	7.91	7.98
1.0% Sulfate	5.86	5.89	4.47	4.31
0.01% Zirconia	5.67	4.79	---[b]	---[b]
0.1% Zirconia	4.49	7.36	---[b]	---[b]

[a]Could not be calculated from force curve (at IEP). [b]Zirconia suspensions were not measured at pH 9.0.

At pH 9.0, there is a larger discrepancy between predicted and measured decay lengths. The theoretical Debye length is nearly 30 nm, while the measured values with no nanoparticles were 17.21 and 20.25 nm for the 5 μm and 30 μm probes, respectively. The values for the nanoparticle suspensions were approximately 8 and 4.5 nm (0.1% and 1.0%, respectively). This discrepancy in the absence of nanoparticles is likely due to the difficulties in accurately controlling the ionic strength with very little added electrolyte. In the systems containing the nanoparticles, the smaller screening lengths arise from the counterions released in the solution from the charged nanoparticles.[122]

One important point to note in these results is that at a given solution, the decay lengths are essentially the same with the different particle sizes. This finding confirms that with both the 5 μm and 30 μm particle probes, the predominant interaction is a similar electrostatic repulsion.

7.4.2 Nanoparticle adsorption

The images in Figure 7-8 show the adsorption occurring on the silica slides for bulk concentrations of sulfate latex nanoparticles of 0.1 and 1.0% vol. While there are noticeably more adsorbed nanoparticles at 1.0%, it is clear that there is significant deposition at both concentrations. Given that these images were taken on surfaces that had been dried, there could have been rearrangement of the nanoparticle on the surface, meaning that these images may to accurately represent the morphology of the adsorbed nanoparticles in the actual test suspensions. Regardless, these images clearly indicate that the latex nanoparticles adsorb to the silica surfaces at the concentrations used in the CP-AFM experiments.

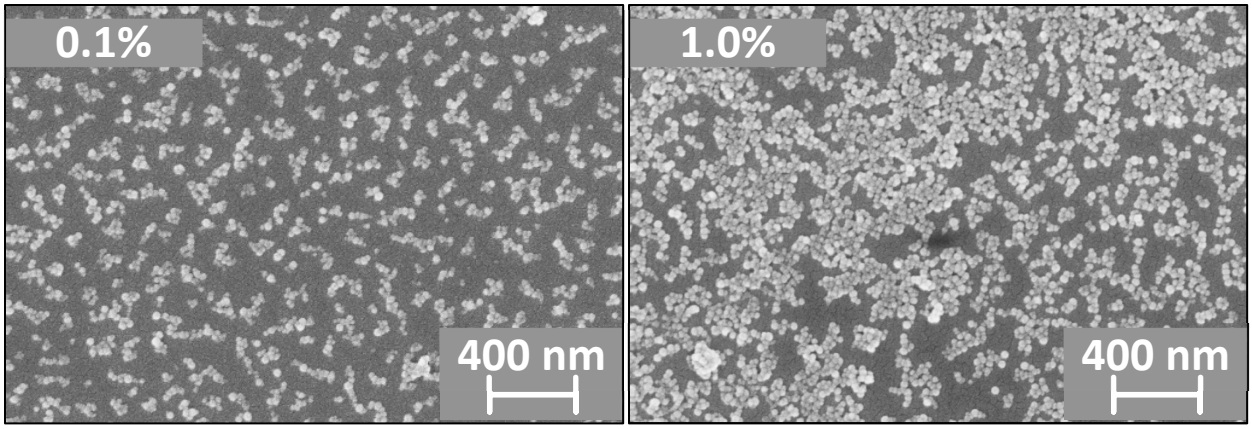

Figure 7-8: SEM micrograph of sulfate latex nanoparticle adsorption on silica slides. Nanoparticle solutions were at pH 2.5, the IEP of silica.

Images of silica surfaces after exposure to the latex nanoparticles at pH 9.0 are shown in Figure 7-9. While the degree of adsorption is, as expected, substantially smaller due to the higher net surface charge on the silica, it is certainly not zero. This is especially true at the higher latex concentration of 1.0% vol. Additionally, in each sample there was a high degree of variability in the number of adsorbed particles at different locations on the surface, so these images are simply a general representation of the overall characteristics. The significance of these images is discussed in greater detail in the Discussion section.

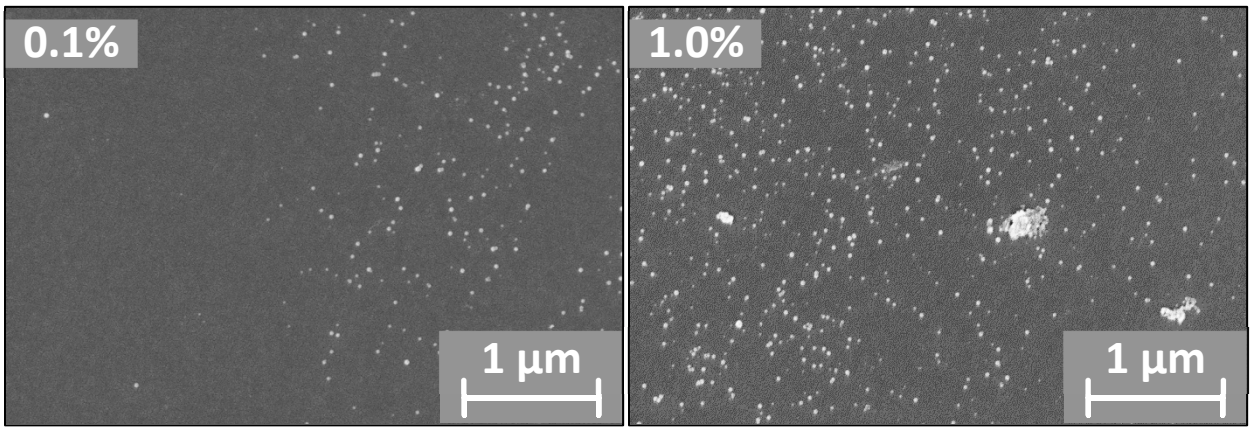

Figure 7-9: Sulfate latex nanoparticle adsorption on silica slides at pH 9.0, for 0.1% (Left) and 1.0% vol. (Right) nanoparticle suspensions.

7.5 Discussion

The primary findings from the experimental results presented in the previous section can be summarized as follows:

1. At the isoelectric point of the silica sphere and plate, the addition of highly charged nanoparticles of either zirconia or sulfate latex to the system produced a significantly increased repulsive force between the silica surfaces. (In the absence of the nanoparticles, only a very weak van der Waals attraction was detected.) At equal bulk volume fractions, the magnitude of the force was slightly greater with the zirconia nanoparticles.
2. At pH 2.5, where the underlying silica surfaces have no net charge and the measured electrostatic interaction thus arises predominantly from the adsorbed nanoparticles, the measured force profiles was essentially independent of the size of the probe particle.
3. In systems where there was a substantial amount of nanoparticle deposition, such the observed electrostatic repulsion arose primarily from the adsorbed nanoparticles (i.e., at pH 2.5 where the underlying silica surfaces are essentially uncharged), the repulsive force was independent of the size of the probe particle.
4. At pH 9.0, where the silica is highly charged, the correct size scaling was observed at the lowest sulfate nanoparticle volume fraction (0.1% vol.). However, at the higher nanoparticle concentration (1.0% vol.), the force was again found to be independent of the probe size.

In the remainder of this section, possible causes of this lack of dependence on probe size are discussed.

7.5.1 Scaling of interparticle forces by particle size

The finding that the interaction force that arises with substantial nanoparticle adsorption is essentially independent of the size of the probe particle was completely unexpected and calls into question the validity of the Derjaguin approximation in these systems. When the underlying silica substrate is essentially uncharged, which will be the case at the IEP of the silica, the electrostatic repulsion will be predominantly determined by the adsorbed nanoparticles. Two questions that come to mind then are (1) are the conditions for the validity of the Derjaguin approximation still valid under these circumstances, and (2) if the Derjaguin approximation is indeed valid, is the radius of the probe particle still the appropriate scaling length?

To address these issues, it is helpful to revisit the basic assumption inherent in the derivation of the approximation. Essentially, the Derjaguin approximation assumes that the surface of the probe particle can be represented as a series of thin, concentric rings and that the force of interaction between each ring and the opposing plate can be calculated as the area of that ring multiplied by the force per unit area between two infinite parallel plates at the same separation as the ring and plate. The force between the probe particle and plate is then calculated by essentially summing the force between each ring and plate. Although not explicitly stated, one other assumption inherent in the Derjaguin approximation is that the properties on the surface of

the particle or plate that determine the interaction force are spatially uniform (i.e., all of the rings have identical surface properties).

An important point about the experimental results presented above that should be emphasized is that that the observed scaling between the magnitude of the force and particle size was not only different from that expected from the Derjaguin approximation but was actually found to be completely independent of the probe size. Such a result could only arise if the interaction region that determined the probe-plate interaction was independent of the probe size. One possible scenario where this would occur would be if the measured interaction force as essentially arising from two opposing nanoparticle – one on the probe particle and one on the plate. In other words, the density of adsorbed nanoparticles was low enough that the probability of more than a single nanoparticle-nanoparticle interaction occurring was sufficiently small that it effectively did not occur.

The likelihood of this scenario can be effectively discounted for two reasons. First, as seen in Figure 7-8, at the higher concentration of the sulfate nanoparticles (1.0% vol.), there is substantial coverage of the silica by the nanoparticles, such that the chances of having only a single pair of nanoparticles interacting would appear extremely small.

The second reason is the magnitude of the measured force itself. Specifically, a rough estimate of the force between two latex nanoparticles can be obtained using the expression[11]

$$F = 32\pi\varepsilon\varepsilon_0\left(\frac{kT}{e}\right)^2 \kappa R \tanh^2\left(\frac{e\psi}{4kT}\right)\exp(-\kappa D) \tag{6.6}$$

where F is the electrostatic repulsive between two spheres of radius R separated by distance D, ψ is the surface potential of the spheres (assumed equal), ε and ε_0 are the relative permittivity and permittivity of a vacuum, respectively, kT is thermal energy, e is the charge of a proton, and κ is the inverse Debye length of the solution. This equation assumes a symmetric electrolyte and linear superposition of potential, which typically requires a separation distance larger than the Debye length.[32] In addition, the Derjaguin approximation is used to account for curvature effects, meaning that the radius of curvature of the particles (11.5 nm in this case) should be larger than the Debye length (5.7 nm here). While this last assumption is only marginally valid here, Equation 6.6 should nonetheless provide a rough approximation to the interaction force between two spherical nanoparticles.

A plot of the force predicted by this equation is shown in the left-hand graph of Figure 7-10. For these calculations, in addition to the physical values listed in the previous paragraph, a surface potential of -40 mV was used. The value was based on the upper bound of the measured zeta potential for the sulfate latex nanoparticles at pH 2.5 (-35.1±5.3 mV). Also shown in the right-hand graph of Figure 7-10 is the force measured between a 30 μm silica particle and plate in 0.1% vol. sulfate latex nanoparticles at pH 2.5 (from Figure 7-4). As seen, while the shape of the two curves are similar, the magnitude of the measured force is roughly two orders of

magnitude greater than that predicted between the two sulfate nanoparticles, indicating that the measured force cannot be explained by a single nanoparticle-nanoparticle interaction.

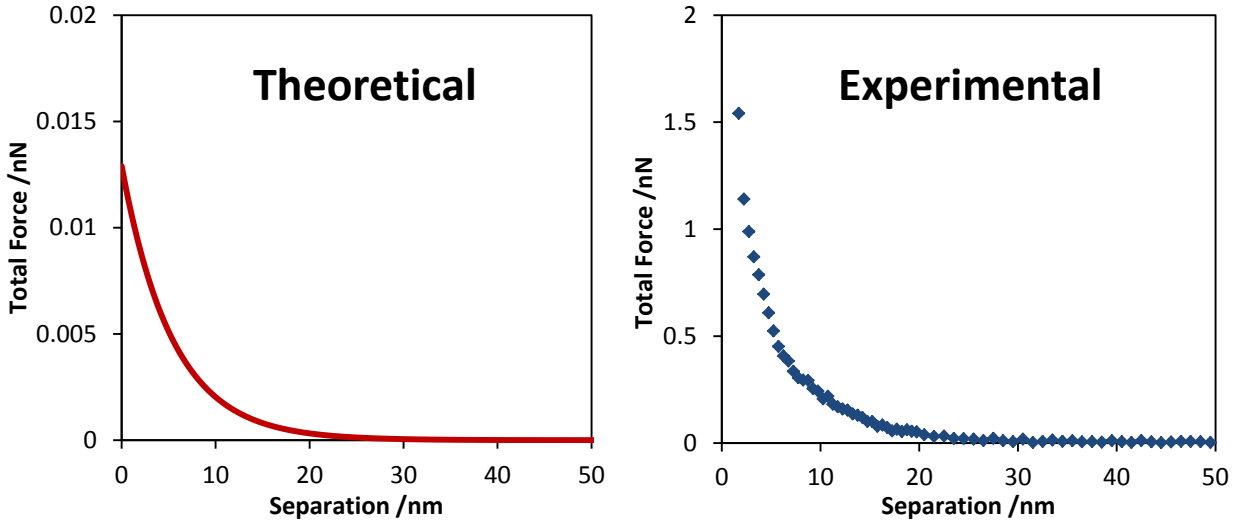

Figure 7-10: Left*:* Theoretical electrostatic force between two sulfate latex nanoparticles (calculated using Equation 6.6). Right*:* Measured total force of a 30 μm sphere in 0.1% vol. sulfate latex at pH 2.5 (Figure 7-4). *Note the difference in y-axis scales in the two graphs (the experimental curve is approximately 2 orders of magnitude greater).*

A second possibility that was considered is that the interaction is predominantly arising from a small patch of nanoparticles and that the size of this patch remains effectively unchanged as the probe size changes. One explanation that could possibly lead to such a phenomenon is would be the adsorbed nanoparticles getting displaced from the surface during the actual force measurement. Specifically, the CP-AFM force measurements are conducted by driving the probe particle toward the plate at a constant drive velocity and them measuring the deflection of the cantilever produced by the surface forces. (The approach speed, 100 nm/s, is small enough that hydrodynamic forces exerted on the probe particle are not significant.) As the particle approaches the plate, significant shear forces are produced by the squeezing flow in the gap region. At the surface of either the particle or plate, the magnitude of the shear rate, $|\dot{\gamma}|$, is given by the following equation

$$|\dot{\gamma}|_r = \frac{3r}{\left(D + \frac{r^2}{2R}\right)^2}\frac{\mathrm{d}D}{\mathrm{d}t} \tag{6.7}$$

where r is the radial distance measured from the point of closest approach, R is the radius of the probe particle, D is the distance of closest approach, and $\mathrm{d}D/\mathrm{d}t$ is the speed at which the probe particle approaches the plate. As expected, the shear rate is zero at the point of closest approach due to symmetry, increases to a maximum at r equal to $(2RD/3)^{1/2}$, then decays back to zero near the outer edge of the particle. What is perhaps most interesting about this equation,

however, is that at small r (i.e., $r << R$), the shear rate becomes independent of r. This can be seen clearly in Figure 7-11 which plots the shear rate at the surface of the particle or plate as a function of radial distance for two different values of D – 10 nm and 20 nm. The approach speed was assumed to be 100 nm/s, and values are shown for both the 5 and 30 µm particles. As seen, within roughly 100 nm or so from the point of closest approach, the shear rates for both the 5 µm and 30 µm particles are essentially the same.

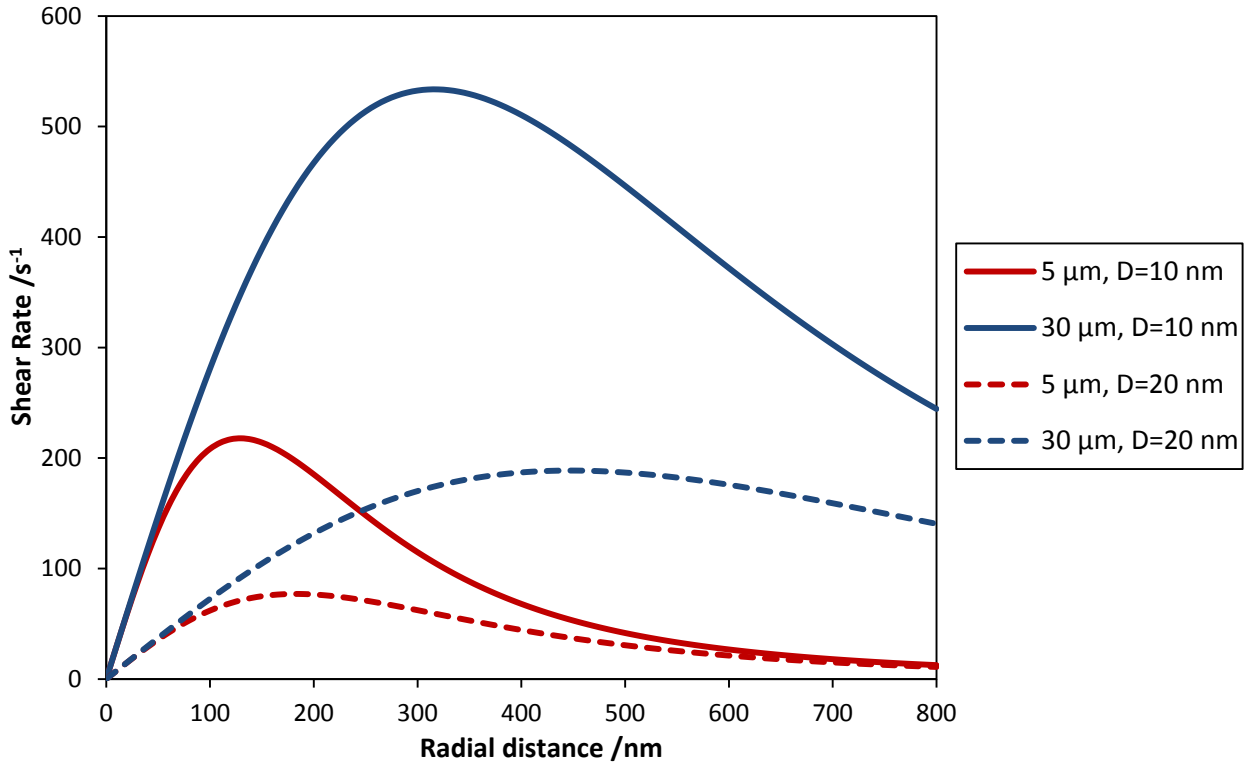

Figure 7-11: A comparison of the shear rate (s^{-1}) at the solid/liquid interface for 5 µm and 30 µm spheres approaching a flat plate at a velocity of 100 nm/s. The shear rate is plotted as a function of radial distance from the point of closest approach of the sphere at two different sphere/plate separation distances (D), 10 nm and 20 nm.

What this result implies is that if there were a critical shear rate necessary to dislodge the nanoparticles, and if this critical shear rate lied very near to the point of closest approach (i.e., in the region where the shear rate was independent of R), then there would be a small patch of nanoparticles remaining around the point of closest approach and the size of this patch would be independent of the radius of the probe particle. A simple schematic illustrating this effect is shown in Figure 7-12.

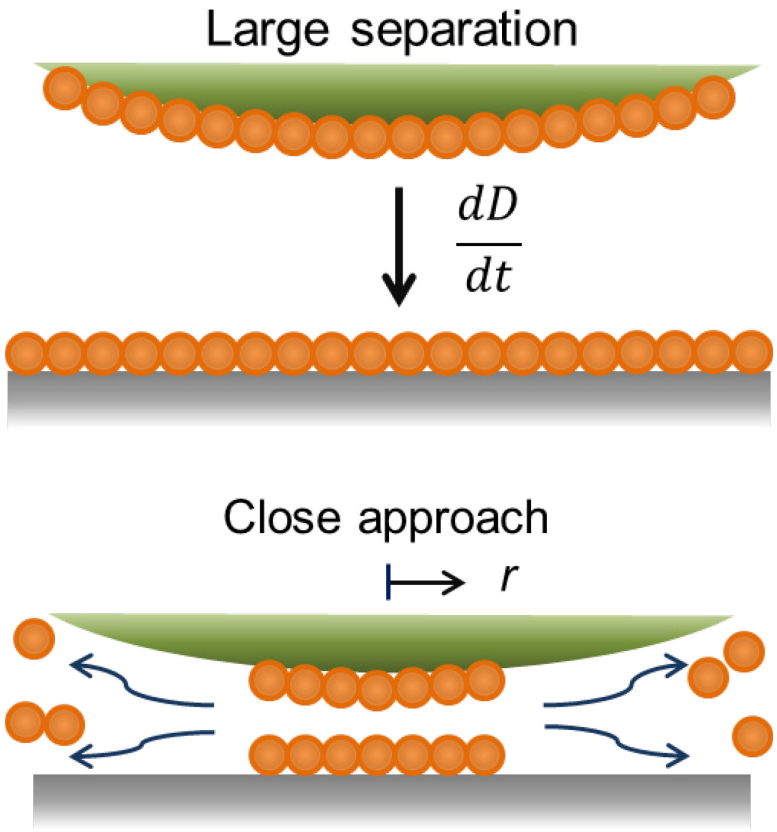

Figure 7-12: Schematic of proposed interaction between a colloidal probe and plate in suspensions of adsorbing nanoparticles that are sheared from the gap region during approach (not to scale). The nanoparticles are sheared from the surface at a certain radial distance, *r*, determined by the shear rate necessary to dislodge the nanoparticles.

Bergendahl studied the removal of various types of natural colloidal particles (i.e., hematite, goethite, and organic matter) from soil and found that a shear rate of 55 s^{-1} caused significant detachment of particles of size 700 – 800 nm.[145] Later, this same author investigated the shear detachment of 1 µm polystyrene particles from glass. It was found that approximately 90% of the polystyrene particles could be detached using a shear rate of around 130 s^{-1}.[146] Finally, Meinders showed that a shear rate of 200 s^{-1} reduced the number of polystyrene particles (size greater than 700 nm) adhered to glass by more than 90%.[147]

Although the sizes of the particles in this earlier work are larger than the nanoparticles used in the present experiments, the values of the shear rate required for particle detachment are certainly within the values attained in the particle-plate gap region of the CP-AFM experiments. Consider, for example, that a shear rate of 100 s^{-1} is required to remove the adsorbed latex nanoparticles. As seen in Figure 7-11, at a particle-plate separation distance of 10 nm, this shear rate is reached for both the 5 µm and 30 µm probe particles within roughly 40 nm from the point of closest approach. What this means is that nanoparticles would remain adsorbed in a circular

patch of radius 40 nm centered around the point of closest approach, but the region outside of this patch would be swept clear of the nanoparticles. Over this circular patch, the local separation distance between the particle and plate would vary by no more than 0.3 nm for the 5 μm probe particle and no more than 0.05 nm for the 30 μm probe particle, so the patches would essentially represent flat plates. (Note that for the 5 μm probe particle, the shear rate would again drop below 100 s^{-1} at a radial distance of approximately 300 nm from the point of closest approach, however at this point the local particle-plate separation distance would have increased to some 18 nm, which is large enough that electrostatic repulsive forces would have decayed to essentially zero.)

Using the hypothetical value of 100 s^{-1} as the critical shear rate (occurring at approximately 40 nm radially from the point of closest approach), this would mean an area of approximately 5000 nm^2 of adsorbed nanoparticles. By comparison, the cross sectional area of an individual 20 nm diameter nanoparticles would be approximately 300 nm^2. Thus it is clearly possible that a patch of sufficient size to accommodate multiple nanoparticles could remain on both the 5 and 30 μm probe particles (same size patch on both probe sizes) such that the nanoparticles in this patch determine the magnitude of the electrostatic interaction between the probe particle and plate.

In addition to the shear flow, the forces between the particles themselves may be contributing to the changes in the effective interaction area. Specifically, the electrostatic interactions between individual nanoparticles (on opposing silica surfaces, as well as between adsorbed particles on the same surface) could contribute to this behavior. The repulsion between nanoparticles could contribute to the susceptibility for the nanoparticles to move on the surface and therefore to being pushed from the interaction area. Thus, while additional experimental work would be required before a definitive statement about the cause of the lack of scaling between the measured forces and the size of the probe particle, this very preliminary analysis indicates that it is possible that removal of adsorbed nanoparticles due to factors such as the high shear rates in the gap region outside of a patch of fixed size could be the cause.

7.6 Conclusions

In this work, experimental colloidal probe CP-AFM measurements were performed to measure the interactions between silica surfaces in the presence of highly charged nanoparticles. Additionally, SEM micrographs were used to confirm the presence of adsorbed nanoparticles, along with the approximate degree of surface coverage. At the silica isoelectric point with the bulk nanoparticle concentrations used, sufficient adsorption took place to produce measurable electrostatic repulsive forces between the probe particle and plate.

The CP-AFM experiments utilized two different nanoparticle types, negatively charged sulfate latex and positively charged zirconia, and two different sizes for the probe particles, 5 and 30 μm. At pH 9.0, where the silica is highly charged, and without added nanoparticles, the

measured force profile was found to scale with the size of the probe particle, in agreement with the scaling predicted from the Derjaguin approximation. At pH 2.5 (the silica IEP) and with no added nanoparticles, essentially no electrostatic force was detected.

In the presence of nanoparticles, a totally different behavior was observed. At pH 2.5 with either sulfate latex or zirconia nanoparticles, no dependence of the measured force on the size of the probe particle was detected. At pH 9.0 and with added sulfate latex nanoparticles, the expected scaling with size was observed at 0.1% vol. bulk nanoparticles, while at 1.0% bulk nanoparticles the lack of dependence on size was again observed. These findings suggest that when the electrostatic repulsion between the silica particle and plate results predominantly from the charged nanoparticles adsorbed to the surfaces, the force is independent on the size of the probe particle.

It is suggested that this lack of dependence on probe size results from removal of the nanoparticles by the high shear rates in the gap region. Specifically, in the region around the point of closest approach, the shear rate at the surface of the probe particle and plate becomes independent of the size of the probe particle. (The shear rate is also exactly zero at the point of closest approach due to symmetry.) It is therefore theorized that the nanoparticles outside of a small patch near the point of closest approach are dislodged during the force measurement and furthermore that the size of this patch is independent of the size of the probe particle.

These findings clearly have implications on the use of CP-AFM to measure the forces between surfaces with adsorbed nanoparticles. Additional experimental study is nonetheless required before a definitive statement on the precise cause of the phenomenon can be identified.

Chapter 8: Conclusions, Contributions, and Future Work

8.1 Conclusions

The work in this dissertation focuses on the relationship between the stability of microparticle suspensions and how it is affected by the presence and adsorption of highly charged nanoparticles in a bidisperse system. The major conclusions are presented in the following:

1. Dispersions of weakly charged microparticles *can* be stabilized by the addition of highly charged nanoparticles, with the nanoparticles providing an electrostatic charge layer on the surface of the microparticles. At or near the isoelectric point, suspensions of silica microparticles will quickly aggregate and settle out of suspension in less than 1 h. With the addition of sufficient concentrations of zirconia or alumina nanoparticles, the silica is restabilized and exhibits no aggregation (observation time approximately 15 h). This is due to the direct adsorption of the nanoparticles on the surface, which occurs quickly and is effectively irreversible.
2. The standard predictors of stability (e.g. zeta potential) do not necessarily apply in the cases of adsorbing nanoparticles on uncharged surfaces. This is particularly evident in the experiments involving polystyrene latex nanoparticles. In these cases, there were significant increases in the effective zeta potential well beyond what would be required to stabilize silica-only suspensions, yet the resulting suspensions were ultimately still unstable. There was a reduction in how quickly the suspensions flocculated (slowed to 3-6 h), however both the adsorbed coverage and zeta potential were greater than those for the zirconia and alumina, which had proved to be effective stabilizers. This was attributed to the lower van der Waals interactions between polystyrene and silica in comparison to various metal oxides; the metal oxides were more strongly attached, and therefore had less potential to migrate or desorb from the surface.
3. While most colloidal-probe force measurements scale with respect to the radius of the probe, certain systems of adsorbing nanoparticles lack all scaling with probe size. This was observed with sulfate latex, zirconia, and alumina nanoparticles. In these systems, the observed forces that result from adsorbed particles were virtually identical when comparing a 5 μm and 30 μm sphere. One possible cause of this phenomenon is the high shear rate that occurs in the gap region between the colloidal probe and plate. Both probe sizes have similar contact regions, but past a critical radius, the shear rate on 30 μm sphere increases significantly more than the 5 μm. If the nanoparticles were sheared from the surface outside this radius, the effective interaction areas of the two particles would be very similar, and thus would give very similar force profiles.

8.2 Contributions

The major contribution of this work to the field of colloid science is conclusively showing that weakly charged dispersions can be effectively stabilized through directly adsorbed nanoparticles with low bulk concentrations. It compares the effectiveness of different nanoparticle materials as well as the conditions and parameters that lead to stability and provides evidence that the effects of the adsorbed nanoparticles are essentially irreversible. Previously, there had been very little information on the adsorption behavior of charged nanoparticles and how it relates to the zeta potential and stability of otherwise weakly charged and unstable microparticles. This work also demonstrates that not all systems where charged nanoparticle adsorption occurs (therefore leading to recharged microparticles) can effectively stabilize the dispersions. This has implications in the practical application of this method to control colloidal stability, as well as in the general understanding of the behavior of bidisperse suspensions.

Additionally, the force measurements focusing on the effects of probe size on the forces observed in suspensions of adsorbing nanoparticles had not been studied previously. The few literature sources where CP-AFM was performed with nanoparticle surfaces had assumed that the force scaled by the probe radius and therefore the measurements could be easily used to approximate the forces that would be present in systems of smaller particles. With the results shown in this dissertation, this assumption is called into question for these systems and demonstrates some of the limitations of these measurements, which will be important for proper interpretation of future experiments.

Journal articles

- S. Ji, D. Herman, J.Y. Walz, *Manipulating microparticle interactions using highly charged nanoparticles.* Colloids Surf., A, 2012. **396**, 51-62.
- D. Herman, J.Y. Walz, *Stabilization of weakly charged microparticles using highly charged nanoparticles.* Langmuir, 2013. **29**, 5982-5994.
- D. Herman, J.Y. Walz, *Adsorption and stabilizing effects of highly charged latex nanoparticles in dispersions of weakly charged silica colloids.* J. Colloid Interface Sci., 2014. DOI:10.1016/j.jcis.2014.11.022
- Chapters 6 and 7 are to be submitted for publication (co-authored with J.Y. Walz).

8.3 Recommendations for future work

While the conclusions from this work have shown that the adsorption of charged nanoparticles can be an effective stabilization method, a number of questions remain to be investigated.

1. A more quantitative assessment is necessary to determine the effects that the van der Waals forces have on the ability to use a certain type of nanoparticle as a stabilization method. The conclusions in Chapter 6 were from basic Lifshitz theory on half-spaces. To

further investigate this, a more rigorous calculation of the van der Waals interaction that accounts for nanoparticle size is required. With this, a set of experiments can be performed to compare the efficacy of different nanoparticle types in conditions where the only nanoparticle-microparticle force is the van der Waals attraction.

2. Further clarification of the scaling effects observed in Chapter 7 is required to make a definitive statement on the behavior of the CP-AFM measurements. The behavior was ascribed to the shear rate in the gap; however no experiments have been done to accurately determine the effects of shear on adsorbed particles of this small size. The experiments would be relatively straightforward; a flow cell would have to be constructed that would allow for accurate control of shear rates. Substrates (e.g. silica) could be inserted and nanoparticles deposited on the surface, then a flow of particle-free solution could be passed over the substrate at various velocities. Subsequent imaging of surfaces (AFM, SEM) could then be performed to assess the degree of desorption at a given shear rate.

   Additionally, the experimental conditions of the CP-AFM measurements can be altered to investigate the conditions that lead to this observed effect. Measurement parameters such as the scan speed can be adjusted (either higher or lower) to determine if there is any dependence for a given particle type. The particle and surface materials can be altered as well. However, CP-AFM experiments are not truly equilibrium measurements. Even if the scan or approach speed is reduced significantly to mitigate dynamic interactions, the probe is still being forced into contact with the substrate. Further measurements using techniques such as total internal reflection microscopy (TIRM) can allow for more measurements that observe the equilibrium behavior of a colloidal sphere near a surface, and could lead to a better approximation of the colloidal interactions of microparticles in suspensions with adsorbing nanoparticles.

3. Depletion measurements have previously been carried out in the systems of adsorbing nanoparticles (though at conditions where there was some electrostatic repulsion between microparticle and nanoparticle), but currently there has been no work to their effect on suspension stability when the underlying microparticle contributes no electrostatics to the system. Given that at least two particle types (zirconia and alumina) were determined to be effective stabilizers, additional experiments at high concentrations would provide insight into the upper concentration limits for stability in these binary suspensions and whether they are susceptible to standard depletion forces at expected concentrations. This would require force measurements at greater than 1% vol., with correlated stability measurements using nanoparticles that have been shown to stabilize the microparticle dispersion.

Appendix A: Colloidal Forces in Increasing Concentrations of Nanoparticles

Before the results discussed in Chapter 7 had been observed (regarding the lack of force scaling with probe size), measurements had been done to determine the forces between the silica surfaces at different concentrations of nanoparticles. While the results of Chapter 7 made it difficult to use the measurements as quantitative predictions of the stability behavior of the silica dispersions with added nanoparticles, they do provide qualitative insight into the adsorption behavior: the amidine and sulfate latex forces can be directly compared, and the zirconia curves can be used to show that repulsive forces are present even at very low nanoparticle concentrations.

A.1 Latex nanoparticles

The plots in Figure A-1 show the differences in the interaction between silica surfaces in different nanoparticle suspensions, ranging from 0% to 0.5% vol. In solutions of sulfate latex nanoparticles, we see a clear development of a repulsion force between the surfaces, though at the concentrations measured there was minimal dependence of the total force on concentration, unlike the stability and zeta potential measurements in the previous chapters. However, the forces are qualitatively consistent with the adsorption images in Chapter 5, which show rather minimal dependence on bulk nanoparticle concentration for the adsorbed particle density of sulfate latex on the silica microparticles.

In comparison to the sulfate latex, the surfaces in the amidine latex suspensions show a significantly greater interaction at each nanoparticle concentration in both magnitude and range. At all non-zero nanoparticle concentrations, we observe a significant repulsive force with a clear dependence on the nanoparticle concentration. The magnitude of the measured amidine forces are a factor significantly greater than the equivalent concentration of sulfate latex, and the range extends beyond 100 nm at the highest concentration (0.5% vol.). This qualitatively similar the measured zeta potentials and adsorption images in Chapter 5, as well as previously observed differences in the adsorption behavior of the two types of nanoparticles. The amidine latex produces significantly greater levels of adsorption and higher zeta potentials, which in turn results in much larger observed forces. Additionally, the very long range nature of the forces in the amidine system suggests multilayer adsorption, which likely produces a steric effect in addition to electrostatic forces.

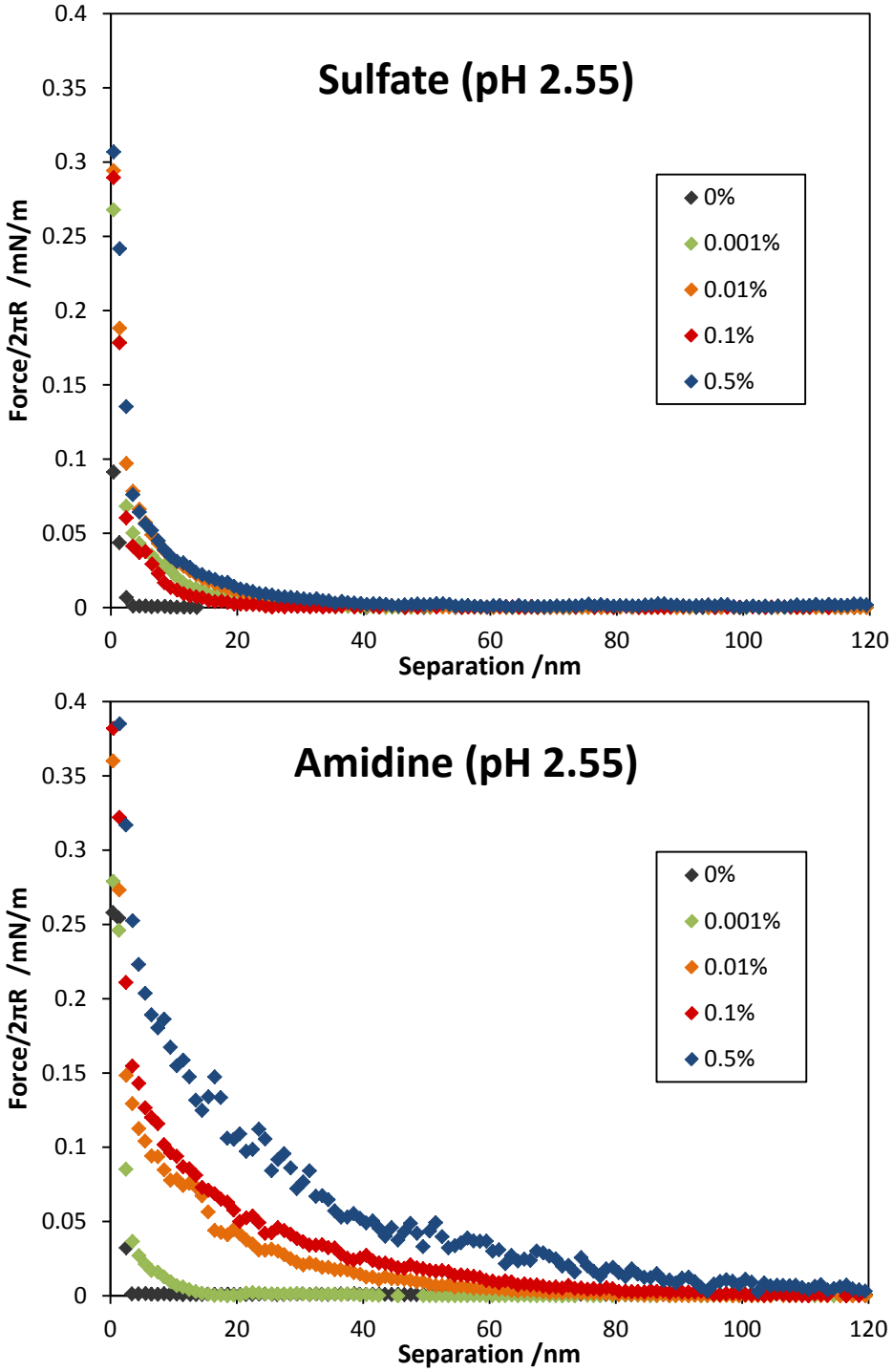

Figure A-1: Force versus separation for SiO_2 probe and substrate in increasing concentrations of nanoparticles (0% to 0.5% vol.) at the IEP. The top plot is with sulfate latex, and the bottom is with amidine latex.

A.2 Zirconia nanoparticles

The goal of this measurement was to see if there was any appreciable effect of zirconia concentration on the forces in the system, given that the stable range for the silica microparticles spanned such a large range of nanoparticle concentrations (slowed flocculation at 10^{-5}% and stability at 10^{-4}% vol. in Chapter 6). As we can see in Figure A-2 the lowest concentration (10^{-6}% vol.) was effectively unchanged from the nanoparticle-free measurement. However for the next lowest measurement, 10^{-5}% vol., there was a significant repulsive force present. Intriguingly, as the concentration of nanoparticle increases beyond this point, there was very little increase in the magnitude or shape of the force curve, and even increasing from 10^{-5}% to 10^{-1}% vol. yielded very little variation. It is possible that the surfaces were effectively saturated with nanoparticles, however since a 30 μm particle was used, it is also possible that the maximum observed force is limited by the same effect of shear rate proposed in Chapter 7. Regardless, repulsive forces were observed as low as 10^{-5}% vol., which is qualitatively consistent with the measurements in Chapter 6.

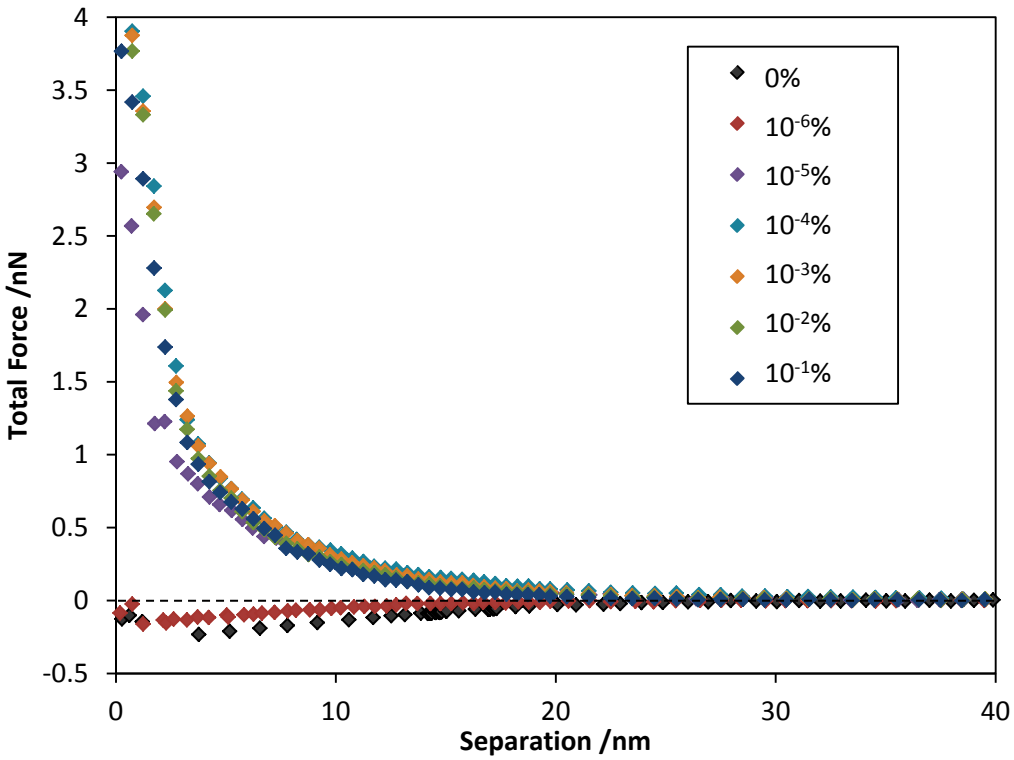

Figure A-2: CP-AFM curves showing the effects total forces between silica surfaces in solutions with increasing concentrations of zirconia nanoparticles. Solutions were at pH 2.55. Zirconia concentrations are % vol.

A.3 Comparison between polystyrene and zirconia forces

Given that the all the nanoparticles that were used in experiments produced a repulsive force between otherwise non-repulsive silica surfaces, yet only the metal oxide particles stabilized the suspensions, a comparison between the zirconia and polystyrene was done. Figure A-3 shows the force between a 5 µm silica sphere and plate in 0.1% vol. solutions of nanoparticles (zirconia and sulfate latex); both systems were shown to essentially produce purely electrostatic interactions (as opposed to the amidine and alumina, which indicated steric effects, and therefore cannot be accurately compared). The zirconia stabilized the silica dispersions, and the measured force is measurably larger than the sulfate latex which did not fully stabilize. The zirconia forces were at least twice the sulfate latex at most separation distances. This is consistent with the zeta potential measurements in Chapters 5 and 6, where the silica had larger zeta potentials than the sulfate (approximately +43 mV versus -23 mV at 0.1% vol.). The increased force and zeta potential is likely due simply to the greater degree of adsorption and coverage for zirconia relative to the sulfate latex. This may result as much from the higher number of the zirconia nanoparticles present at equal volume fractions as from the difference in the strength of adsorption for the two particle types.

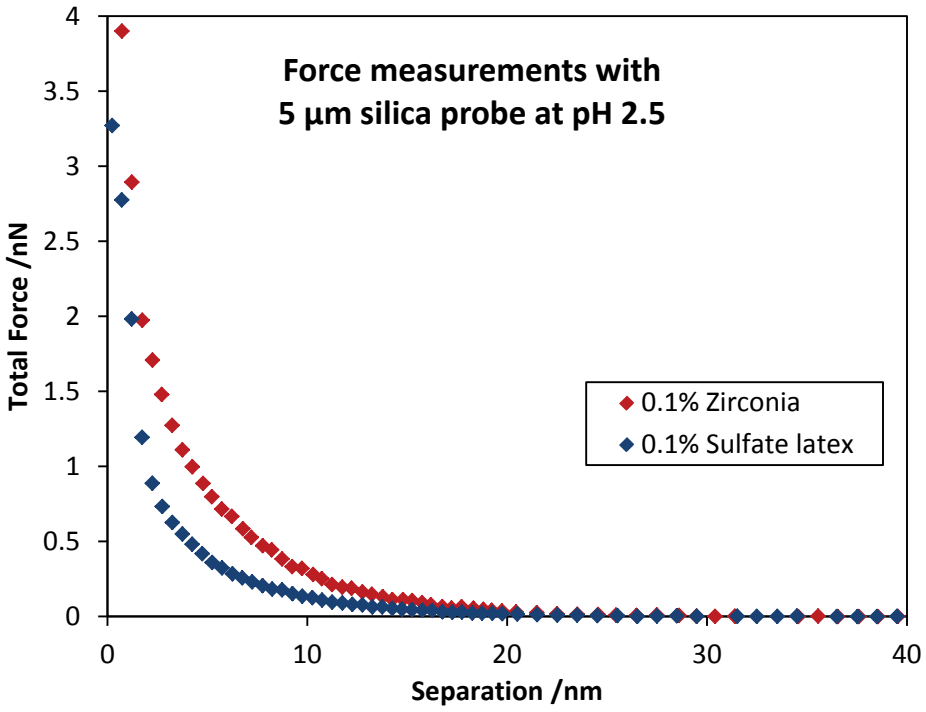

Figure A-3: Comparison between sulfate latex and zirconia at identical concentrations by volume (0.1% vol.). Solutions were at the silica IEP (pH 2.5).

Appendix B: Adsorbed particle size analysis

B.1 SEM image analysis

The particle size distribution of adsorbed nanoparticles, shown as histograms in Chapter 5, was determined by analyzing SEM micrographs of adsorbed latex nanoparticles on silica slides. The goal was to adsorb a quantity of nanoparticles so that the particles could be imaged as individuals on the surface. The software used was ImageJ, a free, public-domain image analysis program.[148] Figure B-1 shows the analysis of a single SEM micrograph.

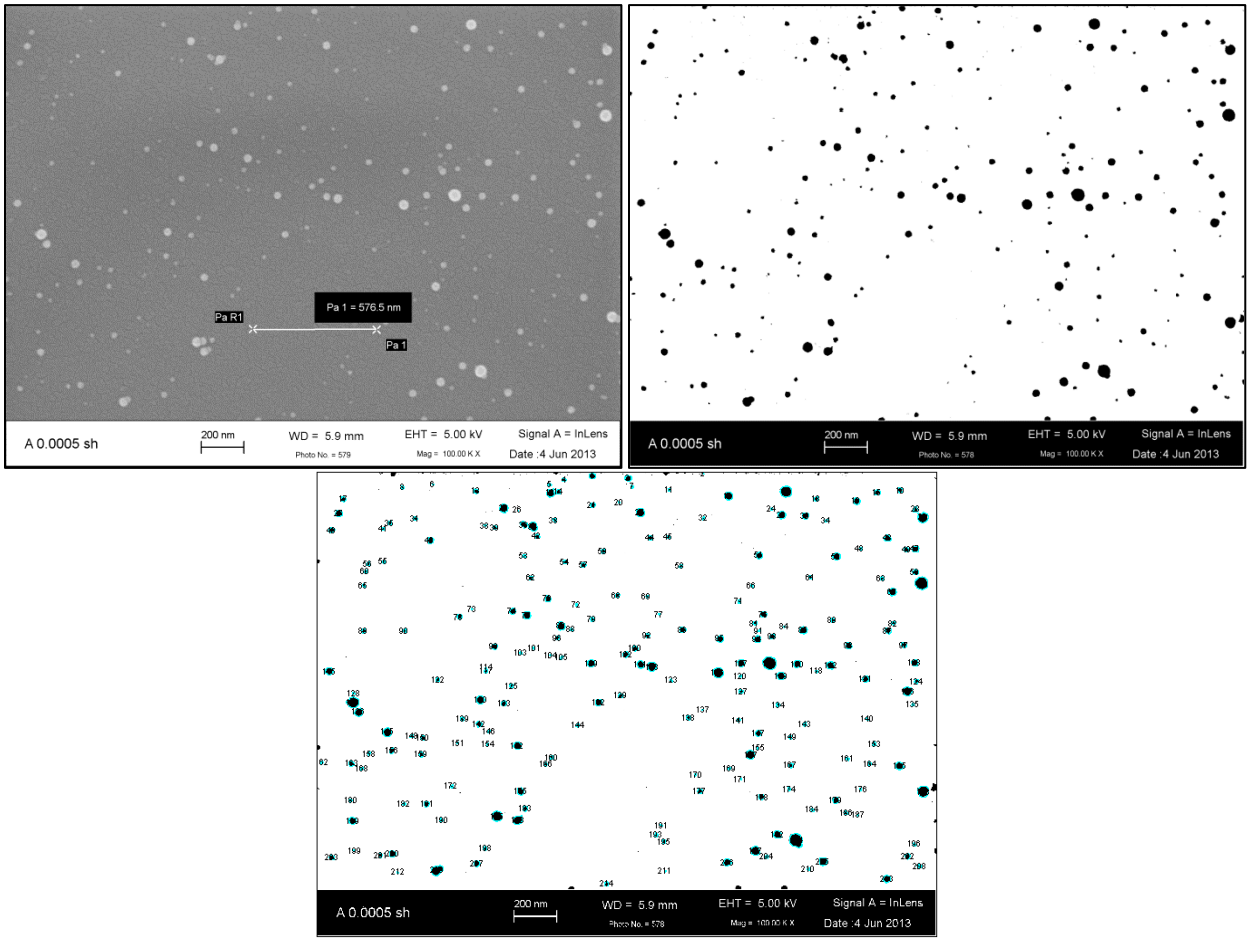

Figure B-1: SEM micrograph analysis. Top left: Unaltered image. Top right: Threshold levels adjusted. Bottom: Particles identified and analyzed.

The particle sizing analysis operates on the assumption that the particles are spherical and therefore the two-dimensional area that a particle occupies in an image is simply equal to πR^2, allowing easy determination of the particle diameter. The processing technique was simple. A suitable SEM image was opened in the program. The measurement scale was calibrated to

nm/pixel using the SEM length scale which is present at the bottom of every image. The image is converted to grayscale (if starting with a color image), and the image contrast adjusted and background masked using the "threshold". This converts the micrograph to a binary image with the particles being 100% black and the background 100% white. The "Analyze Particles" tool was then used, which calculates the area of each individual particle. Limits can be set for the minimum and maximum area to be counted. The area is then used to calculate the radius of the particle.

Due to the resolution of the SEM images, the lower limit for the particle size was set approximately equal to that of a 5 nm diameter particle. This was to prevent detection of artifacts and other stray pixels that would be included when the threshold was properly set. In particular, the silica substrate, when sputter-coated, had a faint texture with a feature size on the order of 2-3 nm and certain regions had a tendency to be more visible than others. The consequence here is that there may be some small nanoparticles, particularly in the amidine latex, that were not counted, however this is unavoidable as it was not possible to distinguish smaller particles from the background.

B.2 AFM imaging

Initially, AFM imaging was used to image adsorbed nanoparticles, rather than SEM. This was done because AFM images have the potential to resolve more detail and the smallest amidine nanoparticles (5 nm or smaller) were approaching the limit of what was clearly visible using SEM. Experiments were done using the Cypher, on samples prepared identically to those discussed in the previous chapters. Samples were imaged using tapping mode, using cantilevers with a nominal spring constant of about 42 N/m (Model# AC160TS, Asylum Research, Santa Barbara, CA).

A selection of images is shown in Figure B-2. In each case, it was clear when there were nanoparticles adsorbed to the surface, but the dimensions of the particles were mostly incorrect. Typically, the projection of the imaged particle off the surface was approximately correct, though usually somewhat smaller than expected (the average particle diameter should be 23 nm, and the images showed particles extending, at most, about 20 nm from the surface). However, the apparent diameter, in the plane of the surface, was typically on the order of 100 nm. This was particularly an issue, as these dimensions were essentially the smallest observed using the AFM. There were some that were smaller, but it was difficult getting clear images and even the best examples were not sufficient to establish a reliable distribution of nanoparticle diameters.

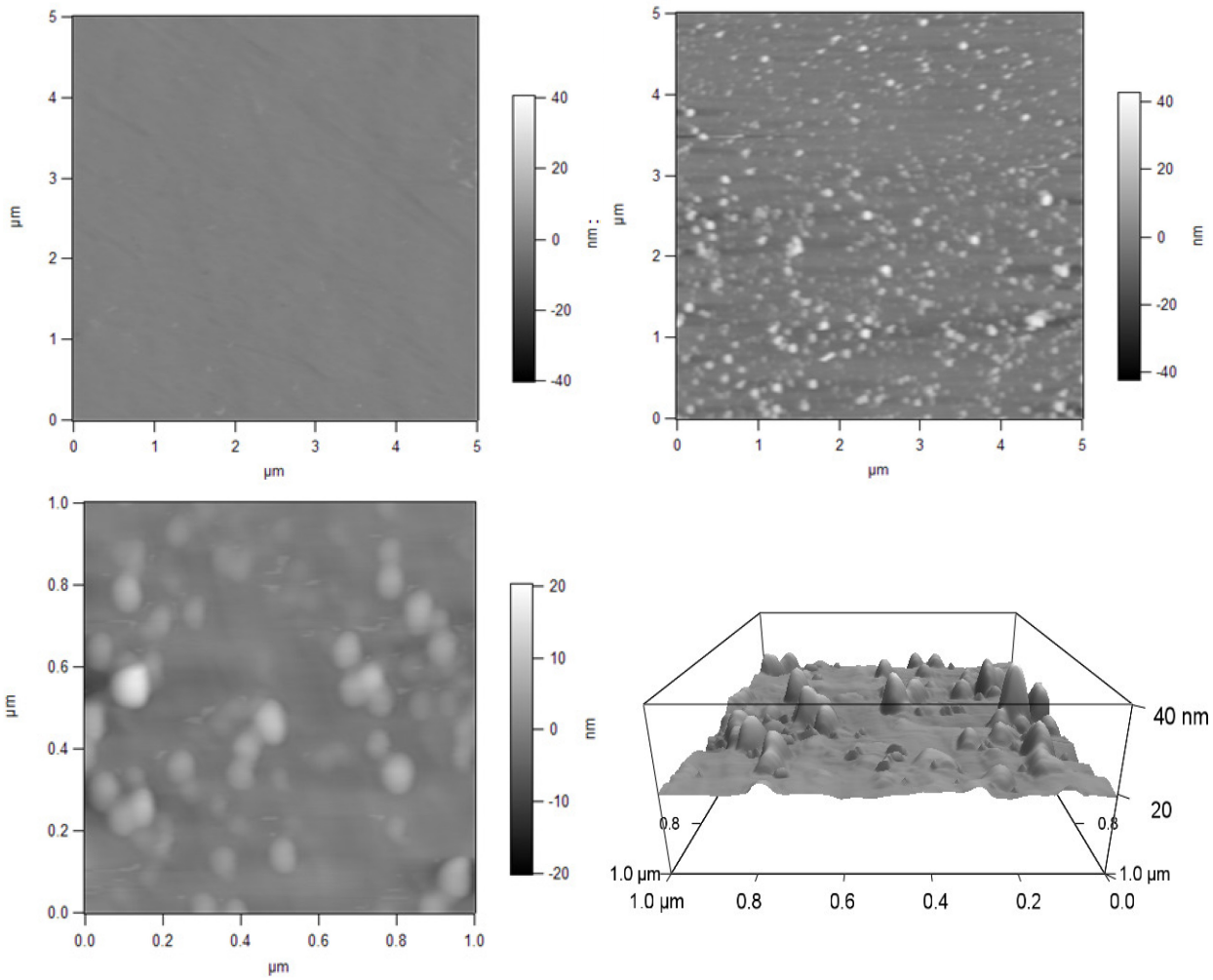

Figure B-2: AFM (Cypher) tapping mode images. Top left: Blank silica slide. Top right: Adsorption from 0.001% vol. amidine solution. Bottom: Higher magnification for 0.001% vol. sample, with 3D plot of surface on the right.

The examples in Figure B-2 were at the higher quality end of the (many) attempts to image the samples. The images in Figure B-3 are better illustrations of a typical image, where at higher magnifications the clarity and shape of the nanoparticles are significantly reduced. The higher magnification AFM images, in particular, often looked "flattened" in a way that eliminated any useful information. Comparing the images to those taken via the SEM, it was decided that it would be easier to simply do analysis on the SEM micrographs rather than spend time trying to improve the AFM images.

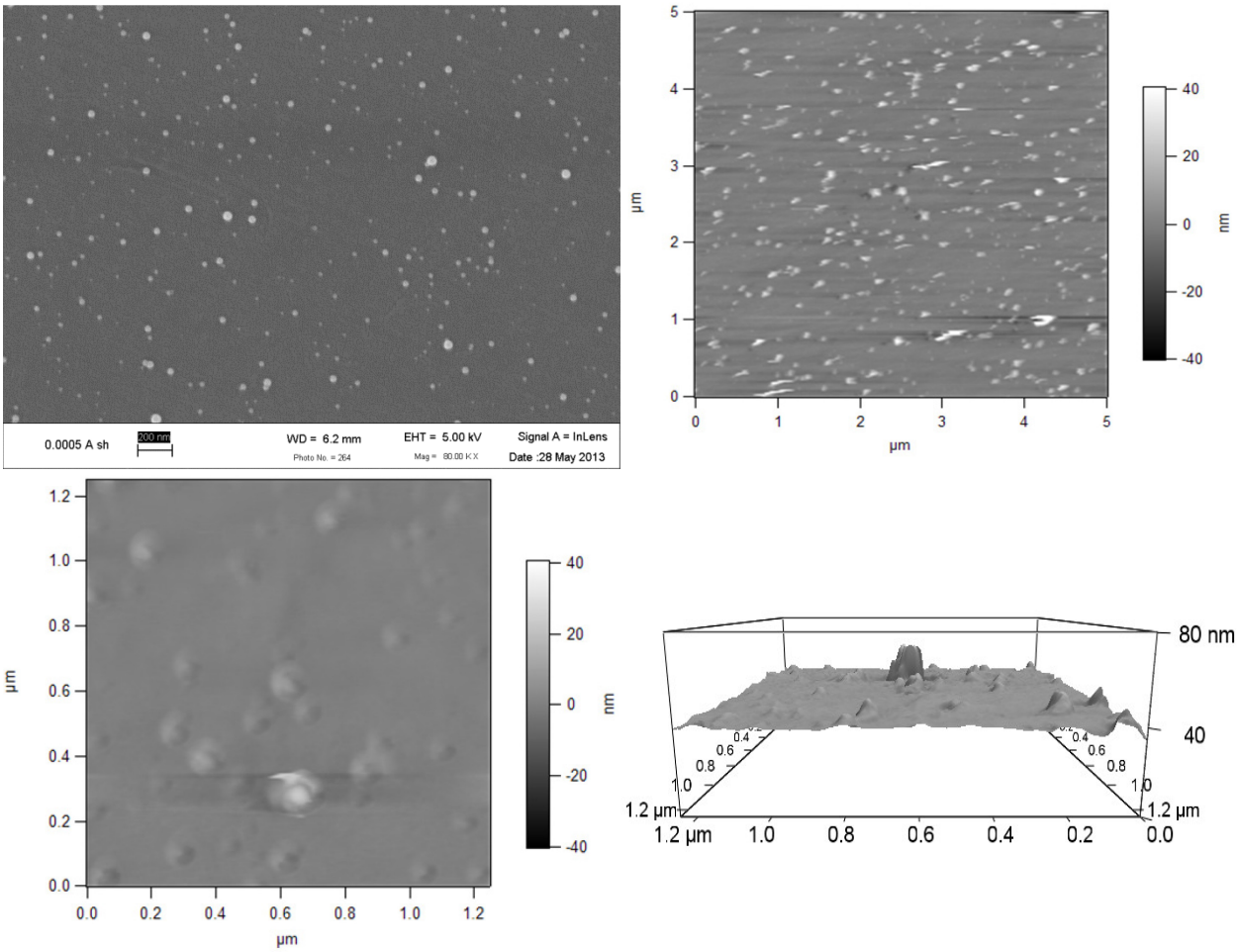

Figure B-3: Comparison of SEM and AFM images using the same amidine latex (on silica) sample. Top left: SEM micrograph. Top right, bottom left: AFM at different magnifications. Bottom left: 3D AFM image.

Appendix C: CP-AFM Measurements using Sulfate and Amidine Latex Colloidal Probes

One of the proposed causes of the differences in the amidine and sulfate latex adsorption was that the amidine latex had a greater affinity for the silica surface and therefore was less likely to desorb. If this was to be the case, it was expected that there would be a greater adhesion force between the amidine latex and silica than there would be with sulfate latex. A set of adhesion measurements was performed using 5 µm sulfate latex and 3.5 µm amidine latex spheres as colloidal probes. The probes were brought into contact with a silica slide surface and then withdrawn, and the force required to remove the sphere from the surface was measured; the adhesion is the negative attractive force shown in Figure C-1. These measurements were carried out at pH 2.5 (approximate IEP of the silica slides) and approximately 30 curves were taken for each measurement

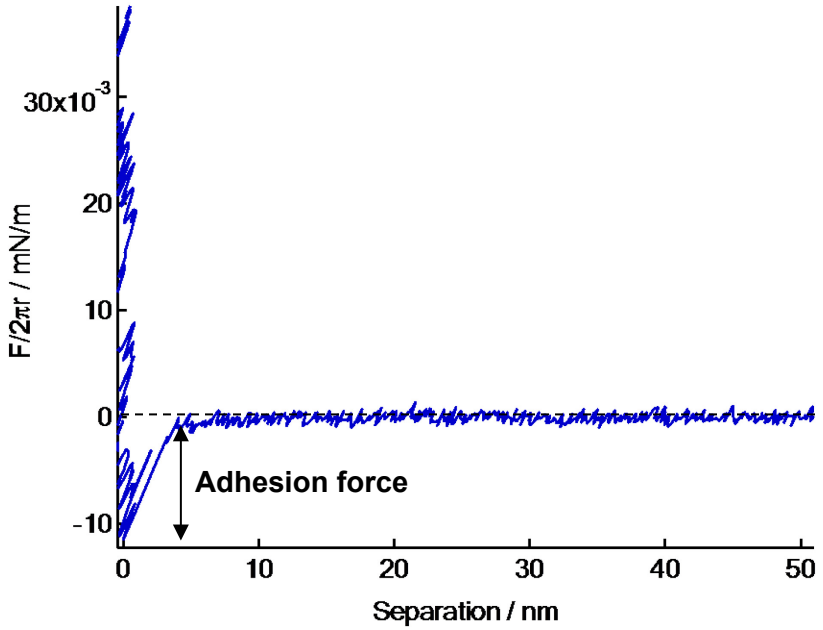

Figure C-1: Single withdrawal force curve: 5 µm sulfate latex probe and silica slide.

The adhesion force was determined from each individual withdrawal curve and then averaged. The resulting average adhesion forces (normalized by 2πR, since the probe sizes were different) are 9.1±3 nN/m for the sulfate latex and 10.9±3 nN/m for the amidine latex (standard deviation used as reported error). While the average amidine adhesion is indeed slightly greater than the sulfate, they are well within one standard deviation of each other, and therefore cannot be said to be significantly different.

Since there was no significant difference at the IEP, additional force measurements were done slightly above the IEP (pH 3) to see if how much the adhesion changed when the amidine had an attractive and sulfate had a repulsive electrostatic interaction with the silica. It was thought that the silica suspensions in the stability experiments, though unstable, may not have been exactly at the IEP and therefore may have had a slight negative charge which would result in higher amidine adsorption. However, at pH 3, both the amidine and sulfate showed repulsive forces on approach, which was not expected. In subsequent zeta potential measurements of the probes, it was observed that the amidine was not positively charged at pH 3. In order to perform the CP-AFM measurements, the probes were dried before being mounted on a cantilever, which apparently causes some change in the surface that leads to a vastly different zeta potential and effectively a charge reversal for the amidine latex at some pH values (the sulfate was still negatively charged before and after drying). Figure C-2 shows the zeta potential of the amidine at various pH values before (diluted and pH-adjusted bulk suspension) and after drying and being resuspended. It is clear that something changed when the particles were dried, as the bulk amidine suspension is positively charged in all the measurements, at pH 3 and 3.5, the average zeta potential is negative.

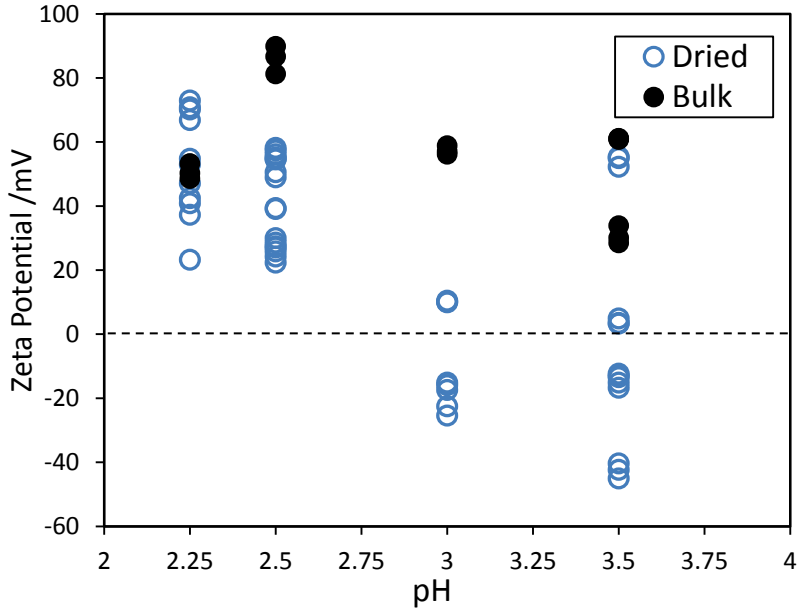

Figure C-2: Amidine latex (3.5 µm probes) zeta potential before (bulk) and after drying.

While the amidine latex is still positively charged at pH 2.5 (where the adhesion measurements in Figure C-1 were performed), since there is clearly some effect due to drying, the adhesion measurements using dry-mounted probes are likely not reliable. In order to avoid drying the latex particles, further measurements were attempted where the latex particles would be trapped in filter pores and the interaction measured with a mounted silica probe (similar to measurements performed by Byrd and Walz[149]). The latex particles were filtered through a

polycarbonate membrane filter with 3 µm pores and then the filter was used as the substrate in the AFM fluid cell, without allowing the latex to dry. The surface was then imaged using a cantilever with an attached silica probe to position the probe directly over the latex sphere, at which point the interaction forces can be measured.

Figure C-3 shows a typical image, with the scan direction indicated. With the attached silica probe, the pores were clearly visible, as were many latex spheres. However, the latex spheres were not trapped sufficiently to remain in place long enough to fully image, position the cantilever, and perform force measurements. As seen in the figure, it was possible to partially image the latex but the spheres were dislodged before the silica probe reached the center of the latex. Different pore sizes, scan speeds, and filtering times were all varied to try to improve this process, but ultimately an effective trapping method was not found due to the limitations of microparticle and pore size. Furthermore, once it was determined that the amidine latex did not fully stabilize the silica system, no additional attempts to determine the adhesion were made.

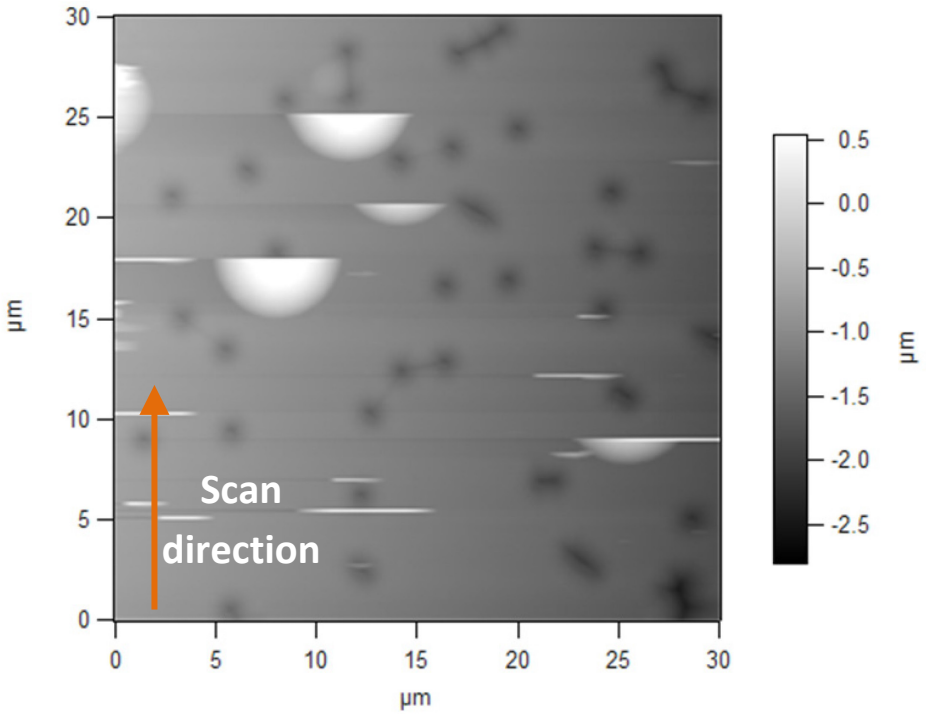

Figure C-3: A membrane with filtered polystyrene particles that was imaged using a cantilever that has an attached 5 µm silica probe.

Appendix D: Chemical Structure of Sulfate and Amidine Groups

Based on the experiments in Chapters 4 and 5, the difference in the levels of adsorption between the sulfate and amidine polystyrene latex is likely a result of the differences in the surface groups (rather than particle size distribution, charge, etc.). The product information from the supplier (Life Technologies, Carlsbad, CA) lists the pKa values for sulfate as <2 and 10-11 for amidine, and that the surface groups occupy approximately 5-10% of the surface area. There was no indication as to how the groups were attached to the particle surfaces or what the actual chemical structure of the groups was. The technical support group at this company was unable to provide greater detail beyond the suggestion that the groups were bound to the polystyrene molecules and that they were likely primary groups (rather than more complex secondary or tertiary structures). The general formula of a terminal sulfate group $R\text{-}O\text{-}SO_3^-$ and an amidine $R_nE(=NR)NR_2$. Amidine groups are easily protonated in solution giving them a positive charge (e.g. $R_nE(=NHH^+)NR_2$).[150] Figure D-1 shows the skeletal structure of simplest sulfate and amidine charge groups (merely used as an example, not necessarily the specific formulae for the actual charge groups on the polystyrene nanoparticles).

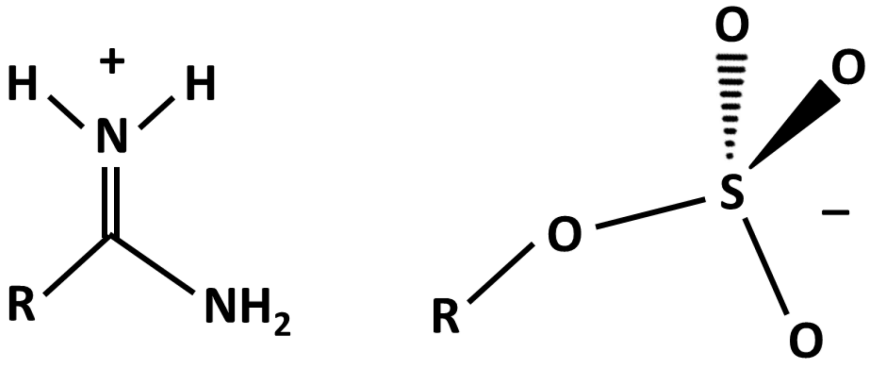

Figure D-1: Skeletal structure of amidine (left) and sulfate (right) terminal groups.

It is possible that the amidine has a greater affinity for the silica surface, e.g. due to increased hydrogen bonding compared to the sulfate, which would increase the attraction and strength of adsorption. It is also possible that the interaction between two amidine particles is less repulsive than that of the sulfate. This could result from the aforementioned hydrogen bonding or other chemical means. This could also result from charge heterogeneity on the surface of the polystyrene. Specifically, polystyrene latex has a natural negative surface charge with no IEP.[151] Given that the positive amidine charges do not occupy the entire surface, there would likely be areas of negative charge between the adsorbed amidine groups and this charge heterogeneity could lead to weaker repulsion between the nanoparticles and thus greater nanoparticle adsorption.

References

1. L.M. Mosley, K.A. Hunter, W.A. Ducker, *Forces between colloid particles in natural waters.* Environ Sci Technol, 2003. **37**, 15, 3303-3308.
2. A. Karathanasis, D. Johnson, *Stability and transportability of biosolid colloids through undisturbed soil monoliths.* Geoderma, 2006. **130**, 3-4, 334-345.
3. J.E. Smay, et al., *Directed colloidal assembly of 3D periodic structures.* Adv Mater, 2002. **14**, 18, 1279-1283.
4. R.W. Puls, C.J. Paul, D.A. Clark, *Surface chemical effects on colloid stability and transport though natural porous media.* Colloids Surf., A, 1993. **73**, 287-300.
5. E. Ringenbach, G. Chauveteau, E. Pefferkorn, *Effect of soluble aluminum ions on polyelectrolyte-alumina interaction. Kinetics of polymer adsorption and colloid stabilization.* Colloids Surf., A, 1995. **99**, 161-173.
6. S. Magdassi, et al., *Silver nanoparticles as pigments for water-based ink-jet inks.* Chem. Mater., 2003. **15**, 2208-2217.
7. E. Della Gaspera, et al., *Low-temperature processed Ga-doped ZnO coatings from colloidal inks.* J Am Chem Soc, 2013. **135**, 9, 3439-3448.
8. V. Tohver, et al., *Nanoparticle halos: A new colloid stabilization mechanism.* Proc. Natl. Acad. Sci. U.S.A., 2001. **98**, 8950-8954.
9. N. Osterman, et al., *Field-induced self-assembly of suspended colloidal membranes.* Phys. Rev. Lett., 2009. **103**, 22, 228301.
10. C.F. Huebner, et al., *Electroluminescent colloidal inks for flexographic roll-to-roll printing.* J. Mater. Chem., 2008. **18**, 41, 4942-4948.
11. W.B. Russel, D.A. Saville, W.R. Schowalter, *Colloidal dispersions*. 1989: Cambridge University Press.
12. T. Graham, *Liquid diffusion applied to analysis.* Philosophical Transactions of the Royal Society of London, 1861. **151**, 183-224.
13. P.C. Hiemenz, R. Rajagopalan, *Principles of colloid and surface chemistry*. 3rd ed. 1997: CRC Press.
14. J. Israelachvili, *Intermolecular and surface forces*. 1992: Academic Press. 450.
15. M. Elimelech, et al., *Particle deposition & aggregation: Measurement, modeling and simulation*. 1995, Oxford: Butterwotrth-Heinemann Ltd.
16. H. Helmholtz, *Ueber einige gesetze der vertheilung elektrischer ströme in körperlichen leitern mit anwendung auf die thierisch-elektrischen versuche.* Annalen der Physik, 1853. **165**, 6, 211-233.
17. G. Gouy, *Sur la constitution de la charge électrique à la surface d'un électrolyte.* J. Am. Ceram. Soc, 1910. **9**, 457-468.
18. D.L. Chapman, *A contribution to the theory of electroencapillarity.* Philosophical Magazine, 1913. **25**, 6, 475-481.
19. P.J. Scales, F. Grieser, T.W. Healy, *Electrokinetics of the silica-solution interface: A flat plate streaming potential study.* Langmuir, 1992. **8**, 3, 965-974.
20. J. Czarnecki, *The effects of surface inhomogeneities on the interactions in colloidal systems and colloid stability.* Adv. Colloid Interface Sci., 1985. **24**, 283-319.
21. J.D. Feick, et al., *Altering surface charge nonuniformity on individual colloidal particles.* Langmuir, 2004. **20**, 3090-3095.
22. J. Jones, et al., *Charge nonuniformity light scattering.* Colloids Surf., A, 2005. **267**, 1-3, 79-85.
23. H.C. Hamaker, *The london--van der waals attraction between spherical particles.* Physica, 1937. **4**, 10, 1058-1072.

24. D.C. Prieve, W.B. Russel, *Simplified predictions of Hamaker constants from Lifshitz theory.* J. Colloid Interface Sci., 1988. **125**, 1, 1-13.
25. R.R. Dagastine, et al., *Calculation of van der Waals forces with diffuse coatings: Applications to roughness and adsorbed polymers.* J. Adhes., 2004. **80**, 5, 365-394.
26. L. Bergstrom, et al., *Estimation of Hamaker constants of ceramic materials from optical data using Lifshitz theory.* J. Am. Ceram. Soc., 1996. **79**, 2, 339-348.
27. L. Bergstrom, *Hamaker constants of inorganic materials.* Adv. Colloid Interface Sci., 1997. **70**, 125-169.
28. V.A. Parsegian, G.H. Weiss, *Spectroscopic parameters for computation of van der Waals forces.* J. Colloid Interface Sci., 1981. **81**, 1, 285-289.
29. A. Milling, P. Mulvaney, I. Larson, *Direct measurement of repulsive van der Waals interactions using an atomic force microscope.* J. Colloid Interface Sci., 1996. **180**, 460-465.
30. W.M. Sigmund, S.-w. Lee, *AFM study of repulsive van der Waals forces between Teflon af™ thin film and silica or alumina.* Colloids Surf., A, 2002. **204**, 43-50.
31. Y. Liu, L. Gao, J. Sun, *Effect of acrylic copolymer adsorption on the colloidal stability of a 3y-tzp suspension.* J. Eur. Ceram. Soc., 2002. **22**, 863-871.
32. S. Liufu, H. Xiao, Y. Li, *Adsorption of poly(acrylic acid) onto the surface of titanium dioxide and the colloidal stability of aqueous suspension.* J. Colloid Interface Sci., 2005. **281**, 1, 155-163.
33. G.J. Fleer, J.M.H.M. Scheutjens, *Block copolymer adsorption and stabilization of colloids.* Colloids Surf., 1990. **51**, 281-298.
34. E.B. Zhulina, O.V. Borisov, V.A. Priamitsyn, *Theory of steric stabilization of colloid dispersions by grafted polymers.* J. Colloid Interface Sci., 1990. **137**, 2, 495-511.
35. J. Liu, E. Luijten, *Colloidal stabilization via nanoparticle halo formation.* Phys. Rev. E, 2005. **72**, 6, 061401.
36. D.H. Napper, *Steric stabilization.* J. Colloid Interface Sci., 1977. **58**, 2, 390-407.
37. M.J. Snowden, et al., *Flocculation of silica particles by adsorbing and non-adsorbing polymers.* J. Chem. Soc., 1991. **87**, 14, 2201-2207.
38. S.G. Ash, E.J. Clayfield, *Effect of polymers on the stability of colloids.* J. Colloid Interface Sci., 1976. **55**, 3, 645-657.
39. A. Sharma, S.N. Tan, J.Y. Walz, *Measurement of colloidal stability in solutions of simple, nonadsorbing polyelectrolytes.* J. Colloid Interface Sci., 1997. **190**, 392-407.
40. J.C. Baird, J.Y. Walz, *The effects of added nanoparticles on aqueous kaolinite suspensions. I. Structural effects.* J. Colloid Interface Sci., 2006. **297**, 1, 161-169.
41. B. Fazelabdolabadi, J.Y. Walz, P.R. Van Tassel, *Influence of charged nanoparticles on colloidal forces: A molecular simulation study.* J. Phys. Chem. B, 2009. **113**, 13860-13865.
42. M. Rasa, A.P. Philipse, J.D. Meeldijk, *Heteroaggregation, repeptization and stability in mixtures of oppositely charged colloids.* J. Colloid Interface Sci., 2004. **278**, 1, 115-125.
43. C. Bondy, *The creaming of rubber latex.* Trans. Faraday Soc., 1939. **35**, 1093-1108.
44. S. Asakua, F. Oosawa, *Interaction between particles suspended in solutions of macromolecules.* Journal of Polymer Science, 1958. **33**, 183-192.
45. S. Asakura, F. Oosawa, *On interaction between two bodies immersed in a solution of macromolecules.* J Chem Phys, 1954. **22**, 1255-1256.
46. M. Piech, J.Y. Walz, *Direct measurement of depletion and structural forces in polydisperse, charged systems.* Journal of colloid and interface science, 2002. **253**, 1, 117-129.
47. A. Sharma, J.Y. Walz, *Effect of long range interactions on the depletion force between colloidal particles.* J. Colloid Interface Sci., 1994. **168**, 2, 485-496.
48. A. Tulpar, P.R. Van Tassel, J.Y. Walz, *Structuring of macroions confined between like-charged surfaces.* Langmuir, 2006. **22**, 2876-2833.
49. A. Tulpar, J.Y. Walz, *Simultaneous measurement of structural and hydrodynamic forces between colloidal surfaces in complex fluids.* Colloids Surf., A, 2007. **300**, 3, 268-280.

50. R.I. Feigin, D.H. Napper, *Depletion stabilization and depletion flocculation.* J. Colloid Interface Sci., 1980. **75**, 2, 525-541.
51. S. Karanikas, A. Louis, *Dynamic colloidal stabilization by nanoparticle halos.* Phys Rev Lett, 2004. **93**, 24, 248303.
52. H. Karimian, A.A. Babaluo, *Halos mechanism in stabilizing of colloidal suspensions: Nanoparticle weight fraction and pH effects.* J. Eur. Ceram. Soc., 2007. **27**, 1, 19-25.
53. C.J. Martinez, et al., *Interparticle interactions and direct imaging of colloidal phases assembled from microsphere-nanoparticle mixtures.* Langmuir, 2005. **21**, 22, 9978-9989.
54. F. Zhang, et al., *Quantitative measurement of nanoparticle halo formation around colloidal microspheres in binary mixtures.* Langmuir, 2008. **24**, 13, 6504-6508.
55. A.T. Chan, J.A. Lewis, *Electrostatically tuned interactions in silica microsphere-polystyrene nanoparticle mixtures.* Langmuir, 2005. **21**, 8576-8579.
56. A.T. Chan, J.A. Lewis, *Size ratio effects on interparticle interactions and phase behavior of microsphere-nanoparticle mixtures.* Langmuir, 2008. **24**, 20, 11399-11405.
57. J.F. Gilchrist, et al., *Phase behavior and 3D structure of strongly attractive microsphere-nanoparticle mixtures.* Langmuir, 2007. **21**, 24, 11040-11047.
58. S.A. Barr, E. Luijten, *Effective interactions in mixtures of silica microspheres and polystyrene nanoparticles.* Langmuir, 2006. **22**, 17, 7152-7155.
59. M. Trulsson, B. Jonsson, C. Labbez, *On the origin of the halo stabilization.* Phys. Chem. Chem. Phys., 2013. **15**, 2, 541-545.
60. V. Tohver, et al., *Nanoparticle engineering of complex fluid behavior.* Langmuir, 2001. **17**, 26, 8414-8421.
61. X. Hong, G.A. Willing, *Transition force measurement between two negligibly charged surfaces: A new perspective on nanoparticle halos.* Langmuir, 2009. **25**, 9, 4929-4933.
62. S. Ji, J.Y. Walz, *Interaction potentials between two colloidal particles surrounded by an extremely bidisperse particle suspension.* Journal of colloid and interface science, 2013. **394**, 611-618.
63. S. Ji, D. Herman, J.Y. Walz, *Manipulating microparticle interactions using highly charged nanoparticles.* Colloids Surf., A, 2012. **396**, 51-62.
64. J.T.G. Overbeek, M.J. Sparnaay, *Exeriments on long-range attracitve forces between macroscopic objects.* J. Colloid Interface Sci., 1952. **7**, 3, 343-345.
65. M.J. Sparnaay, *Attractive forces between flat plates.* Nature, 1957. **180**, 334-335.
66. B.V. Derjaguin, T.N. Voropayeva, *Surface forces and the stability of colloids and disperse systems.* J. Colloid Interface Sci., 1964. **19**, 2, 113-135.
67. D. Tabor, R.H.S. Winterton, *Surface forces: Direct measurement of normal and retarded van der Waals forces.* Nature, 1968. **219**, 1120-1121.
68. D. Tabor, R.H.S. Winterton, *The direct measurement of normal and retarded van der Waals forces.* Proc. R. Soc. London, Ser. A, 1969. **312**, 345-450.
69. J. Israelachvili, D. Tabor, *The measurement of van der Waals dispersion forces in the range 1.5 ro 130 nm.* Proc. R. Soc. London, Ser. A, 1972. **331**, 19-38.
70. J. Israelachvili, et al., *Recent advances in the surface forces apparatus (SFA) technique.* Rep. Prog. Phys., 2010. **73**, 3, 036601.
71. D.C. Prieve, *Measurement of colloidal forces with TIRM.* Adv. Colloid Interface Sci., 1999. **82**, 93-125.
72. D.C. Prieve, N.A. Frej, *Total internal reflection microscopy: A quantitative tool for the measurement of colloidal forces.* Langmuir, 1990. **6**, 396-403.
73. A. Sharma, J.Y. Walz, *Direct measurement of the depletion interaction in a charged colloidal dispersion.* J. Chem. Soc., Faraday Trans., 1996. **92**, 24, 4997-5004.
74. D.L. Sober, J.Y. Walz, *Measurement of long range depletion energies between a colloidal particle and a flat surface in micellar solutions.* Langmuir, 1995. **11**, 2352-2356.

75. V.A. Parsegian, N. Fuller, R.P. Rand, *Measured work of deformation and repulsion of lecitin bilayers.* Proc. Natl. Acad. Sci. U.S.A., 1979. **76**, 6, 2750-2754.
76. T.G.M. van de Ven, et al., *Colloidal particle scattering: A new method to measure surface forces.* Langmuir, 1994. **10**, 3046-3056.
77. H.-J. Butt, B. Cappella, M. Kappl, *Force measurements with the atomic force microscope: Technique, interpretation and applications.* Surf. Sci. Rep., 2005. **59**, 1-6, 1-152.
78. G. Binnig, C.F. Quate, *Atomic force microscope.* Phys. Rev. Lett., 1986. **56**, 9, 930-933.
79. M. Rief, et al., *Single molecule force spectroscopy on polysaccharides by atomic force microscopy.* Science, 1997. **275**, 1295-1297.
80. W.A. Ducker, T.J. Senden, R.M. Pashley, *Direct measurement of colloidal forces using an atomic force microscope.* Nature, 1991. **353**, 239-241.
81. K.M. Andersson, L. Bergstrom, *DLVO interactions of tungsten oxide and cobalt oxide surfaces measured with the colloidal probe technique.* Journal of colloid and interface science, 2002. **246**, 2, 309-315.
82. F.J. Montes Ruiz-Cabello, P. Maroni, M. Borkovec, *Direct measurements of forces between different charged colloidal particles and their prediction by the theory of Derjaguin, landau, Verwey, and Overbeek (DLVO).* J Chem Phys, 2013. **138**, 23, 234705.
83. S. Zauscher, D.J. Klingenberg, *Normal forces between cellulose surfaces measured with colloidal probe microscopy.* Journal of colloid and interface science, 2000. **229**, 2, 497-510.
84. C.T. McKee, J.Y. Walz, *Interaction forces between colloidal particles in a solution of like-charged, adsorbing nanoparticles.* J. Colloid Interface Sci., 2012. **365**, 72-80.
85. G.K. James, J.Y. Walz, *Experimental and theoretical investigation of the depletion and structural forces produced by ionic micelles.* Colloids Surf., A, 2014. **441**, 406-419.
86. N.C. Christov, et al., *Oscillatory structural forces due to nonionic surfactant micelles: Data by colloidal-probe AFM vs theory.* Langmuir, 2010. **26**, 2, 915-923.
87. M. Kappl, H.-J. Butt, *The colloidal probe technique and its application to adhesion force measurements.* Part. Part. Syst. Char., 2002. **19**, 129-143.
88. G.A. Willing, et al., *New approach to the study of particle-surface adhesion using atomic force microscopy.* Journal of colloid and interface science, 2000. **226**, 1, 185-188.
89. S.M. Wiederhorn, et al., *Cell adhesion to borate glasses by colloidal probe microscopy.* Acta biomaterialia, 2011. **7**, 5, 2256-2263.
90. T.S. Rodrigues, H.-J. Butt, E. Bonaccurso, *Influence of the spring constant of cantilevers on hydrodynamic force measurements by the colloidal probe technique.* Colloids Surf., A, 2010. **354**, 1-3, 72-80.
91. K. Theander, R.J. Pugh, M.W. Rutland, *Forces and friction between hydrophilic and hydrophobic surfaces: Influence of oleate species.* Journal of colloid and interface science, 2007. **313**, 2, 735-746.
92. S. Zauscher, D.J. Klingenberg, *Friction between cellulose surfaces measured with colloidal probe microscopy.* Colloids Surf., A, 2001. **178**, 213-229.
93. X. Zhang, et al., *Friction behavior of nano-textured polyimide surfaces measured by AFM colloidal probe.* Appl. Surf. Sci., 2014. **320**, 328-333.
94. W.A. Ducker, T.J. Senden, R.M. Pashley, *Measurement of forces in liquids using a force microscope.* Langmuir, 1992. **8**, 1821-1936.
95. S.C. Clark, J.Y. Walz, W.A. Ducker, *Atomic force microscopy colloid-probe measurements with explicit measurement of particle-solid separation.* Langmuir, 2004. **20**, 7616-7622.
96. J.L. Hutter, J. Bechhoefer, *Calibration of atomic-force microscope tips.* Rev. Sci. Instrum., 1993. **64**, 7, 1868-1873.
97. D.H. Van Winkle, C.A. Murray, *Layering in colloidal fluids near a smooth repulsive wall.* J. Chem. Phys., 1988. **89**, 6, 3885-3891.
98. A. Trokhymchuk, et al., *Computer modeling of ionic micelle structuring in thin films.* J. Phys. Chem. B, 2003. **107**, 3927-3937.

99. J. Drelich, et al., *AFM colloidal forces measured between microscopic probes and flat substrates in nanoparticle suspensions.* J. Colloid Interface Sci., 2006. **301**, 2, 511-522.
100. R. von Klitzing, et al., *Confinement of linear polymers, surfactants, and particles between interfaces.* Adv. Colloid Interface Sci., 2010. **155**, 1-2, 19-31.
101. Y. Zeng, R. von Klitzing, *Structuring of colloidal suspensions confined between a silica microsphere and an air bubble.* Soft Matter, 2011. **7**, 11, 5329-5338.
102. J. Liu, E. Luijten, *Stabilization of colloidal suspensions by means of highly charged nanoparticles.* Phys. Rev. Lett., 2004. **93**, 24, 247802.
103. Y.-I. Chang, C.-C. Chang, W.-Y. Cheng, *Can nanoparticles stabilize microparticle suspension?* Sep Purif Technol, 2011. **79**, 393-398.
104. J.A. Long, D.W.J. Osmond, B. Vincent, *The equilibrium aspects of weak flocculation.* J. Colloid Interface Sci., 1973. **42**, 3, 545-553.
105. A. Sharma, S.N. Tan, J.Y. Walz, *Effect of nonadsorbing polyelectrolytes on colloidal interactions in aqueous mixtures.* J. Colloid Interface Sci., 1997. **191**, 236-246.
106. W. Heller, H.L. Bhatnagar, M. Nakagaki, *Theoretical investigations on the light scattering of spheres. XIII. The "wavelength exponent" of differential turbidity spectra.* J. Chem. Phys., 1962. **36**, 5, 1163-1170.
107. G. Sauerbrey, *Use of quartz vibrator for weighting thin layers and as a microbalance.* Z. Phys., 1959. **155**, 206-222.
108. G.M. Bell, S. Levine, L.N. McCartney, *Approximate methods of determining the double-layer free energy of interaction between two charged colloidal spheres.* J. Colloid Interface Sci., 1970. **33**, 3, 335-359.
109. P. Taboada-Serrano, et al., *Surface charge heterogeneities measured by atomic force microscopy.* Environ. Sci. Technol., 2005. **39**, 6352-6360.
110. R. Duffadar, et al., *The impact of nanoscale chemical features on micron-scale adhesion: Crossover from heterogeneity-dominated to mean-field behavior.* J. Colloid Interface Sci., 2009. **337**, 2, 396-407.
111. N. Kozlova, M.M. Santore, *Micrometer scale adhesion on nanometer-scale patchy surfaces: Adhesion rates, adhesion thresholds, and curvature-based selectivity.* Langmuir, 2007. **23**, 4782-4791.
112. J.N. Ryan, M. Elimelech, *Colloid mobilization and transport in groundwater.* Colloids Surf., A, 1996. **107**, 1-56.
113. W.J.C. Holt, D.Y.C. Chan, *Pair interactions between heterogeneous spheres.* Langmuir, 1997. **13**, 1577-1586.
114. L. Song, P.R. Johnson, M. Elimelech, *Kinetics of colloid deposition onto heterogeneously charged surfaces in porous media.* Environ. Sci. Technol., 1994. **28**, 1164-1171.
115. D. Velegol, P.K. Thwar, *Analytical model for the effect of surface charge nonuniformity on colloidal interactions.* Langmuir, 2001. **17**, 7687-7693.
116. P.K. Thwar, D. Velegol, *Force measurements between weakly attractive polystyrene particles.* Langmuir, 2002. **18**, 7328-7333.
117. S.J. Miklavic, et al., *Double layer forces between heterogeneous charged surfaces.* J. Phys. Chem., 1994. **98**, 9022-9032.
118. G. Silbert, et al., *Long-ranged attraction between disordered heterogeneous surfaces.* Phys. Rev. Lett., 2012. **109**, 16, 168305.
119. Y. Mao, M.E. Cates, H.N.W. Lekkerkerker, *Depletion force in colloidal systems.* Physica A, 1995. **222**, 10-24.
120. W. Xu, A.D. Nikolov, D.T. Wasan, *Role of depletion and surface-induced structural forces in bidisperse suspensions.* AlChE J., 1997. **43**, 12, 3215-3222.
121. X.L. Chu, A.D. Nikolov, D.T. Wasan, *Effects of interparticle interactions on stability, aggregation and sedimentation in colloidal suspensions.* Chem. Eng. Commun., 1996. **148-150**, 1, 123-142.

122. H. Huang, E. Ruckenstein, *Repulsive force between two microparticles decorated with highly charged nanoparticles.* Colloids Surf., A, 2013. **436**, 862-867.
123. D. Herman, J.Y. Walz, *Stabilization of weakly charged microparticles using highly charged nanoparticles.* Langmuir, 2013. **29**, 5982-5994.
124. C.A. Schneider, W.S. Rasband, K.W. Eliceiri, *NIH image to ImageJ: 25 years of image analysis.* Nature Methods, 2012. **9**, 7, 671-675.
125. J. Feder, *Random sequential adsorption.* Journal of Theoretical Biology, 1980. **87**, 237-254.
126. Z. Adamczyk, et al., *Structure and ordering in localized adsorption of particles.* J. Colloid Interface Sci., 1990. **140**, 1, 123-137.
127. C.H. Ko, S. Bhattacharjee, M. Elimelech, *Coupled influence of colloidal and hydrodynamic interactions on the RSA dynamic blocking function for particle deposition onto packed spherical collectors.* J. Colloid Interface Sci., 2000. **229**, 2, 554-567.
128. Z. Adamczyk, et al., *Influence of polydispersity on random sequential adsorptoin of spherical particles.* J. Colloid Interface Sci., 1997. **185**, 1, 236-244.
129. P. Hanarp, et al., *Influence of polydispersity on adsorption of nanoparticles.* J. Colloid Interface Sci., 2001. **241**, 1, 26-31.
130. P. Danwanichakul, T. Charinpanitkul, *Random sequential adsorption of polydisperse spherical particles: An integral-equation theory.* Physica A, 2007. **377**, 102-114.
131. D. Velegol, J.D. Feick, L.R. Collins, *Electrophoresis of spherical particles with a random distribution of zeta potential or surface charge.* J. Colloid Interface Sci., 2000. **230**, 1, 114-121.
132. A. Sharma, J.Y. Walz, *Direct measurement of the depletion interaction in a charged colloidal dispersion.* J. Chem. Soc., Faraday Trans., 1995. **92**, 24, 4997-5004.
133. D. Herman, J.Y. Walz, *Adsorption and stabilizing effects of highly charged latex nanoparticles in dispersions of weakly charged silica colloids.* J. Colloid Interface Sci., 2014.
134. S.M. Gatica, M.W. Cole, D. Velegol, *Designing van der Waals forces between nanocolloids.* Nano Lett., 2005. **5**, 1, 169-173.
135. H.-Y. Kim, et al., *Van der Waals dispersion forces between dielectric nanoclusters.* Langmuir, 2007. **23**, 1735-1740.
136. S. Rentsch, et al., *Probing the validity of the Derjaguin approximation for heterogeneous colloidal particles.* Phys Chem Chem Phys, 2006. **8**, 21, 2531-2538.
137. H.-J. Butt, *Measuring electrostatic, van der Waals, and hydration forces in electrolyte solutions with an atomic force microscope.* Biophys. J., 1991. **60**, 6, 1438-1444.
138. B.V. Derjaguin, *Untersuchungen über die reibung und adhäsion, iv.* Kolloid Zeits, 1934. **69**, 155-164.
139. S. Bhattacharjee, M. Elimelech, *Surface element integration: A novel technique for evaluation of DLVO interaction between a particle and a flat plate.* J. Colloid Interface Sci., 1997. **193**, 273-285.
140. S.L. Carnie, D.Y.C. Chan, J.S. Gunning, *Electrical double layer interaction between dissimilar spherical colloidal particles and between a sphere and a plate: The linearized Poisson-Boltzmann theory.* Langmuir, 1994. **10**, 2993-3009.
141. S.L. Carnie, D.Y.C. Chan, J. Stankovich, *Computation of forces between spherical colloidal particles: Nonlinear Poisson-Boltzmann theory.* J. Colloid Interface Sci., 1994. **165**, 116-128.
142. R. Roth, R. Evans, S. Dietrich, *Depletion potential in hard-sphere mixtures: Theory and applications.* Phys. Rev. E, 2000. **62**, 5360-5377.
143. J.N. Israelachvili, R.K. Tandon, L.R. White, *Measurement of forces between two mica surfaces in aqueous polyethylene oxide solution.* J. Colloid Interface Sci., 1980. **78**, 2, 430-443.
144. B.A. Todd, S.J. Eppell, *Probing the limits of the Derjaguin approximation with scanning force microscopy.* Langmuir, 2004. **20**, 4892-4897.
145. J. Bergendahl, D. Grasso, *Colloidal generation during batch leaching tests: Mechanics of disaggregation.* Colloids Surf., A, 1998. **135**, 193-205.

146. J. Bergendahl, D. Grasso, *Prediction of colloid detachment in a model porous media: Hydrodynamics.* Chem. Eng. Sci., 2000. **55**, 1523-1532.
147. J.M. Meinders, H.J. Busscher, *Adsorption and desorption of colloidal particles on glass in a parallel plate flow chamber - influence of ionic strength and shear rate.* Colloid. Polym. Sci., 1994. **272**, 478-486.
148. M.D. Abramoff, P.J. Magalhaes, S.J. Ram, *Image processing with ImageJ.* Biophotonics International, 2004. **11**, 7, 36-42.
149. T.L. Byrd, J.Y. Walz, *Investigation of the interaction force between cryptosporidium parvum oocysts and solid surfaces.* Langmuir, 2007. **23**, 7475-7483.
150. P.M. Dewick, *Essential of organic chemistry*. 2013: John Wiley & Sons. 704.
151. K. Ohsawa, M. Murata, H. Ohshima, *Zeta potential and surface charge density of polystyrene-latex; comparison with synaptic vesicle and brush border membrane vesicle.* Colloid. Polym. Sci., 1986. **264**, 12, 1005-1009.